2011

Effects of Air Bubbles on Storm Surge

Rahman, Md. Azizur

University of Rajshahi

EFFECTS OF AIR BUBBLES ON STORM SURGE

Ph.D Thesis

Submitted

By

Md. Azizur Rahman

Department of Mathematics
University of Rajshahi
Rajshahi, Bangladesh

DEDICATED

TO

THE MEMORY OF MY PARENTS

Declaration

I hereby declare that the whole works now submitted as a thesis entitled "EFFECTS OF AIR BUBBLES ON STORM SURGE" in the department of Mathematics, University of Rajshahi, Bangladesh for the degree of Doctor of Philosophy is the result of my own investigation. The thesis contains no material which has been accepted for the award of my other degree or diploma elsewhere (except for publication in the journal), and, to the best of my knowledge, the thesis contains no material written by another person, except where due reference is made in the text.

Azizur
The Author

Certificate

This is to certify that the thesis entitled "**EFFECTS OF AIR BUBBLES ON STORM SURGE**" being submitted by **Md. Azizur Rahman** for the award of the degree of Doctor of Philosophy is a record of the original bonafide research work carried out by him. He has worked under our joint guidance and supervision and has fulfilled the requirements for the submission of this thesis. The results presented in this thesis have not been submitted in part or full to any other University or Institute for award of any degree or diploma.

21.06.11

(Dr. Md. Ashabul Hoque)

Supervisor

Department of Mathematics

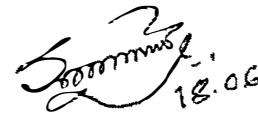University of Rajshahi

Rajshahi-6205, Bangladesh

21.6.11

(Dr. M. Zillur Rahman)

Co-supervisor

Department of Applied Mathematics

University of Rajshahi

Rajshahi-6205, Bangladesh

18.06.2011

(Sujit Kumar Debsarma)

Co-supervisor

SAARC Meteorological Research Centre

E-4/C, Agargaon, Dhaka-1207

Bangladesh

Acknowledgement

First and foremost, I would like to express my deepest gratitude to my reverend supervisor **Dr. Ashabul Hoque**, Professor, Dept of Mathematics, University of Rajshahi, Bangladesh for his wonderful supervision, valuable suggestion and continuous encouragement through the thesis work. I shall remain grateful to him.

I would like to express my gratitude to my co-supervisors **Dr. M. Zillur Rahman,** Professor, Department of Applied Mathematics, University of Rajshahi, Bangladesh and **Sujit Kumar Debsarma**, Scientist, Theoretical Division, SAARC Meteorological Reseach Center (SMRC), Agargaon, Dhaka, Bangladesh for their help and valuable suggestions throughout the work.

I express my gratitude to respectable teacher Dr. Akhil Chandra Paul Chairman, Department of Mathematics, University of Rajshahi, Bangladesh for providing me all kinds of departmental help.

I express my special gratitude to respectable teacher Dr. Gour Chandra Paul, Associate Professor, Department of Mathematics, University of Rajshahi, Bangladesh for giving me all kinds of help and encouragement. I also express my gratitude to all of my teachers especially, Dr. Md. Altab Hossain, Dr. Md. Zulfikar Ali, Dr. Nasima Akhter, Late Professor Dr. Monsur Rahman, Dr. Md. Sazuwar Raihan for their valuable suggestions and encouragement during the thesis work.

I am also grateful to **Dr. Samarendra Karmakar** (the former Director of Bangladesh Meteorological Department) for giving me permission to work at Bangladesh Meteorological Department.

Finally, I would like to thank all of my family members and friends for their cordial encouragement and help through the thesis work.

The Author

Contents

Chapter 4: Verification of the Storm Surge model

Chapter 5: General Conclusions

ABSTRACT

The development of real time operational surge prediction system in the Bay of Bengal incorporating air bubble effects is still limited and is needed immediate attention. In this respects the study has been focused the wave energy dissipation, sea level rise due to air entrainment during storm surge and its various consequences. Furthermore, the thesis has also been investigated the two most severe cyclones of 1991 and AILA, 2009 that crossed the coast of Bangladesh. The energy dissipation by entrained air bubbles under breaking waves is studied theoretically both in spilling and plunging breakers. Results show that there is a correlation between the sudden reductions of wave height and entrained air bubbles into water. The study also focuses that in plunging breaking waves, the wave energy is dissipated on a very short way, whereas, in a spilling breaker this way is of the order of some wave lengths. Mathematical formulations of depth-averaged hydrodynamic equations have also been developed in terms of air bubbles. The results show that the water level increases with the increasing of air bubbles. Moreover, we have also found that wave energy increases with the increasing of void fraction.

A nonlinear storm surge model in terms of air bubble effect has been developed for the Bay of Bengal along Bangladesh coast. The model is included the analysis area of the head Bay of Bengal. These equations have been solved by finite difference method where the coasts and islands are included in the stair step method. The dynamic effect of pressure gradient outside the storm surge region in the model is found to be negligible in comparison with the dominant effect of wind. Using the model storm surges are simulated for the severe cyclones April, 1991 and "AILA" 2009. The simulation is made at some coastal and island locations of Bangladesh and simulated water levels are found higher in presence of air bubbles. That is, it observes that approximately 1.5%-3.5% water level increases with the increasing of void fraction from 10%-70% associated with AILA, 2009, whereas it increases up to 2%-4.5% for void fraction 10%-70% in the cyclone April, 1991. The results are in good agreement with the reported post storm survey information.

General Introduction

Breaking waves at the near shore area of the oceans inject air bubbles (Fig. 1). Air entrained by breaking waves plays an important role in the surf zone in the transport of mass and energy across the air-sea interface (Melville, 1992). Wave breaking with extensive air bubble entrainment occurs in the shallow water region. Soloviev and Lukas (2010) concluded that breaking waves disrupt the air–sea interface producing a two-phase layer, namely air bubbles in water and sea-spray droplets in air. Hoque (2008) showed the contribution of entrained air bubbles on wave set up in raising the water level. It is believed that the entrained air bubbles are responsible to change the surge height, direction and velocity.
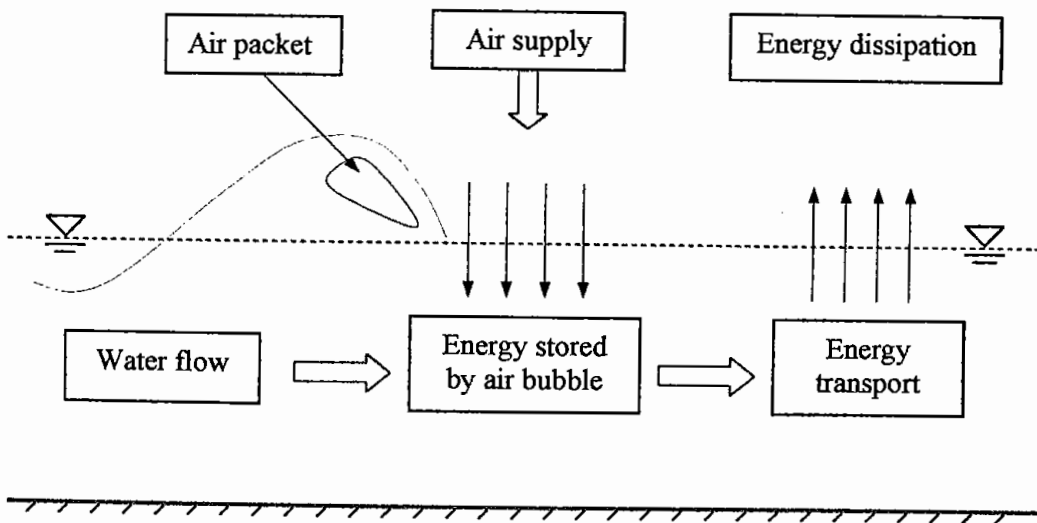
Figure 1: Air entrainment and detrainment cycle (after Hoque, 2002).

The coastal region of Bangladesh lies between latitude 21° to 23° north and longitude 89° to 93° east. The coastline is approximately 710 kilometers long and the coastal zone covers an area of about 2.85 million hectares, which is 23 percent of the area of total country. Most of the land of the coastal region is low-lying and this makes the country quite vulnerable to cyclonic storm surge. The growing threats for the coastal regions of

Bangladesh are the sea level rise caused by global warming. Also the inundation and salinity intrusion are great concerns of coastal region due to the tropical cyclones and cyclonic storm surges in the Bay of Bengal. These natural calamities ravage the area almost regularly and are considered as the main obstacle to the development of this region and the country as a whole.

The forecasting and analysis of storm surge in the region of Bay of Bengal have been investigated by many authors (Debsharma, 2009; Sinha *et al*, 1997; John and Ali, 1980a; Ali, 1980; Ali *et al*, 1997$_{a,b}$). Though a number of studies are carried out on the analysis and prediction of tide, surge, their interaction and the effects of various factors on water levels, but studies incorporating air bubbles and their effect on water levels during storm surges are very limited.

In this study we intend to develop a hydrodynamic model including air bubbles effects to simulate the storm surges due to tropical storms in the Bay of Bengal along Bangladesh coast. The content of this thesis is divided into five chapters. An outline of each chapter is described briefly in the followings:

In chapter 1, a brief review of the literatures relevant to the studies made in the thesis has been given.

In chapter 2, the energy dissipation by entrained air under breaking waves is studied theoretically both in spilling and plunging breakers. Result shows that there is a correlation between the sudden reductions of wave height and entrained air bubbles into water. This theoretical study also focuses that in plunging breaker the wave energy is dissipated on a very short way whereas in a spilling breaker this way is of the order of some wavelengths. This chapter also describes the mathematical formulation of depth-averaged hydrodynamic equations in terms of air bubble effects. The results show that the water level increases with the increasing of air bubbles. Moreover, we have also found that wave energy increases with the increasing of void fraction.

In chapter 3, a nonlinear storm surge model in terms of air bubble effect has been developed for the Bay of Bengal along Bangladesh coast. The model was included the analysis area of the head Bay of Bengal. These equations have been solved by finite difference method where the coasts and islands are included in the stair step method.

In chapter 4, using the model developed in chapter 3 storm surges are simulated for the severe cyclones in April, 1991 and AILA, 2009. The simulation is made at some coastal and island location of Bangladesh.

In chapter 5, a brief conclusion drawn from the studies described in earlier chapters and an outline of the future course of studies has been discussed. Finally, the total bibliography that has been needed for completing this thesis is given.

List of Figure Captions

.

List of Tables

List of Symbols

Main Symbols	Meanings
H	wave height
h	water depth
u, v	horizontal velocity components
w	vertical velocity component
η	surface elevation
L	wave length
P	fluid pressure
u, v, w	Reynolds averaged component of velocity in the direction of x, y and z respectively,
t	time,
p	pressure,
ρ	density of air-water mixture,
f	coriolis parameter, $f = 2\omega\sin\phi$
g	acceleration due to gravity,
τ_x, τ_y	x and y components, respectively, of the frictional stress (Reynolds stress).
T	time
ϕ	velocity potential
z	vertical axis
k	wave number
ω	wave frequency
Δh	entrained air volume
$\bar{u}, \bar{v}$	depth averaged horizontal velocity component
KE	kinetic energy
PE	potential energy

E_f	energy flux
c	wave celerity
P_d	dynamic pressure
c_g	group velocity
$C(z)$	part of the volume locally occupied by bubbles per unit width
K_1	decay parameter
C_0	reference void fraction at the mean water surface
ρ_a	air density
ρ_w	water density
w_r	rise velocity of bubble
σ	surface tension
R	air bubble radius
p_a	air pressure
p_w	water pressure
u_a	horizontal velocity of air
u_w	horizontal velocity of water
w_w	vertical velocity of water
w_a	vertical velocity of air
w_r	rise velocity of bubbles
ΔSE	change of static energy
ΔPE	change of potential energy

Abbreviations

$KSBS$	kinematic surface boundary condition
BBC	bottom boundary condition
BOB	Bay of Bengal
BP	Breaking point
BMD	Bangladesh Meteorological Department
BST	Bangladesh Standard Time

Chapter-1

Review of Long Waves

Summary

This chapter highlights the cause of long waves (e.g. storm surge, tsunami, tide etc) and its impact to Bangladesh. Cyclone-induced storm surges are very common phenomena in Bangladesh. We have reviewed different kinds of long waves and have shown the list of the most destructive cyclone-induced storm surges that hit Bangladesh and the surrounding area. The input parameters and the various methods of storm surge prediction are also reviewed.

1.1 Introduction

Bangladesh is located between 20° to 26° north and 88° to 92° east. It is bordered on the west, north and east by India, on the south-east by Myanmar, and on the south by the Bay of Bengal (Fig. 1.1). Most of the land of the coastal region is low-lying (particularly in its southern coastal regions where the elevation of the land does not exceed 10-15 m above sea level in height) and this low-lying makes the country quite vulnerable to cyclonic storm surge. The triangular shape of the Bay of Bengal has its apex along its northern shoreline which includes the full coast of Bangladesh. This shape funnels the storm surge pushed by the severe tropical storms (known as cyclones or cyclonic storms in the region) onto the Bangladesh coast. The shape is accentuated by the shallow waters which allow the build-up of high storm surges. The devastation caused by these surges can be especially destructive, and deadly, when they occurs at astronomical high tide. Much of it sits on the delta of the Ganges-Brahmaputra-Meghna Rivers and is very susceptible to coastal flooding.

Bangladesh is a very densely populated country because the population of about 150 million and population density of more than 1,209 persons per km^2, and 75% of the population lives in rural areas, (World Bank, 2002).
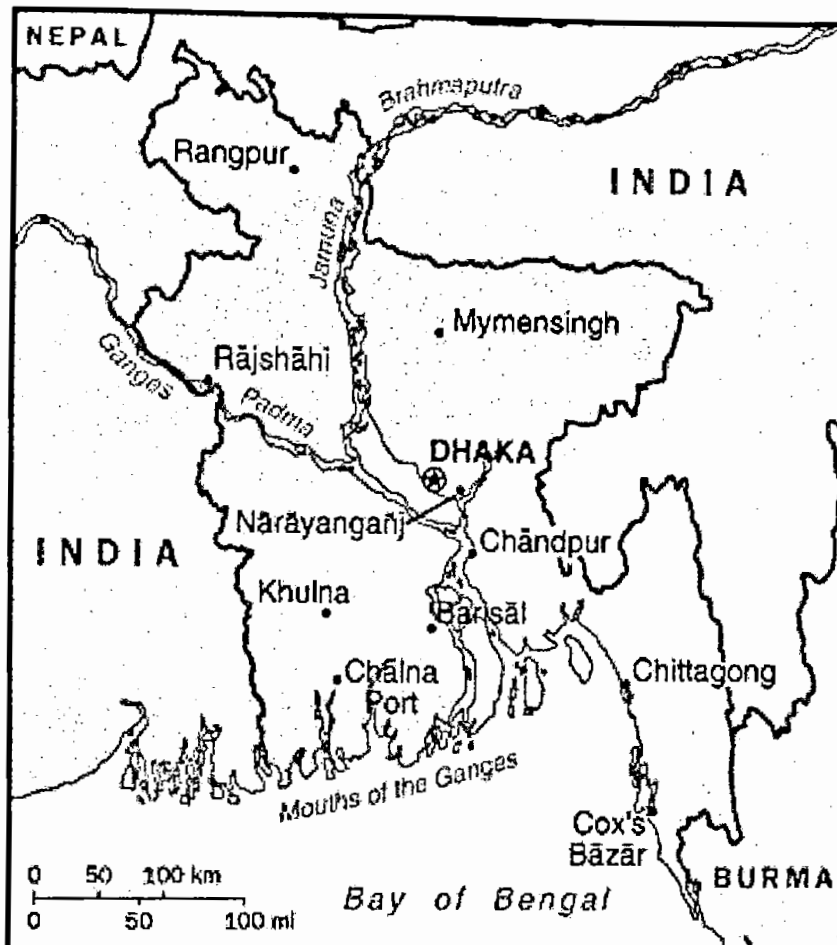
Figure 1.1: Map of Bangladesh

A series of works were conducted on long waves and its vulnerability (e.g. Aimin Shi, 2005; Joseph-Louis Lagrange, 1781; Dean and Dalrymple, 1984; Huq et al., 1995; Hoque and Rahman, 2006). Aimin Shi (2005) investigated the fundamental behavior of long water waves propagating through branching channels of uniform depth and width. Joseph-Louis Lagrange (1781) derived the linearized governing equations for small-amplitude waves, and obtained the solution in the limiting case of long plane waves in shallow water. Dean and Dalrymple (1984) studied long wave equations and discussed its various effects. Huq et al. (1995) estimated that 1m rise in

sea level would inundate 18% of Bangladesh's total land, directly threatening 11% of the country's population with inundation (based on current population distribution). Hoque and Rahman (2006) showed that the Coriolis force dominated the long waves. From the above discussion, it is clear that long waves have major effects that should be accounted in our research. Therefore, the motivation of this chapter is to gain experience on long waves, losses of lives and damages of properties to the coastal area of Bangladesh.

1.2 Long waves

Waves propagating in shallow water are often called long waves. Mathematically, it can be defined as $\dfrac{h}{L} << \dfrac{1}{20}$ where h and L represent the water depth and wave-length, respectively. Tidal waves, tsunamis, storm surges and other waves with extremely long periods and wavelengths are the examples of long waves or shallow water waves.
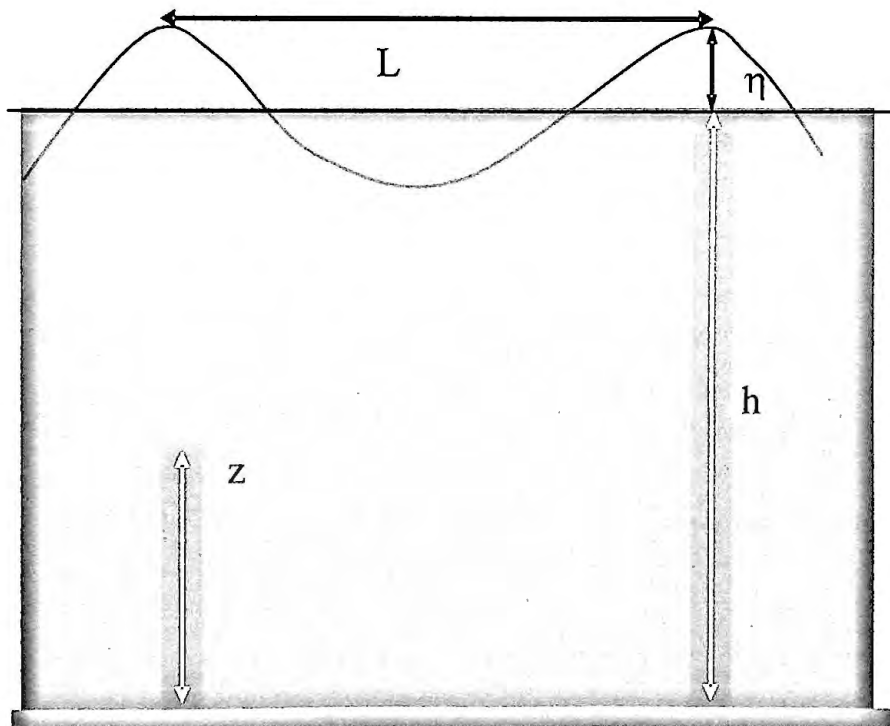
Figure 1.2: Definition sketch of long waves.

1.2.1 Tidal waves

Tides are periodic rises and falls of large bodies of water. It is caused by the gravitational interaction between the earth and the moon. Since the moon passes overhead about an hour later each day, it was long suspected that the moon was associated with tides. The gravitational attraction of the moon causes the oceans to bulge out in the direction of the moon. Another bulge occurs on the opposite side, since the earth is also being pulled toward the moon (and away from the water on the far side). Since the earth is rotating while this is happening, two tides occur each day. A water molecule in the ocean is attracted gravitationally by the earth, but it also experiences a much smaller gravitational attraction from the moon. But this gravitational attraction of the moon is not limited to the water molecules; in fact, the moon exerts a gravitational force on every object on and in the earth. Tides occur because the earth is a body of finite extent and these forces are not uniform. Some parts of the earth are closer to the moon than other parts, and since the gravitational force drops off as the inverse square distance, those parts experience a larger gravitational tug from the moon than parts that are further away.
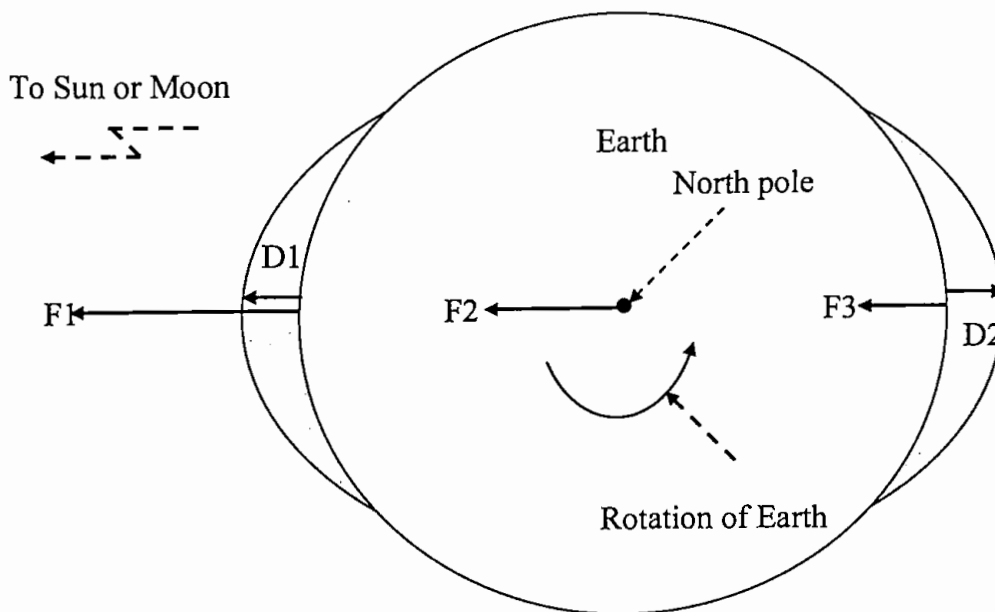
Figure 1.3: Envelope of tide generating forces (After S. D. Hicks, 2006)

In this situation, the differential forces act on the body (the earth in this example). The effect of differential forces on a body is to distort the body. The body of the earth is rather rigid, so such distortion effects are small but finite. However, the fluid in the earth's oceans is much more easily deformed and this leads to significant tidal effects. In figure 1.3, at F_2, the center of mass of the earth, the gravitational attraction must be a value to keep the earth in its orbit around the sun. At F_1, a point on the side of the earth facing the sun, the gravitational force is greater than at the center. At F_3, a point on the side on the earth away from the sun, the gravitational force is less than at the center. Quantitatively, the tide-generating forces are the differences between the gravitational attraction at the center of the earth and the gravitational attractions at the points of interest, as altered by distances from the sun.

1.2.2 Tsunami

Tsunami is a Japanese word represented by two characters: "tsu" and "nami". The character "tsu" means harbor, and the character "nami" means wave. So the word "tsunami" means "harbor wave", because tsunamis cause little or no visible effect in deep sea, and often Japanese fishermen would be out at sea fishing in deep sea when a tsunami came, and in the evening they came home and found their home or village devastated by the tsunami, and thus they theorized that tsunamis only happen in harbors and elsewhere close inshore.

Tsunami is a series of waves of extremely long wave length and long period generated in a body of water by an impulsive disturbance that displaces the water. Tsunamis are primarily associated with earthquakes in oceanic and coastal regions. Also landslides, volcanic eruptions and large meteorite impacts all have the potential to generate a tsunami. Tsunamis can be generated when the sea floor abruptly deforms and vertically displaces the overlying water. Such large vertical movements of the earth's crust can occur at plate boundaries. The effects of a tsunami can range from unnoticeable to devastating. Figure 1.4 shows the recent tsunami at Japan that causes the great loss of lives and properties.
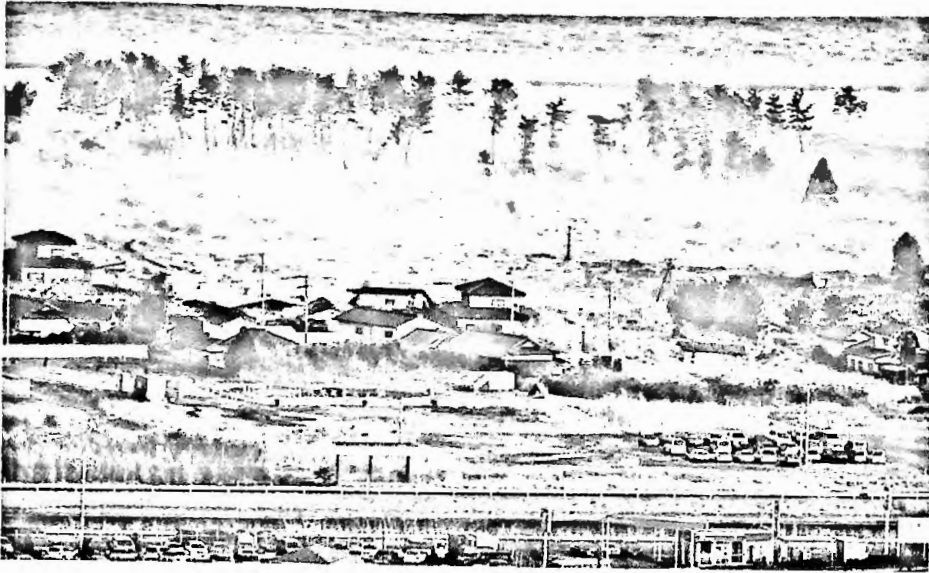
Figure 1.4: Photo of tsunami in Japan, 2011 (Internet).

1.2.3 Cyclone and cyclone-induced storm surge

Cyclones develop over warm seas near the equator. Air heated by the sun rises very swiftly, which creates areas of very low pressure. As the warm air rises, it becomes loaded with moisture which condenses into massive thunderclouds. Cool air rushes in to fill the void that is left, but because of the constant turning of the earth on its axis, the air is bent inwards and then spirals upwards with great force. The swirling winds rotate faster and faster, forming a huge circle which can be up to 2,000 km across. The centre of the storm is a calm and cloudless which is called the eye, where there is no rain, and the winds are fairly light. When warm air rises from the seas and condenses into clouds, massive amounts of heat are released. The result of this mixture of heat and moisture is often a collection of thunderstorms, from which a tropical storm can develop (Fig. 1.5).

A raising or a lowering of sea level produced by wind and by changes in atmospheric pressure over the sea associated with a storm is known as a storm surge (Fig. 1.6). The atmospheric pressure force usually acts in a statical sense; its dynamic contribution being quite negligible (Heaps, 1967; Prandle, 1975; Ali, 1980a).

Figure 1.5: Photo of cyclone-induced storm surge

The amplitude of the surge depends directly on the strength of the wind. Since wind can not produce a strong motion in deep water, a cyclone in deep water can not generate a high surge. As the cyclone moves to shallower water near the coast, surge begins to amplify. The water being shallow, it is easier for stronger wind to stir almost the whole depth of water and pile them up against the coast by its onshore component. According to the definition a storm surge can be either positive or negative. A negative surge is defined as the fall of water surface below the mean sea level. It occurs on the left hand side of a cyclone where the wind is in the off-shore direction A positive surge is obtained on the right hand side of the cyclone due to the onshore component of wind. A storm surge is sometimes divided into three categories: forerunner, surge and resurgence (Fig. 1.7). The Bay of Bengal is the major vulnerable area of storm surges.
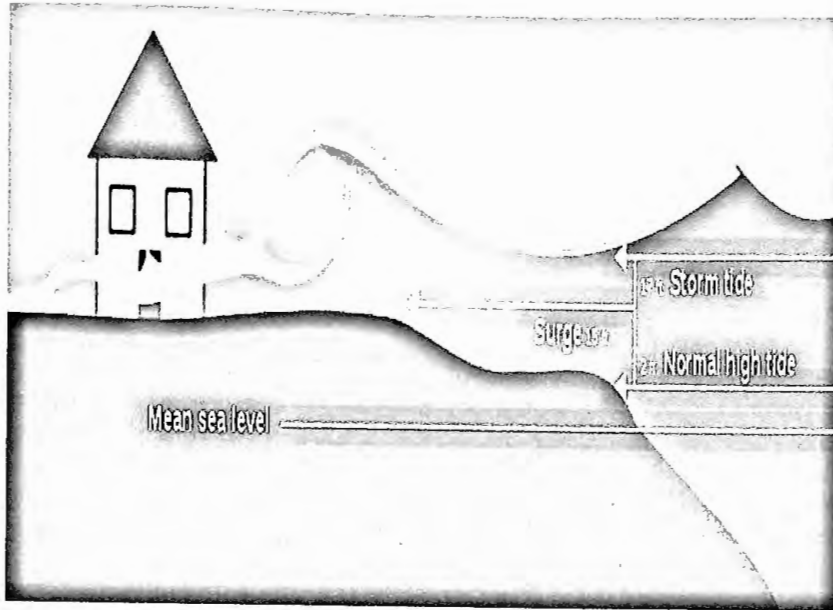
Figure 1.6: Sketch of storm surge (internet)

Bangladesh is low-lying country with the Ganges-Brahmaputra-Meghna river system on one side, and tidal and cyclonic activity from the Bay of Bengal on the other side (Fig. 1.1).
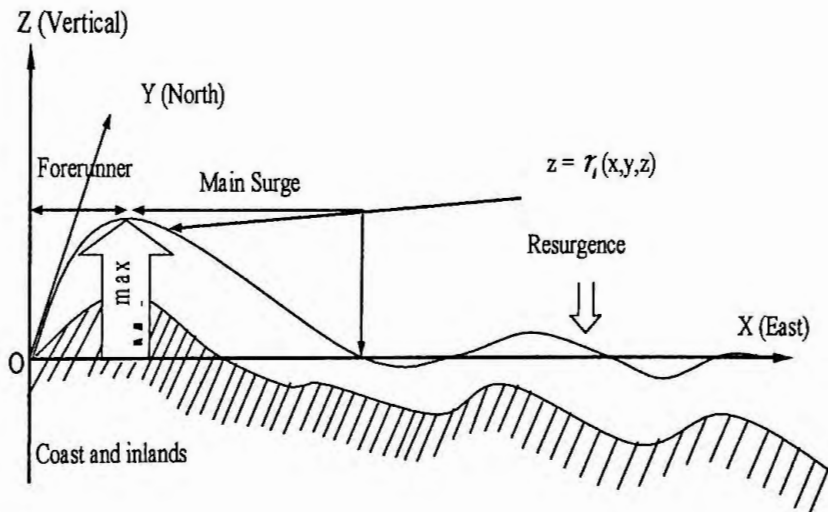
Figure 1.7: Stages of storm surge.

The Sunderban, the world's largest mangrove forest in the southern part of Bangladesh plays a pivotal role in mitigating the storm's ferocity. Table 1.1 shows the list of the most destructive cyclone-induced storm surges that hit Bangladesh and the surrounding area (Karim, 2006). On the basis of the cyclone April, 1991 storm surge and the cyclone SIDR of 2007, Bangladesh Government has taken a massive project of mangrove plantations to reduce the impact of storm surges and to stabilize sediments.

Table 1.1: Some major cyclones induced storm surges in Bangladesh (Internet)

Year	Wind speed (km/h)	Storm surge (m)	Central pressure (mb)	Human death (no.)	Cattle death (no.)	Damage of forest (ha)	Financial loss million (USD)
1970	222	10.6	950	500,000	280,000	--	86
1985	154	3 ~ 5	--	11,069	135,033	--	--
1991	225	5 ~ 8	898	150,000	70,000	--	1780
2007	220	3 ~ 4	944	10,000	107,923	3,500	480
2008	110	--	968	8000	--	--	552

1.2.4 Track of tropical cyclones

Bangladesh suffers from devastating tropical cyclones and cyclonic storm surges frequently. When cyclones make landfall, the northern portion of the Bay of Bengal causes storm surge. During the period from 1960 to 2009, twenty seven (27) cyclones hit the coast of Bangladesh. Tracks of major cyclones crossed Bangladesh coast during in the 20th century is shown in Fig. (1.8). Cyclone "SIDR" was one of the 10 strongest cyclones to hit Bangladesh between 1876 and 2007. It was born in Bay of Bengal on 11th, November, 2007 and intensified into a category 4 storm system (on the Saffir-Simpson Scale) with peak sustained winds of up to 215 km/h (135 mp/h) (peaking at 260 km/hour).
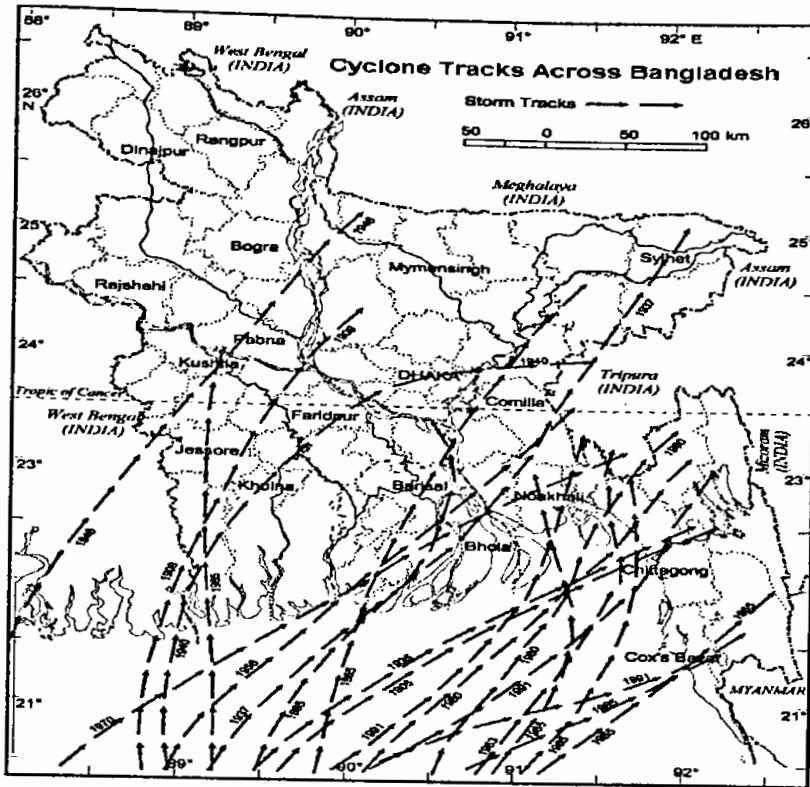
Figure 1.8: Tracks of major cyclones crossed Bangladesh coast.

The cyclone made landfall in Bangladesh in the evening of November 15, 2007. SIDR and its surge resulted in thousands of deaths and massive destruction of coastal communities. The actual path of cyclone SIDR is shown in Fig. (1.9). The cyclone "AILA", crossed the coast of west Bengal-Khulna (Bangladesh) coast near sagar island of India and lay centered at west Bengal and adjoining western part of Bangladesh. Late on 21 May 2009, the joint typhoon warning center reported that a tropical disturbance had persisted about 950 kilometers to the south of Kolkata and had developed within the southwest monsoon. During 22 May 2009, the disturbance developed as a depression and slowly intensify as a deep depression to the next day. AILA became a severe cyclonic storm at 06UTC on May 25 and made landfall at its peak intensity. The cyclone April, 1991 struck the coastal region of Bangladesh causing a massive storm surge and widespread flooding.
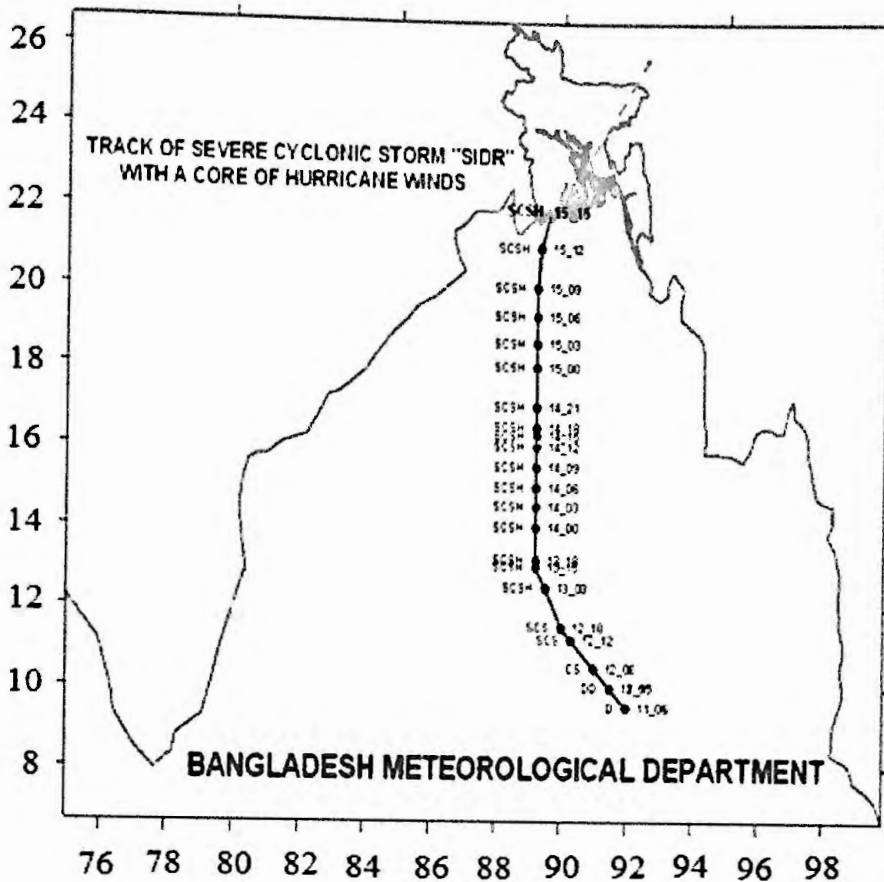
Figure 1.9: Track of cyclone SIDR, 2007 (BMD).

Although cyclones frequently hit in this region, this cyclone was one of the strongest cyclones in the history of Bangladesh. The 260 km/hr wind speed caused more than 6 meter high storm surge that flooded a large area of the coastal region of the country. Due to the lackness of the warning system at least 138,000 people were killed and damage was estimated $1.5 billion.

1.3 Climate change and sea-level rise

Climate change refers to the increase in global mean temperature leading to melting of sea ice and subsequent sea-level rise. According to the Inter-governmental Panel on Climate Change (IPCC, 2007), a rising sea level would have a wide range of impacts on coastal environments and infrastructures with storm surge. There is a high level of uncertainty about how much sea-level rise we can expect for the 21st Century. In 2007, assessment reports (IPCC) has estimated between 18-59cm of sea-

11

level rise and up to 30% of coastal wetlands to be lost. As sea level continues to rise, more low-lying coastal regions (e.g. Bangladesh) in developing countries will be affected by coastal flooding and coastline erosion. As a developing country, Bangladesh is too poor to be able to adapt to such a rise in sea level. In fact, many of the nations that are most vulnerable to sea-level rise do not have the resources for the necessary adaptation.

1.4 Protection of cyclone-induced storm surge

Surges associated with tropical storms often lash the coastal region of Bangladesh. The inundation that results due to the surges has caused the loss of many lives and properties. It is well known phenomenon that during storm events, wave breaking with extensive air bubble entrainment occurs in the shallow water region and these air bubbles can change the dynamical processes in the sea. Particularly, we believe that air bubbles may have a contribution in changing water levels and wave velocity during a storm period. So, it is our intension to develop a mathematical model based on air bubble effects that will helpful to the coastal community.

1.5 Data input of the storm surge model

Having good knowledge of the input parameters and their role in the surge development is very important before developing any technique for forecasting surges in the Bay of Bengal. The input parameters include the oceanographic and hydrographic data, meteorological input (the satellite derived storm characteristics), hydrological parameters, basin characteristics and coastal geometry, wind stress and sea bed friction and information about the astronomical tides. In many cases these parameters strongly influence the surge development. These data inputs are briefly discussed below (R. A. Devendra, 1982).

1.5.1 Oceanographic and hydrographic data

The oceanographic and hydrographic data includes bathymetry, astronomical tides and inshore currents in closed regions. Accurate bathymetry maps are needed for

improved prediction due to the shallowness of the northern Bay of Bengal and the consequent large bottom friction. In general, we need accurate bathymetric maps out to a depth of 100 metres, at approximate intervals of 3 metres upto the 30 metre contour. The another kind of rise of sea level which occurs as a result of the predictical movements of the celestial bodies relative to the earth are astronomical tides.

1.5.2 Meteorological input

This is mainly concerned with the characteristics of the tropical storm. The main characteristics required are the pressure drop, maximum sustained winds, the radius of maximum winds, surface wind distribution, vector motion of the storm, point of landfall and duration of the storm.

1.5.3. Hydrological input

The main hydrological inputs are i) river discharge in the sea and ii) rainfall distribution. As the worlds largest river systems, Ganga-Brahmaputra-Meghna, joined, the discharge of fresh water carried by the rivers is very important to modify the surge simulation in the Bay of Bengal. And the dynamic effect of these inlets and estuaries is the potentially deep inland penetration of surge origination in the sea.

1.5.4 Basin characteristics and coastal geometry

The location of the highest surge depends predominantly on the coastal geometry of the basin. Dube *et al* (1982) suggests that the curving coasts not only shift the peak surge position but also affect its height. Storm blowing straight into it may funnel the water toward the north because of the north and northward converging nature of the Bay of Bengal. Convergence then leads to the pilling up of a strong surge in that area (Proudman, 1955), whereas it may affect the sea level only slightly on a straight part of the coast, where the water can escape sideways.

1.5.5 Surface and Bottom stress

The atmosphere transfers energy to the ocean through normal and tangential stresses on the sea surface, which are generated by pressure gradients and a vertical wind profile. The formulation of surface stress is usually in the form of quadratic law. The surface and bottom friction may be comparable in the case of strong winds (exceeding 10 ms^{-1}) and strong currents (exceeding 1 ms^{-1}). Sea bed friction is also formulated in terms of a quadratic law, but the data is not available on the appropriate drag coefficients.

1.6 Methods of storm surge prediction

The various methods used for storm surge prediction are given below:

1.6.1 Empirical methods

Empirical formulas have been devised for many coastal regions of the world by correlating the sea surface elevation with sea-level pressure, the strength and direction of the prevailing wind (e.g Miazaki, 1957; Isozaki, 1970; Cheng, 1967; Conner et al., 1957 etc.). Miazaki (1957) and Isozaki (1970) made the empirical formula for the coastal region of Japan and Cheng (1967) made the prediction rule for the coastal region of Hongkong. Conner et al. (1957) designed a simple empirical model to forecast surge along the coast of Mexico. Chowdhury and Ali (1974) developed empirical methods for forecasting storm surges in the Bay of Bengal. These methods have not been found to be much useful in the absence of sufficiently large series of accurate observation.

1.6.2 Analytical methods

The analytical method is the solution of hydrodynamic equations under some assumptions. Due to some non-linear part of these differential equations the mathematical theory is very limited. An analytical solution of the general equations is not possible without making major simplifying assumptions in which many important parameters may have to be dropped. Paul Glaister (1988) solved analytically the

shallow water equations representing the motion in the sea. The assumptions usually made for analytical solution are:

i)   The effect of earth's rotation is dropped in many cases to simplify the equations.

ii)   The wind field associated with the cyclone is assumed to be uniform and steady, which is not the case in reality.

iii) Frictional effects, which play a significant role in shallow waters, are dropped in many analytical models.

iv)   Non-linearity arising in the acceleration terms is dropped and the surge is described by linear equations with time-independent coefficients.

v)   Finally, the sea is considered as a channel of uniform depth with straight coastal boundaries. Variable depths and complicated coastal boundaries are difficult to handle theoretically, because the equations will no longer have constant coefficients.

1.6.3 Numerical method

The best technique for the storm surge prediction is the numerical method. The numerical method is the solution of the hydrodynamic equations at a discrete set of points in space at discrete instant of time. This method is also applicable when the forces and the boundary conditions are described by very complicated functions, as is almost always the case in reality. Numerical modeling of storm surges in the Bay of Bengal and Arabean sea was pioneered by Das (1972). He conducted a numerical experiment and computed the surge generated by an idealized cyclone striking the coast of Bangladesh.

1.7 Conclusions

In this chapter, it has been attempted only to explore the characteristic and ferocity of different type of natural disaster. Furthermore, it has also been focused the protective role of air bubbles against cyclone induced storm surge.

Chapter 2

Long Wave Equations

Summary

This chapter is concerned about the long wave equations and its various consequences based on air bubble effects. Due to air bubble entrainment, water becomes two phases flow and it will be complicated. To investigate each phase, an averaging technique is used for developing long wave equations. Result shows that there is a correlation between the sudden reductions of wave height and entrained of air bubbles. Moreover, it is also found that the energy dissipation occurs very short way in plunging breakers comparatively to spilling breakers.

2.1 Introduction

When a cyclone moves to shallower water near the coast, surge begins to unstable and finally it breaks. So wave breaking in the shallow region is a regular and fascinating phenomenon for coastal engineering. It is believed that the sloping bottom causes the breaking process; where a large amount of air bubbles enter into water in the surf zone, resulting in complicated flow field of air-water. Air bubbles entrainment by breaking waves destroy the original flow structure and dissipate wave energy. Some part of wave energy may transfer to the entrained air bubbles and dissipate with the bubble escaping at the free surface.

Sevral researchers investigated the mechanism of air bubbles and its various properties (e.g. Chanson *et al*, 2002; Fuhrboter, 1970, Horikawa and Kuo, 1966; Hoque, 2002; Hoque and Aoki, 2008). Chanson *et al* (2002) suggested that wave breaking near the coastline associated with significant sediment transport and resulting flow becomes in three phases: air (gas), water (liquid), and sediment (solid). Fuhrboter (1970) discussed the sudden reduction of wave height and wave energy

inside the surf zone by the entrained air bubbles into water. Horikawa and Kau (1996) proposed that this entrained air bubbles are responsible for dissipating wave energy, especially at initial stages.

From the physical observations and satellite images, we can also see that water becomes white due to cyclone-induced storm surge both in deep water and shallow water. But studies of air entrainment in long waves are limited yet. So the aim of this chapter is to develop the long wave equations in terms of air bubble effects.

2.2 Basic assumption

2.2.1 A simple phenomenon

The following sketch (Fig. 2.1) represents the simple phenomena of air bubble entrainment.
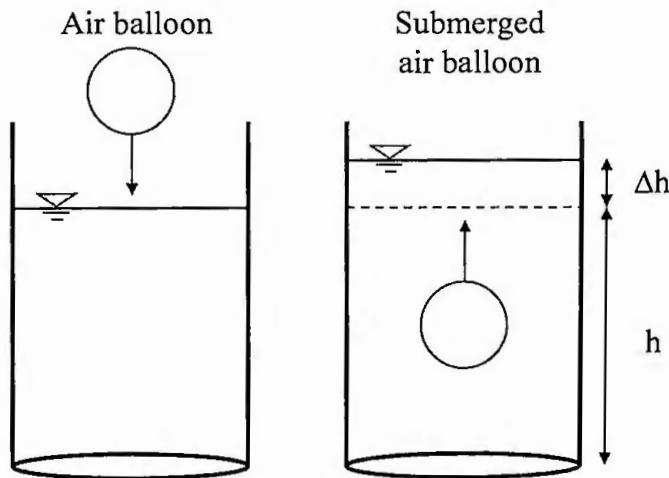
Figure 2.1: Sketch of air bubble entrainment.

If an air balloon inserts into water then water level rises Δh above the initial water depth h. This shows that the potential energy will be increased and after a certain time air bubble will be detrained. That means, air bubble will work as an agent of energy transformation. This assumption might be helpful to investigate the surf zone air bubbles.

2.2.2 Distribution of void fraction in the surf zone

Distribution of void fraction in the vertical direction is considered that is proposed by Wu (1981a) and Hoque (2002):

$$C(z) = C_0 \, \exp(k_1 z) \tag{2.1}$$

where C (z) is the part of the volume locally occupied by bubbles per unit width (time-averaged concentration), k_1 is a decay parameter characterizing vertical distribution of air bubbles and C_0 denotes the reference concentration at the mean water surface $z = 0$.

The following boundary conditions are automatically satisfied:

C $(z) = C_0$ at the surface $z = 0$

and

C $(z) \rightarrow 0$, for $z \rightarrow -\infty$
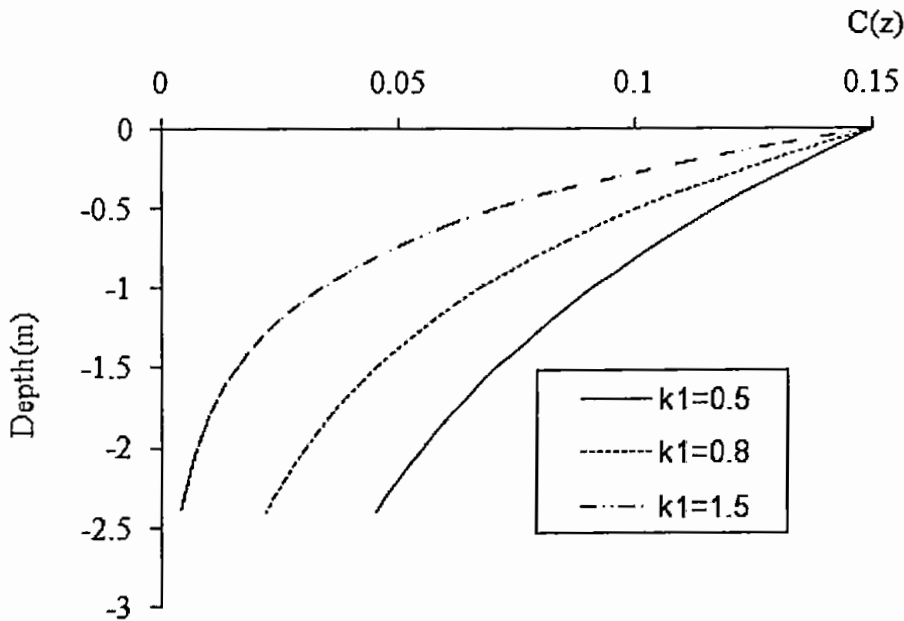
Figure 2.2: Vertical distributions of void fraction by Eq. (2.1) ($C_0 = 0.15$).

Figure 2.2 shows how the mathematical model predicts the vertical distribution of void fraction due to the wave breaking. Significant decay can be seen in void fraction

profiles with increasing k_1 for fixed reference void fraction C_0. The total volume of entrained air into water per unit width is defined as

$$\Delta h = \int_{h-\Delta h}^{\eta} C(z)dz \tag{2.2}$$

Equation (2.2) becomes with the help of Eq. (2.1) as

$$\Delta h = \frac{C_0}{k_1} \frac{1-e^{-k_1 h}}{1-C_0 e^{-k_1 h}} \tag{2.3}$$

2.2.3 Averaging procedure

To calculate the behavior of every single bubble in the bubble cloud the averaging procedure proposed by Hoque (2002) has been used.

The following wave parameters were derived by Hoque (2002) for air-water mixture:

$$u = u_w \tag{2.4a}$$

$$w = w_w + C w_r \tag{2.4b}$$

$$p = p_w \tag{2.4c}$$

$$\rho = (1-C)\, \rho_w \tag{2.4d}$$

where, subscript 'w' and w_r denotes the water and rise velocity of bubbles respectively. Moreover, u, w, p and ρ represent the average horizontal velocity, vertical velocity, pressure and density respectively.

2.3 Wave energy for long waves

The energy in wave is an important to the understanding of several phenomena including the generation of waves by wind, the changes that occur as a wave propagates from deep water to shallow water and the spectral characteristics of waves. The total energy in a wave is the sum of its kinetic energy manifest by the water particle motion and its potential energy owing to the water surface displacement from the still condition. The definitions of potential energy, kinetic energy and energy flux are given below in terms of air bubble effects.
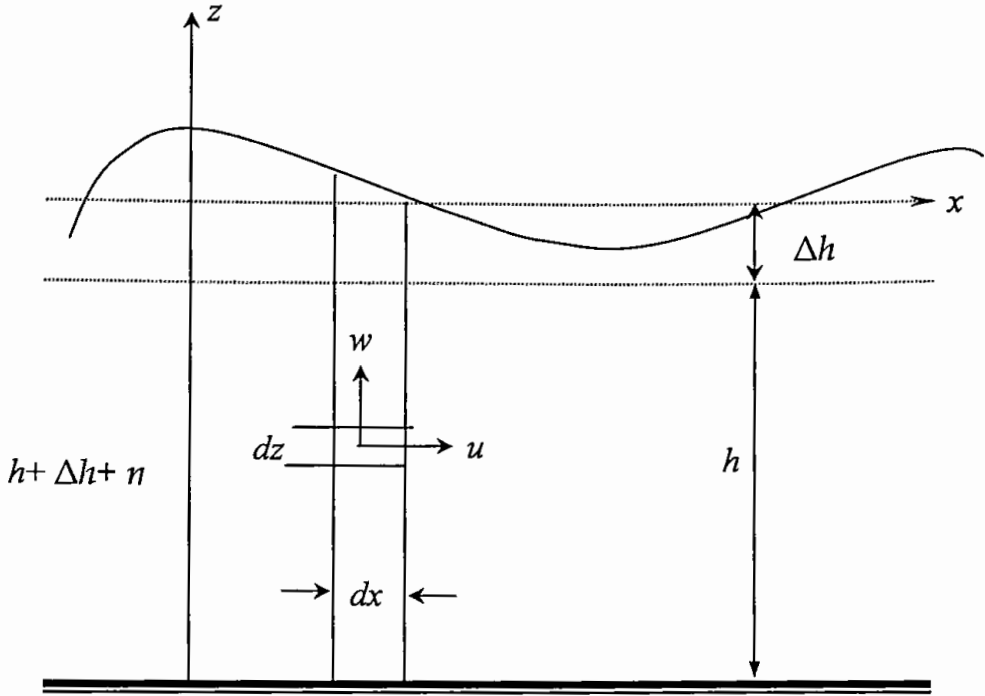
Figure 2.3: Two dimensional wave structure.

2.3.1 Potential energy

Potential energy of the wave system is defined as the work done to deform a horizontal free surface into disturbed state. The increase in potential energy *d(PE)* due to air bubbles is define as the difference between the potential energy of water with air bubbles and without air bubbles in presence of long waves, i.e.

$$d(PE) = \overline{\int_{-h-\Delta h}^{\eta} \rho_w (1 - C_0) gz\,dz} - \left\{ \overline{\int_{-h-\Delta h}^{-\Delta h} \rho_w gz\,dz + \int_0^{\eta} \rho_w gz\,dz} \right\}$$

The above equation can be simplified in dimensionless form as

$$P = \frac{d(PE)}{\rho_w g H^2 / 16} = C_0 \left[-1 + 16 \left\{ \frac{(1 - e^{-k_1 h})}{(k_1 H)^2} - \frac{(1 - C_0)}{(k_1 H)^2} k_1 h \frac{e^{-k_1 h}}{(1 - C_0 e^{-k_1 h})} \right\} \right] \quad (2.5)$$
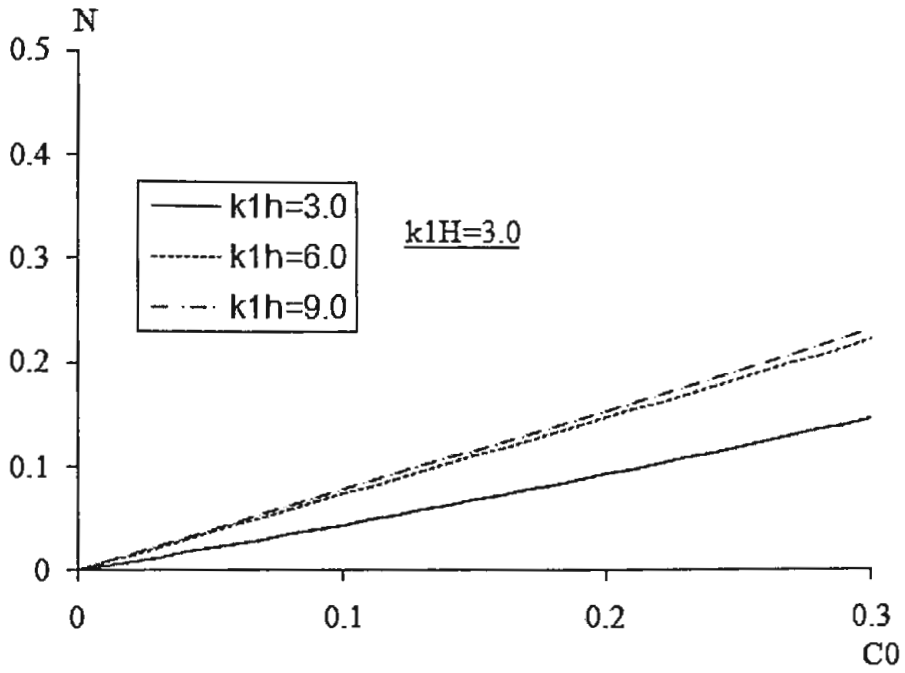
(a)
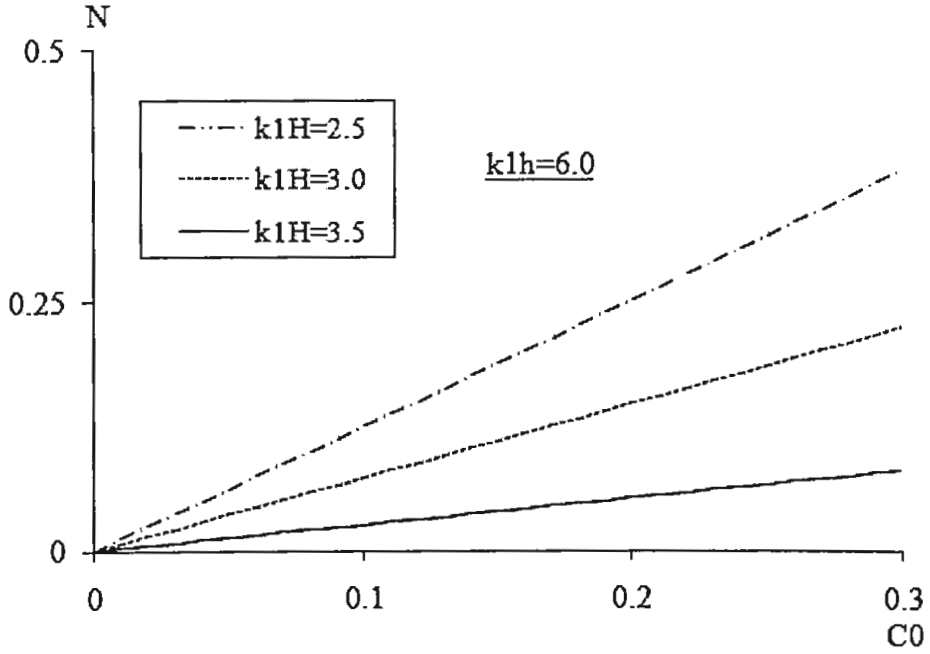
(b)
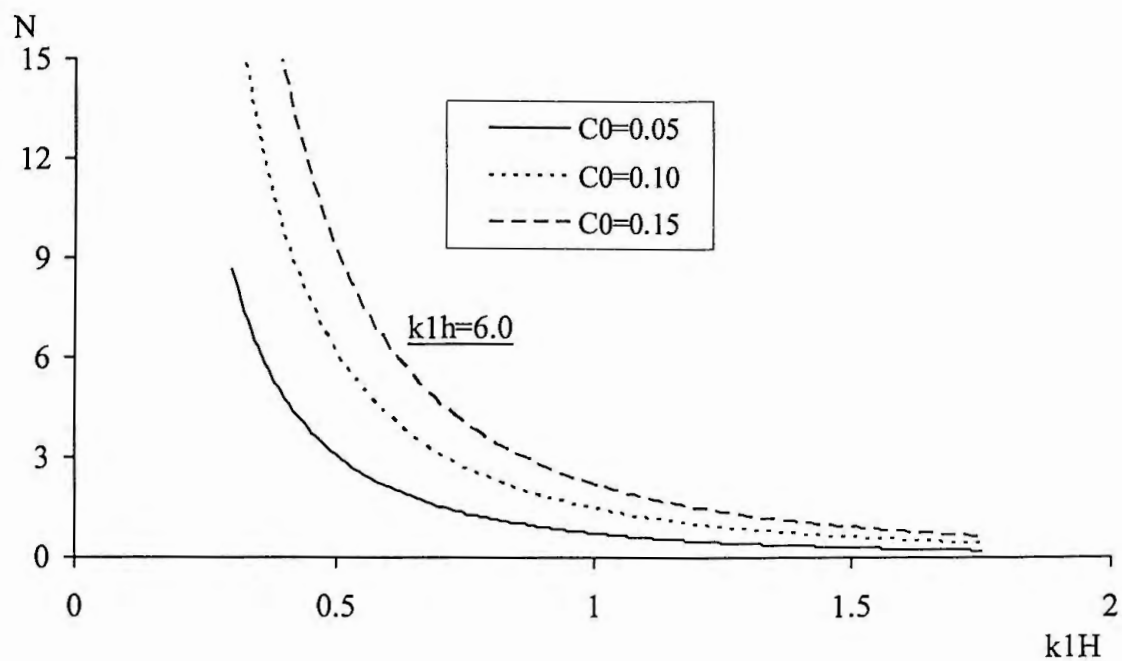
(c)
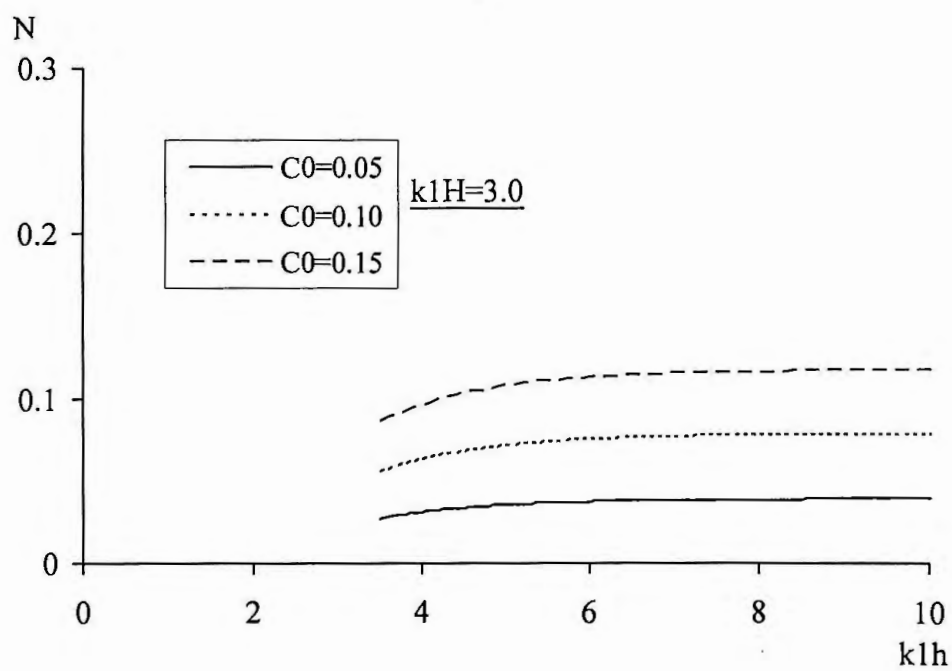
(d)

Figure 2.4: Dimensionless Potential energy varies with C_0, k_1h and k_1H.

Figure 2.4 illustrates the relationship among dimensionless potential energy and C_0, k_1h and k_1H that is calculated from Eq. (2.5). The dimensionless potential energy P increases as C_0 increases for different values of k_1h and k_1H (Fig. 2.4). Figure 2.4 (c) shows a significant change of N for $k_1H<1.5$ whereas, it becomes flatten with k_1h for different values of C_0.

2.3.2 Kinetic energy

The kinetic energy is due to the moving water particles; the average kinetic energy per unit surface area must be integrated over depth and averaged over one wave period. The appropriate expression of kinetic energy can be written as

$$KE = \frac{1}{T} \int_0^T \int_{-h-\Delta h}^0 \frac{1}{2} \rho u_w{}^2 dz dt$$

$$= \frac{1}{T} \int_0^T \int_{-h-\Delta h}^{\eta} \frac{1}{2} \rho_w (1 - C_0 e^{k_1 z}) \frac{\pi^2 H^2}{T^2} \frac{\cosh^2 k(h+z)}{\sinh^2 kh} \cos^2 (kx - \sigma t) dz dt$$

Simplifying the above expression, we have the kinetic energy in dimensionless form as

$$Q = \frac{KE}{\rho_w g H^2 / 16} = \frac{(kh)^2}{2\sinh^2 kh} \left[\frac{\sinh 2kh + 2kh}{2kh} + \frac{C_0}{k_1 h}(1 - e^{-k_1 h}) + C_0 \left(\frac{k_1 h(\cosh 2kh - e^{-k_1 h}) - 2kh \sinh 2kh}{(k_1 h)^2 - 4(kh)^2} \right) \right] \tag{2.6}$$

(a)

(b)

24
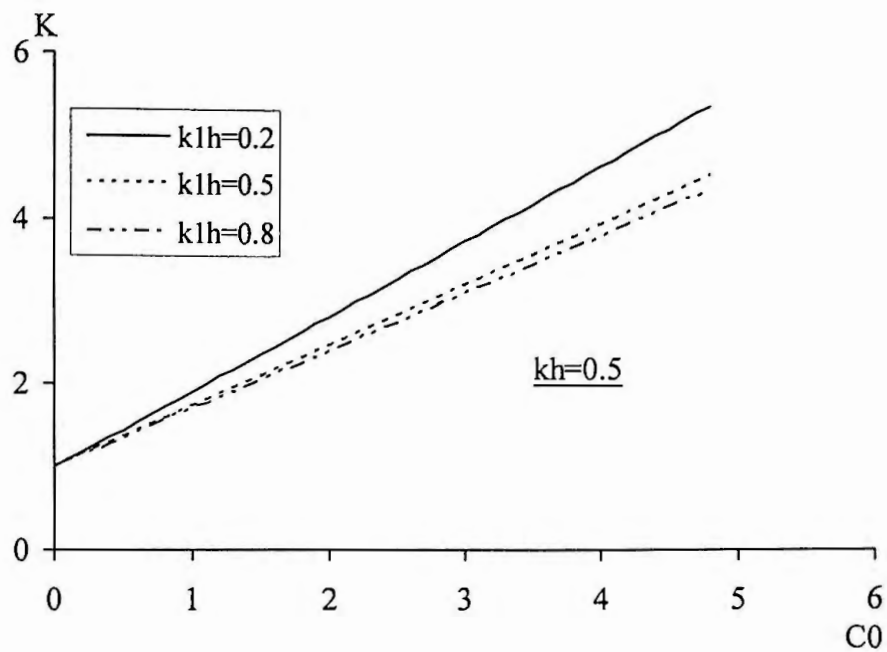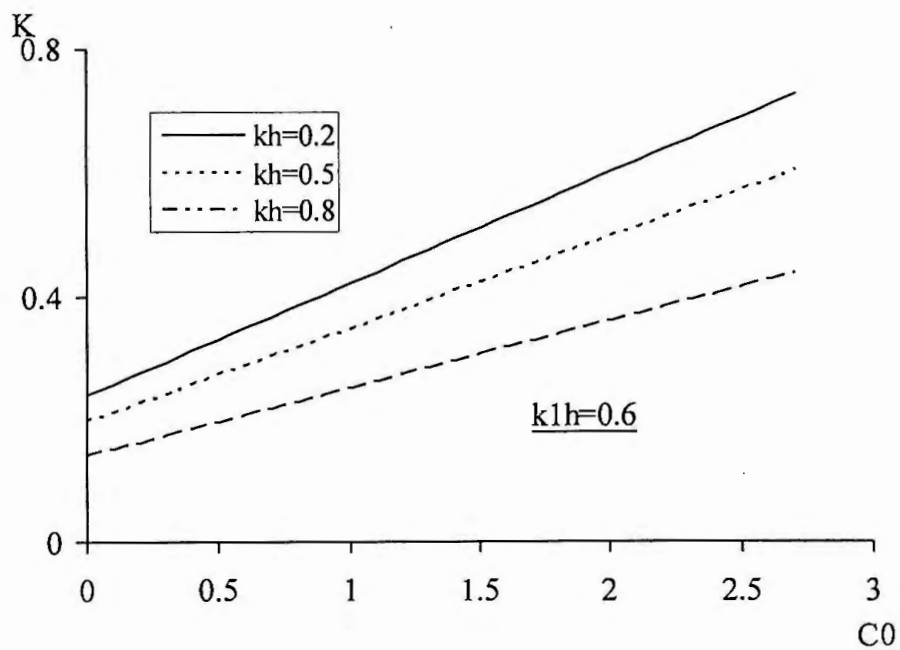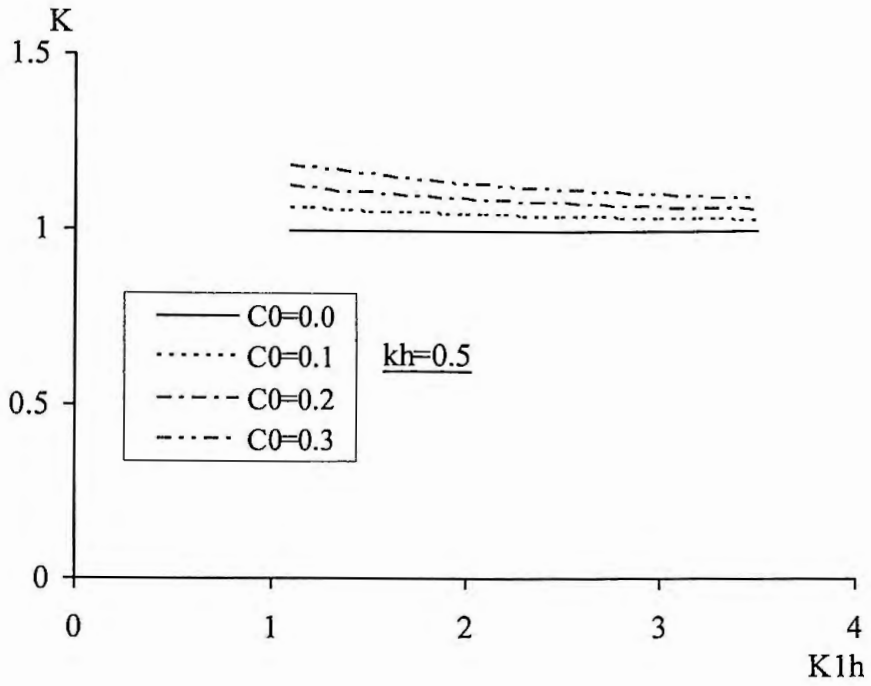
(c)
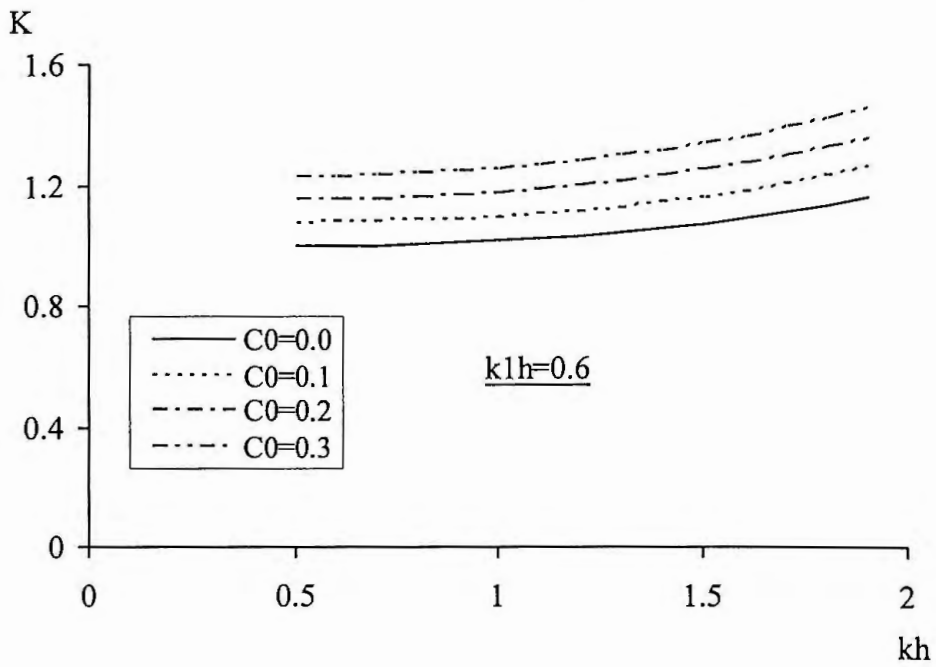
(d)

Figure 2.5: Dimensionless kinetic energy is a function of C_0, k_1h and k_1H.

Figure 2.5 shows the dimensionless kinetic energy obtained from Eq. (2.6). In the presence of water waves the kinetic energy increases with the increasing of air bubble (Fig. 2.5 (a) and 2.5 (b)). It can also be seen (Fig. 2.5 (c)) that the effect of air bubbles is almost constant for $kh > 1.2$ and this range may be deep-water wave conditions.

2. 4 Energy dissipation

2.4.1 Static energy

When air bubbles entrain into the water, the water level rises by Δh (Fig. 2.1). The excess static energy per unit horizontal area due to entrained air bubbles inside the surf zone can be determined by

$$\Delta SE = SE - SE_0 = \int_{-h-\Delta h}^{0} \rho gz dz - \int_{-h-\Delta h}^{\Delta h} \rho_w gz dz \tag{2.7}$$

where, ρ and ρ_w represent the density of air-water mixture and water density respectively. Inserting the value of ρ from Eq. (2.4d) into Eq. (2.7), we have

$$(dE)_{stat} = \int_{-h-\Delta h}^{0} \rho_w (1 - C_0 e^{k_1 z}) gz dz - \int_{-h-\Delta h}^{-\Delta h} \rho_w gz dz \tag{2.8}$$

The first term on the right hand side in Eq. (2.8) can be recognized as total potential energy including air bubble effect and the second term without air bubbles. After simplification the above equation can be written as

$$(dE)_{stat} = \rho_w gh^2 bC_0 \left[\frac{1 - e^{-k_1 h}}{(k_1 h)^2} - \frac{(1-C_0)}{k_1 h} \frac{e^{-k_1 h}}{(1 - C_0 e^{-k_1 h})} \right] dx \tag{2.9}$$

where, dx is the length of the water column.

Inside the surf zone, wave height and energy are reduced suddenly by strong interactions. It is believed that the major part of wave energy is spent by surface interaction. According to the linear wave theory, the local total wave energy within the one wavelength can be expressed as

$$E = \frac{1}{8} \rho_w gLH^2 \tag{2.10}$$

where H, L, b, and ρ_w represent the wave height, wavelength, width and water density respectively.

For a sudden reduction of wave height (dH) inside in Fig. 2.6, the reduced wave energy (dE) can be evaluated by

$$dE = \frac{1}{4}\rho_w gbLHdH \tag{2.11}$$
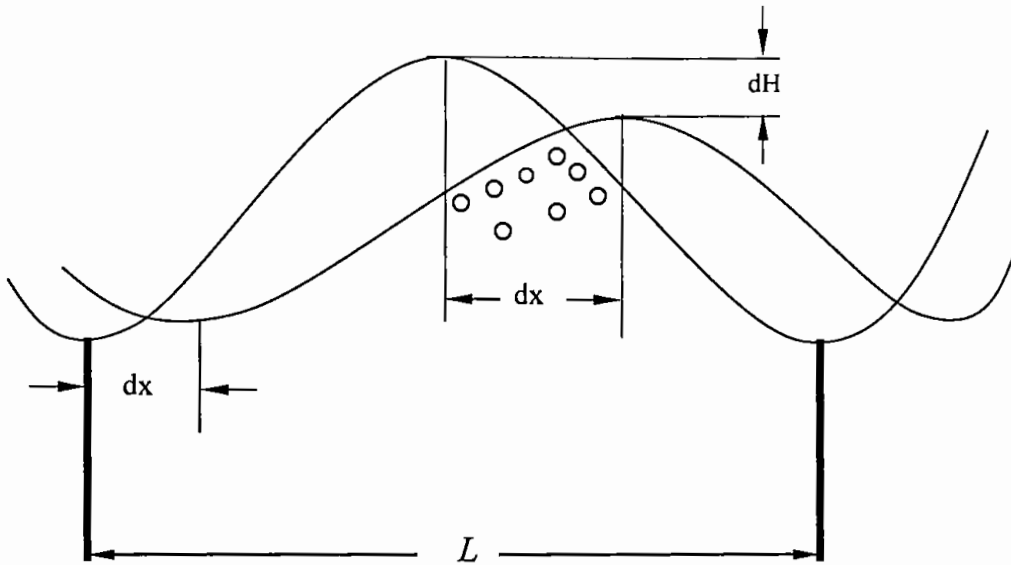
Figure. 2.6: Wave height reduction due to air entrainment.

The wave length L shall be stated to be constant during wave breaking. This loss of energy must be transformed into other sorts of energy, so in turbulent motion and at last into heat by friction. By using the fact that the loss of wave energy is expressed in terms of that of turbulent energy. But before the energy is going into turbulence, there is a transfer mechanism by air entrainment and foam production.

Combining Eqs. (2.11) and (2.9) which give

$$\frac{dH}{dx} = \frac{4h^2 C_0}{LH}\left[\frac{1-e^{-k_1 h}}{(k_1 h)^2} - \frac{(1-C_0)}{k_1 h}\frac{e^{-k_1 h}}{(1-C_0 e^{-k_1 h})}\right] \tag{2.12}$$

This is the differential equation for $H = H(x)$, the wave height inside the surf zone. Eq. (2.12) can be solved for two cases: (a) plunging breaker (b) spilling breaker.

2.5 Solution

In a plunging breaker, the energy is released suddenly into a downwardly directed mass of water. The crest advances faster than the base of the breaker, curls and then descends violently into the wave trough. A considerable amount of air is trapped when this happens and this air escapes explosively behind the wave (Fig. 2.7(a)), throwing water high above the surface. The plunging breaker is characterized by a loud explosive sound.

(a)   (b)

Figure 2.7: Photograph of (a) plunging breaker and (b) spilling breakers.

In a spilling breaker, the energy which the wave has transported over many miles of sea is released gradually over a considerable distance. The wave peaks up until it is very steep but not vertical. Only the topmost portion of the wave curls over and descends on the forward slope of the wave, where it then slides down into the trough. Light foam may wash gently up the shore (Fig. 2.7(b)).

2.5.1 Plunging breaker

For a plunging breaker, in first approximation the depth of aeration h can be considered to be of same order of magnitude as the breaker height H_b and to be constant during the process of breaking. So we have $h \propto H_b =$ constant.

Here integration of Eq. (2.12) gives with $H(x) = H_b$ for $x = 0$ as

$$H = H_b \sqrt{8C_0 \left[\frac{1 - e^{-k_1 H_b}}{(k_1 H_b)^2} - \frac{(1 - C_0)e^{-k_1 H_b}}{k_1 H_b (1 - C_0 e^{-k_1 H_b})} \right] \frac{x}{L} + 1}$$

(2.13)
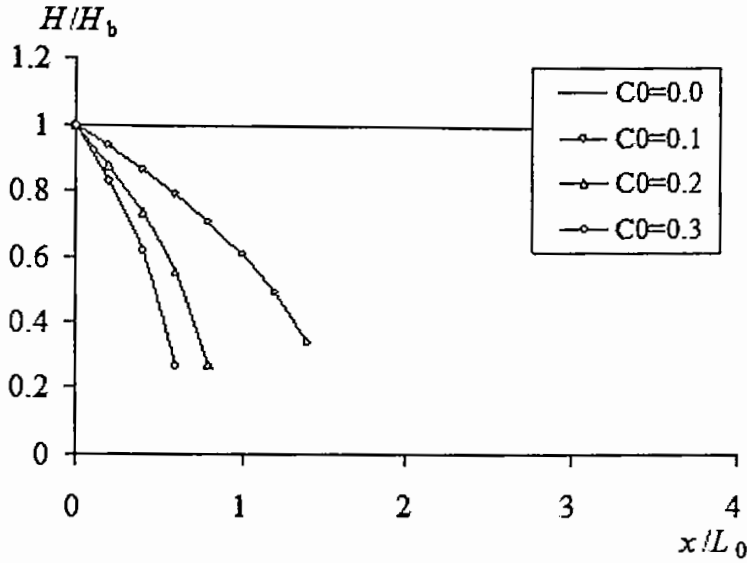
Figure 2.8: Wave height reduction for plunging breaker.

Figure 2.8 shows the variation of wave height as a function of x/L which compares the wave height curves for different C_0 (C_0 = 0.10, 0.20, 0.30) with the exact expression of linear theory. Thus, with the different specification of C_0, a part of wavelength is enough for the total destruction of the wave. The reference void fraction, C_0 was measured about 0.20 for plunging breaker (Hoque, 2002).

2.5.2 Spilling breaker

For a Spilling breaker, the depth of aeration is in a linear relation to the reduction of wave height $H(x)$. So we can consider $h \propto H(x)$. Integrating Eq. (2.12), while noting $H(x) = H_b$ at the breaking point $x = 0$, results in

$$H = H_b \exp\left\{ 4C_0 \left[\frac{1 - e^{-k_1 H_b}}{(k_1 H_b)^2} - \frac{(1 - C_0)e^{-k_1 H_b}}{k_1 H_b (1 - C_0 e^{-k_1 H_b})} \right] \frac{x}{L} \right\}$$

(2.14)
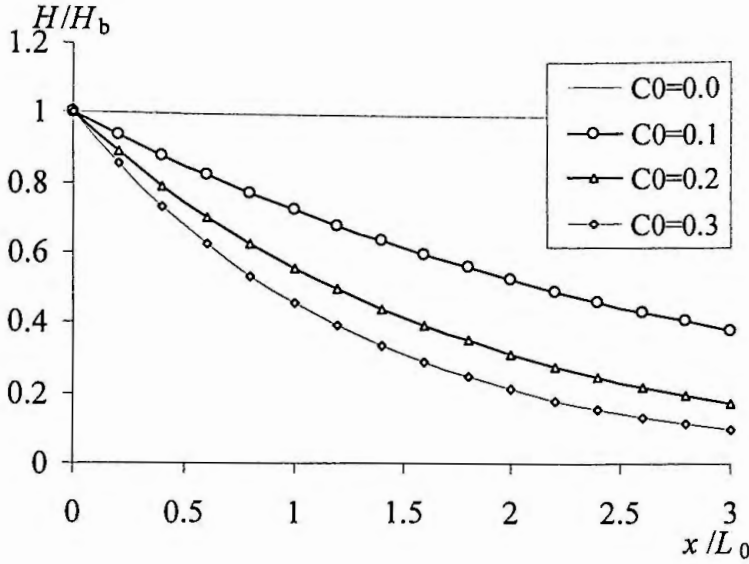
Figure 2.9: Wave height reduction for spilling breaker.

Figure 2.9 shows the variation of wave height as a function of x/L for different values of C_0. Among these various exponential curves, curve for $C_0 = 0.15$ is the best choice, because Hoque (2002) was measured this value near the free surface in the spilling breakers.

2.6 Wave equations

The basic hydrodynamic equations of continuity and momentum for the dynamical process in the sea may be written as

$$\frac{\partial u}{\partial x} + \frac{\partial v}{\partial y} + \frac{\partial w}{\partial z} = 0 \tag{2.15}$$

$$x \text{ com: } \frac{\partial u}{\partial t} + u\frac{\partial u}{\partial x} + v\frac{\partial u}{\partial y} + w\frac{\partial u}{\partial z} - fv = -\frac{1}{\rho}\frac{\partial p}{\partial x} + \frac{1}{\rho}\frac{\partial \tau_x}{\partial z} \tag{2.16}$$

$$y \text{ com: } \frac{\partial v}{\partial t} + u\frac{\partial v}{\partial x} + v\frac{\partial v}{\partial y} + w\frac{\partial v}{\partial z} + fu = -\frac{1}{\rho}\frac{\partial p}{\partial y} + \frac{1}{\rho}\frac{\partial \tau_y}{\partial z} \tag{2.17}$$

$$z \text{ com: } \frac{\partial w}{\partial t} + u\frac{\partial w}{\partial x} + v\frac{\partial w}{\partial y} + w\frac{\partial w}{\partial z} = -\frac{1}{\rho}\frac{\partial p}{\partial z} - g \tag{2.18}$$

where Eq. (2.15) represents the continuity equation and Eqs. (2.16-2.18) represent the components of equation of motion.

30

2.6.1 Boundary conditions

Molecular velocity has been neglected in the above equations. At any boundary, whether it is fixed (bottom) or at free surface (water surface) certain physical conditions must be satisfied by the fluid velocities. The equations describing the surface that constitutes the boundary are the mathematical expression for the kinematic boundary condition. Denoting the wind stress and bottom stress components as (F_S, G_S) and (F_B, G_B) respectively, and the surface pressure as P_a, the boundary conditions become,

$$\left.\begin{array}{l} u = v = w = 0 \\[4pt] (\tau_x, \tau_y) = (F_B, G_B) \\[4pt] u\dfrac{\partial(h+\Delta h)}{\partial x} + v\dfrac{\partial(h+\Delta h)}{\partial y} = -w(-h-\Delta h) \end{array}\right\} \quad \text{at } z = -h - \Delta h \qquad (2.19)$$

$$\left.\begin{array}{l} (\tau_x, \tau_y) = (F_S, G_S) \\[4pt] p = p_a \\[4pt] \dfrac{\partial \eta}{\partial t} + u\dfrac{\partial \eta}{\partial x} + v\dfrac{\partial \eta}{\partial y} = w \end{array}\right\} \quad \text{at } z = \eta \qquad (2.20)$$

Eqs. (2.19) and (2.20) represent the bottom boundary condition and the kinematic surface boundary condition respectively.

In shallow water, it is reasonable to assume that the wave length is large compared to the water depth. With this assumption, it may be shown (Welander, 1961) that Eq. (2.18) reduces to the hydrostatic pressure approximation

$$\frac{\partial p}{\partial z} = -\rho g \qquad (2.21)$$

which on integration gives

$$p = p_a + \rho g(\eta - z) \qquad (2.22)$$

where $p = p_a$ is the atmospheric pressure at the surface.

2.6.2 Continuity equation in terms of air bubbles

By depth integration, Eq. (2.15) can be written as

$$\int_{-h-\Delta h}^{\eta} \left(\frac{\partial u}{\partial x} + \frac{\partial v}{\partial y} + \frac{\partial w}{\partial z} \right) dz = 0$$

or, $\quad \int_{-h-\Delta h}^{\eta} \frac{\partial u}{\partial x} dz + \int_{-h-\Delta h}^{\eta} \frac{\partial v}{\partial y} dz + w(\eta) - w(-h - \Delta h) = 0 \qquad (2.23)$

Using Leibnitz's rule of integration, *KSBC* and *BBC*, Eq.(2.23) become after some manipulation,

$$\frac{\partial [\bar{u}(h + \Delta h + \eta)]}{\partial x} + \frac{\partial [\bar{v}(h + \Delta h + \eta)]}{\partial y} + \frac{\partial \eta}{\partial t} = 0 \qquad (2.24)$$

where, $\bar{u} = \dfrac{1}{h + \Delta h + \eta} \int_{-h-\Delta h}^{\eta} u\, dz$ and $\bar{v} = \dfrac{1}{h + \Delta h + \eta} \int_{-h-\Delta h}^{\eta} v\, dz$ are depth average velocity.

Equation (2.24) is the equation of continuity for long waves in terms of air bubbles effect.

2.6.3 Momentum equation in terms of air bubbles

After simplification, Eq. (2.16) can be written as

$$\frac{\partial u}{\partial t} + \frac{\partial (u^2)}{\partial x} + \frac{\partial (uv)}{\partial y} + \frac{\partial (uw)}{\partial z} - fv = -g\frac{\partial \eta}{\partial x} - \frac{1}{\rho_w(1 - C_0 e^{k_1 z})}\frac{\partial p_a}{\partial x} + \frac{1}{\rho_w(1 - C_0 e^{k_1 z})}\frac{\partial \tau_x}{\partial z}$$

$$(2.25)$$

Integrating Eq. (2.25) vertically and taking the limits from $-h - \Delta h$ to η, we have

$$\int_{-h-\Delta h}^{\eta} \frac{\partial u}{\partial t} dz + \int_{-h-\Delta h}^{\eta} \frac{\partial (u^2)}{\partial x} dz + \int_{-h-\Delta h}^{\eta} \frac{\partial (uv)}{\partial y} dz + \int_{-h-\Delta h}^{\eta} d(uw) - fv \int_{-h-\Delta h}^{\eta} dz = -g\frac{\partial \eta}{\partial x} \int_{-h-\Delta h}^{\eta} dz$$

$$+ \frac{\partial p_a}{\partial x} \int_{-h-\Delta h}^{\eta} \frac{1}{\rho_w(1 - C_0 e^{k_1 z})} dz + \int_{-h-\Delta h}^{\eta} \frac{\partial \tau_x}{\partial z} \frac{dz}{\rho_w(1 - C_0 e^{k_1 z})} \qquad (2.26)$$

Equation (2.26) is based on the assumption that τ_{xx} and τ_{yx} do not depend on z.

If we define,

$$(\bar{u},\bar{v}) = \frac{1}{h+\Delta h+\eta} \int_{-h-\Delta h}^{\eta}(u,v)\,dz \ , \ (\overline{u^2},\overline{v^2}) = \frac{1}{(h+\Delta h+\eta)} \int_{-h-\Delta h}^{\eta}(u^2,v^2)\,dz$$

$$\overline{uv} = \frac{1}{h+\Delta h+\eta} \int_{-h-\Delta h}^{\eta}uv\,dz \ \text{ and } \ B(C_0) = [h+(1+C_0)\eta + \frac{2C_0}{k_1}\frac{1-e^{-k_1 h}}{1-C_0 e^{-k_1 h}}]$$

where the over bars denote the depth average velocity and B is the function of C_0 (air bubble parameter). Using Leibnitz rule of integration and above definitions, Eq. (2.26) can be summarized as

$$\frac{\partial[(h+\Delta h+\eta)\bar{u}]}{\partial t} + \frac{\partial[(h+\Delta h+\eta)\overline{u^2}]}{\partial x} + \frac{\partial[(h+\Delta h+\eta)\overline{uv}]}{\partial y} - f\,\bar{v}(h+\Delta h+\eta) =$$

$$-g(h+\Delta h+\eta)\frac{\partial\eta}{\partial x} + \frac{B(C_0)}{\rho_w}\frac{\partial p_a}{\partial x} + \frac{(F_S - F_B)B(C_0)}{\rho_w(h+\Delta h+\eta)} \tag{2.27}$$

Within the framework of a vertically integrated system, it is impossible to evaluate the terms involving $\overline{u^2}$, $\overline{uv}$ etc. without taking recourse to some assumptions about them. The assumptions and some of the reasons for their justification are briefly discussed below.

$$\overline{u^2} = \overline{(\bar{u}+u')(\bar{u}+u')} = (\bar{u})^2 + \overline{u'u'} \tag{2.28}$$

where u' is the deviation from the depth-averaged value $\bar{u}$ and $\overline{u'} = 0$. The term $\overline{u'u'}$ is appeared due to the shear effect which would become zero for uniform velocity. Some authors (Nihoul, 1975; Johns, 1981) discussed shear effects for long waves. Among them Johns (1981) suggested the value of this term in the ranges

$$0.996 < \left|\overline{u^2}/\bar{u}^2\right| < 1.04 \tag{2.29}$$

for all instant of time. Hence it is usual to make approximations as

$$\left.\begin{array}{l} \overline{u^2} = \bar{u}^2 \\[2mm] \overline{uv} = \bar{u}\bar{v} \\[2mm] \overline{v^2} = \bar{v}^2 \end{array}\right\} \tag{2.30}$$

Additionally, a parameterization of the bottom stress must be made in terms of the depth-averaged current. This is frequently done by conventional quadratic law

$$F_B = \rho_w \, c_f \bar{u} (\bar{u}^2 + \bar{v}^2)^{\frac{1}{2}}$$

$$G_B = \rho_w \, c_f \bar{v} (\bar{u}^2 + \bar{v}^2)^{\frac{1}{2}}$$

(2.31)

where $c_f = 2.6 \times 10^{-3}$ is an empirical bottom friction coefficient.

Substituting the values from Eqs. (2.30) and (2.31) into Eq. (2.27), we (the over bars have been dropped for convenience) have

$$\frac{\partial[(h + \Delta h + \eta)u]}{\partial t} + \frac{\partial[(h + \Delta h + \eta)u^2]}{\partial x} + \frac{\partial[(h + \Delta h + \eta)uv]}{\partial y} - fv(h + \Delta h + \eta) =$$

$$- g(h + \Delta h + \eta)\frac{\partial \eta}{\partial x} + \frac{B(C_0)}{\rho_w}\frac{\partial p_a}{\partial x} + \frac{B(C_0)[F_S - \rho_w c_f u(u^2 + v^2)^{\frac{1}{2}}]}{\rho_w(h + \Delta h + \eta)}$$

(2.32)

This is the equation of motion in x-direction including air bubble effects. Similarly, the equation of motion in y-direction can be written as

$$\frac{\partial[(h + \Delta h + \eta)v]}{\partial t} + \frac{\partial[(h + \Delta h + \eta)vu]}{\partial x} + \frac{\partial[(h + \Delta h + \eta)v^2]}{\partial y} + fu(h + \Delta h + \eta) =$$

$$- g(h + \Delta h + \eta)\frac{\partial \eta}{\partial y} + \frac{B(C_0)}{\rho_w}\frac{\partial p_a}{\partial y} + \frac{B(C_0)[G_S - \rho_w c_f v(u^2 + v^2)^{\frac{1}{2}}]}{\rho_w(h + \Delta h + \eta)}$$

(2.33)

Applying the boundary conditions in Eqs.(2.32) and (2.33) and after some simplifications, we have

$$\frac{\partial u}{\partial t} + u\frac{\partial u}{\partial x} + v\frac{\partial u}{\partial y} - f v = -g\frac{\partial \eta}{\partial x} - \frac{B(C_0)}{\rho_w(h + \Delta h + \eta)}\frac{\partial p_a}{\partial x}$$

$$+ \frac{B(C_0)[F_S - \rho_w c_f u(u^2 + v^2)^{\frac{1}{2}}]}{\rho_w(h + \Delta h + \eta)^2}$$

(2.34)

and

$$\frac{\partial v}{\partial t} + u\frac{\partial v}{\partial x} + v\frac{\partial v}{\partial y} + f\,u = -g\frac{\partial \eta}{\partial y} - \frac{B(C_0)}{\rho_w(h+\Delta h+\eta)}\frac{\partial p_a}{\partial y}$$

$$+ \frac{B(C_0)[G_S - \rho_w c_f v(u^2+v^2)^{\frac{1}{2}}]}{\rho_w(h+\Delta h+\eta)^2} \tag{2.35}$$

Equations (2.34) and (2.35) are the equation of motion in terms of air bubbles in simplified form.

2.7 Conclusions

Based on the air bubble effects, long wave equations and its various consequences were studied and developed. It was observed that air bubbles were significant effects on potential energy and kinetic energy. Furthermore, energy dissipation by entrained air under breaking waves was studied theoretically both in spilling and plunging breakers. Result showed that there was a correlation between the sudden reductions of wave height and entrained air bubbles into water. This theoretical study also provided that in plunging breaker the wave energy was dissipated on a very short way whereas in a spilling breaker this way was of the order of some wave lengths.

Chapter-3

Storm Surge Modeling including Air Bubble Effects

Summary

This chapter highlights the theoretical study of vertically integrated two-dimensional hydrodynamic storm surge models including air bubble effects. The finite difference method is used where the coasts and islands are included in the stair step method. The dynamic effect of pressure gradient outside the storm surge region in the model is found to be negligible in comparison with the dominant effect of wind. Moreover, we have found the significant effects of air bubble on water level elevation during storm surge propagation.

3.1 Introduction

Bangladesh is a land of natural calamities. The Bay of Bengal is one of the regions in the world, which is frequently affected by storm surges associated with tropical cyclones. Statistics show that about 5% of the global tropical cyclones form over the Bay of Bengal (Fig. 3.1). On an average, 5 or 6 storms form in this region every year. Bangladesh is situated at the northern tip of the Bay of Bengal. Long continental shelf, shallow bathymetry, complex coastal geometry with many kinks and islands, and long tidal range between east and west coasts of Bangladesh are well-known features for the highest storm surge and of the longest duration (Fig. 3.2). About 60 % of all deaths due to storm surges have occurred in the low-lying arable coastal areas of the countries bordering Bay of Bengal and the adjoining Arabian Sea (Dube et al., 1997). The great killer cyclones of November 12, 1970 and April 29, 1991, took away lives of 300,000 and 138,882 people from Bangladesh, respectively.
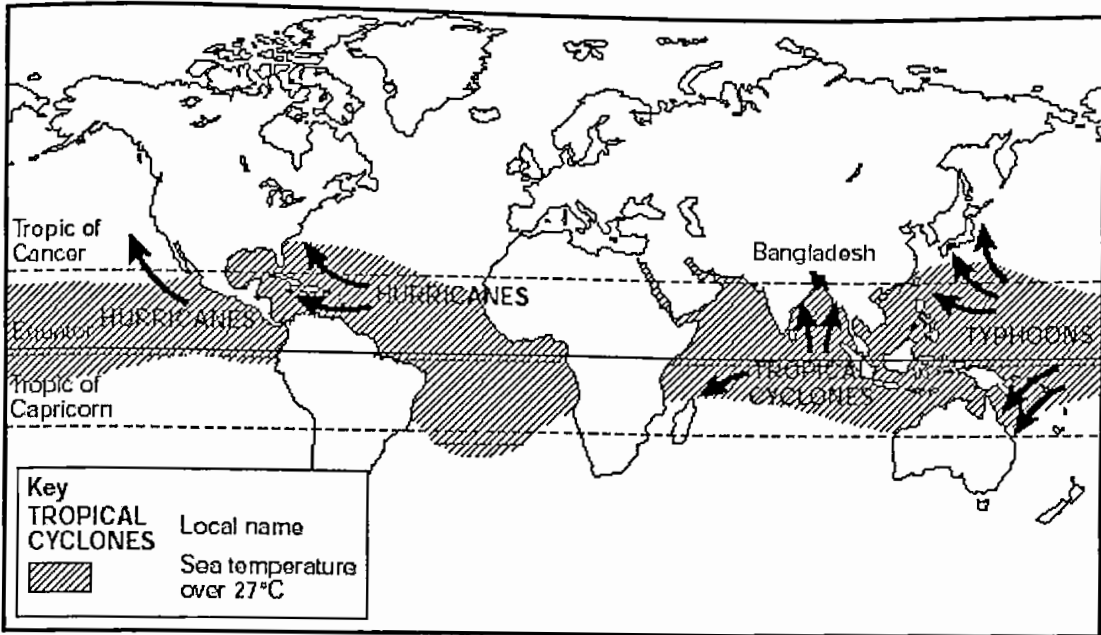
Figure 3.1: Global distribution of tropical storms (after Gray, 1975).

According to the Inter-governmental Panel on Climate Change (IPCC, 2007), a rising sea level due to storm surge would have a wide range of impacts on coastal environments and infrastructures. Frank and Hussain (1971) proposed that about 90% of marine fishermen suffered casualties and about 65% of total annual fishing capacity of coastal areas was destroyed. In 2002, IIT Kharagpur transferred the PC-based storm surge models to BMD. These include one North Indian Ocean (the Bay of Bengal and the Arabian Sea) model (medium resolution), one Bay of Bengal model (medium resolution), one Head of the Bay of Bengal model (fine resolution) and one Myanmar model (fine resolution).

A detailed review of the problem of storm surges in the Bay of Bengal is given by Ali (1979), Ali *et al.* (1997a, 1997b), Rao (1982), Roy (1984), Murty (1984), Murty et. al (1986), Das (1994a, b), Dube et. al. (1997), Debsarma (1997), Chittibabu (1999).
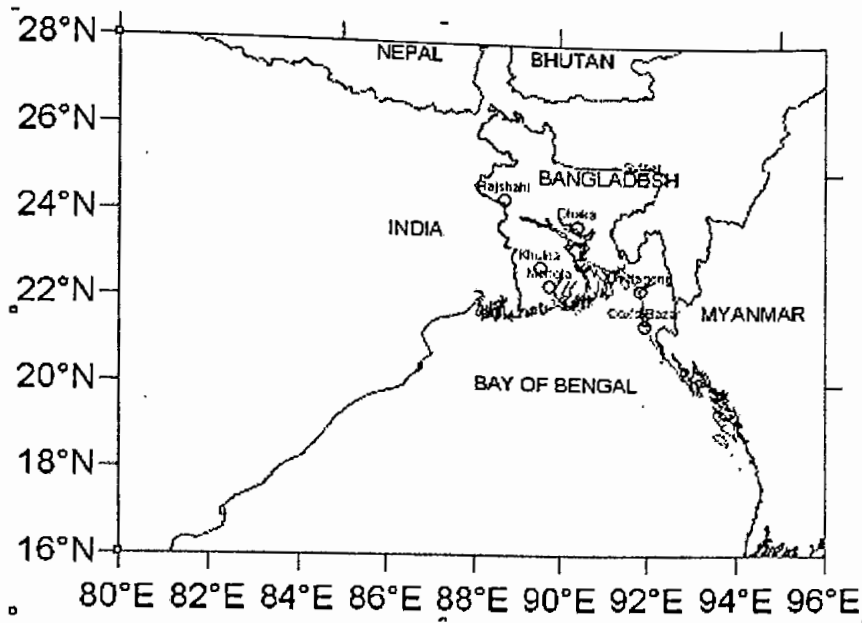
Figure 3.2: Map of Bangladesh showing complex coastal geometry

Numerical modelling of storm surges in Indian seas (Bay of Bengal and Arabian Sea) was pioneered by Das (1972). He conducted a numerical experiment and computed the surge generated by an idealised cyclone striking the coast of Bangladesh. Rao and Majumdar (1966) and Ghosh (1981) developed a technique for forecasting storm waves for the Indian coasts. Jelesnianski (1972) developed SPLASH (Special Program to List Amplitudes of Surges from Hurricanes) and SLOSH (Sea, Lake and Overland Surges from Hurricanes) models. Ali (1979, 1996) studied storm surges and sea level rise in the Bay of Bengal. Ali *et al* (1997a, 1997b) investigated the river discharge, storm surges and tidal interaction in the Meghna river mouth in Bangladesh; and back water effect of tides and storm surges on fresh water discharge through the Meghna estuary.

Das *et al* (1983) and Dube *et al* (1985, 1986, 1989, 1991, 1997) developed numerical models to investigate the dynamic effect of curving coasts and the direction of motion of the storm relative to the coast on the location of the peak surge. Debsarma (1997) made visualization of May 1997 storm surge by using IIT model. Chittibabu (1999) developed storm surge prediction models for the Bay of Bengal and the Arabian Sea.

From the above discussions it is clear that although many researchers worked on storm surges and its various consequences but none of them do not consider the effects of air bubble entrainment. In this chapter, we have developed some hydrodynamic equations based on air bubble effects that will be helpful to compute the surface elevation in the coastal area, especially in Bangladesh.

3.2 Formulation of the model

3.2.1 Shallow water equations in terms of air bubbles

The basic hydrodynamic equations for the dynamical process in the sea may be written as

$$\frac{\partial u}{\partial x} + \frac{\partial v}{\partial y} + \frac{\partial w}{\partial z} = 0 \tag{3.1}$$

$$\frac{\partial u}{\partial t} + u\frac{\partial u}{\partial x} + v\frac{\partial u}{\partial y} + w\frac{\partial u}{\partial z} - fv = -\frac{1}{\rho}\frac{\partial p}{\partial x} + \frac{1}{\rho}\frac{\partial \tau_x}{\partial z} \tag{3.2}$$

$$\frac{\partial v}{\partial t} + u\frac{\partial v}{\partial x} + v\frac{\partial v}{\partial y} + w\frac{\partial v}{\partial z} + fu = -\frac{1}{\rho}\frac{\partial p}{\partial y} + \frac{1}{\rho}\frac{\partial \tau_y}{\partial z} \tag{3.3}$$

The equation of continuity (Eq.(3.1)) and equation of motion (Eqs.(3.2) and (3.3)) form the basic equations for numerical storm surge model. By depth integration (from bottom to surface) the above three basic equations can be written as

$$\frac{\partial u}{\partial x} + \frac{\partial v}{\partial y} + \frac{1}{h + \Delta h + \eta}\frac{\partial \eta}{\partial t} = 0 \tag{3.4}$$

$$\frac{\partial u}{\partial t} + u\frac{\partial u}{\partial x} + v\frac{\partial u}{\partial y} - f\,v = -g\frac{\partial \eta}{\partial x} - \frac{B(C_0)}{\rho_w(h + \Delta h + \eta)}\frac{\partial p_a}{\partial x}$$
$$+ \frac{B(C_0)[F_S - \rho_w c_f u(u^2 + v^2)^{\frac{1}{2}}]}{\rho_w(h + \Delta h + \eta)^2} \tag{3.5}$$

$$\frac{\partial v}{\partial t} + u\frac{\partial v}{\partial x} + v\frac{\partial v}{\partial y} + f\,u = -g\frac{\partial \eta}{\partial y} - \frac{B(C_0)}{\rho_w(h + \Delta h + \eta)}\frac{\partial p_a}{\partial y}$$
$$+ \frac{B(C_0)[G_S - \rho_w c_f v(u^2 + v^2)^{\frac{1}{2}}]}{\rho_w(h + \Delta h + \eta)^2} \tag{3.6}$$

3.2.2 Boundary and initial conditions

Appropriate conditions have to be satisfied along the lateral boundaries of the sea area under consideration for all time in addition to the fulfillment of the surface and bottom conditions. Theoretically the only boundary condition needed in the vertically integrated system is that the normal transport vanish at the coast, that is,

$$u \cos \alpha + v \sin \alpha = 0 \quad \text{for all } t \geq 0 \tag{3.7}$$

where α denotes the inclination of the outward directed normal to the x-axis. Thus on a y-directed boundary $u = 0$ and $v = 0$ on an x-directed boundary $v = 0$.

At the open-sea boundary, the normal currents across the boundary may be prescribed, yielding a condition such as Eq. (3.7) modified by a non-zero term on the right hand side of the equation. A radiation type of condition may be applied, which leads to Heaps (1973).

$$u \cos \alpha + v \sin \alpha + \left(\frac{g}{h + \Delta h} \right)^{\frac{1}{2}} \eta = 0 \tag{3.8}$$

Application of a radiation type of condition (3.8) at the open sea boundary of a model allows the propagation of energy (disturbances) only outwards from the interior in the form of simple progressive waves. It also helps to eliminate the transient response more quickly as a result of the frictional dissipation in the system. Flather (1976) noted that application of a radiation condition in the numerical model might remove the unrealistically large currents and grid scale oscillations in the vicinity of the open boundary, which may possibly be produced by the application of conventional open-sea boundary condition (i.e., $\eta = 0$ at $y = 0$). As usual it is assumed that the motion in the sea is generated from an initial state of rest, so that $\eta = u = v = 0$ everywhere for $t = 0$.

3.2.3 Determination of forcing functions

The forcing terms in the basic equations are the Coriolis force, the surface pressure, wind stress components and the seabed friction. In view of the strong associated winds and consequently high values of the wind stress forcing, the forcing due to barometric changes (i.e., $\partial p_a / \partial x$ and $\partial p_a / \partial y$) may be neglected in the surge prediction models.

The Coriolis force can be determined by knowing the latitudinal position of the area and the bottom stress may be parameterized in terms of depth averaged currents by a quadratic law. The problem thus remains to compute the surface winds and the wind stresses.

Up to date no good theory exists on which a computation of the surface winds can be based. A number of numerical models are used for the storm surges in which the wind speed is related to the pressure gradient. Some of the pressure formulas used for tropical cyclones are given below:

$$p(r) = p(\infty) - \frac{\Delta p}{[1+(r/R)^2]^{1/2}} \quad \text{(Isozaki, 1970)} \tag{3.8}$$

$$p(r) = 1010 - \frac{\Delta p}{[1+(r/R)^2]} \quad \text{(Das et al., 1974)} \tag{3.9}$$

$$p(r) = p(\infty) - \Delta p \exp(-r/R) \quad \text{(Johns and Ali, 1980)} \tag{3.10}$$

where $p(r)$ represents sea level pressure at a radial distance of any point in a cyclone from its centre and $p(\infty)$ that of at the cyclone periphery, R is the radius of maximum winds and Δp is the pressure drop.

The wind distribution in the cyclone is then calculated from the cyclostrophic wind or gradient wind formula. The cyclostrophic wind corresponding to the pressure field given by Eq. (3.9) is

$$V^2 = 4V_m^2 [\mu^2 \div (1+\mu^2)^2] \tag{3.11}$$

where $\mu = r/R$ and V_m is the maximum wind at R. The maximum wind (in knots) and the pressure drop (hPa) may be related by

$$V_m = C'(\Delta p)^{\frac{1}{2}} \quad \text{(Fletcher's Formula)} \tag{3.12}$$

where C' is a numerical constant (14.2 for the Bay of Bengal).

Johns and Ali (1980) used the following gradient wind formula for computing the wind distribution corresponding to the pressure field Eq. (3.10)

$$V = -\frac{fr}{2} + \left[\frac{f^2 r^2}{4} + \frac{r}{\rho_a} \frac{\partial p}{\partial r} \right]^{\frac{1}{2}} \tag{3.13}$$

where ρ_a is the density of the air, taken as 1.293 kg m^{-3}.

A number of other cyclone models compute the wind field by one of the following expressions

$$V = V_m \left(\frac{r}{R} \right)^{3/2}, \quad 0 \leq r \leq R \quad \text{(Jelseninanski, 1965)} \tag{3.14}$$

$$V = V_m \left(\frac{R}{r} \right)^{1/2}, \quad r > R, \quad \text{(Das et al., 1974)} \tag{3.15}$$

$$V = V_m \left(\frac{2Rr}{R^2 + r^2} \right) \quad \text{(Jelesnianski, 1972)} \tag{3.16}$$

With the surface winds estimated one can proceed to the computation of the stress at the sea surface. The surface stress for nonlinear problem can be expressed by conventional quadratic law as

$$F_S = \rho_a \, c_D \, u_a \, (u_a^2 + v_a^2)^{\frac{1}{2}} \tag{3.17}$$

$$G_S = \rho_a \, c_D \, v_a \, (u_a^2 + v_a^2)^{\frac{1}{2}} \tag{3.18}$$

where u_a and v_a are the x and y components of surface wind, c_D is the drag coefficient. Observational studies suggest that the drag coefficient may be related to the wind speed by $c_D = (1.00 + 0.07 \, v_{10}) \times 10^{-3}$ (3.19)

in which v_{10} is the wind speed at 10m from the mean sea level. This expression is generally valid for wind speed less than 14 ms^{-1}. At wind speeds between 10 and 30 m s^{-1}, c_D varies from 2 x 10^{-3} to 3 x10^{-3} with no significant dependence on wind speed. Most of the workers used a uniform value of drag coefficient (=2.8 x 10^{-3}).

3.3 Numerical solution

In this model, a system of rectangular Cartesian coordinates is used in which the origin, O, is in the equilibrium level of the sea surface. O_x and O_y are directed towards the east

and north respectively and O_z is directed vertically upwards (Fig. 3.3). The displaced position of the free surface is given by $z = \eta(x, y, t)$ and the position of the sea bed by $z = -h - \Delta h$, where, $h = h(x,y)$

For numerical treatment, it is convenient to express Eqs. (3.4) - (3.6) in flux form as

$$\frac{\partial[(h + \Delta h + \eta)u]}{\partial x} + \frac{\partial[(h + \Delta h + \eta)v]}{\partial y} + \frac{\partial \eta}{\partial t} = 0 \tag{3.20}$$

$$\frac{\partial[(h + \Delta h + \eta)u]}{\partial t} + \frac{\partial[(h + \Delta h + \eta)uu]}{\partial x} + \frac{\partial[(h + \Delta h + \eta)uv]}{\partial y} - f\, v(h + \Delta h + \eta) =$$

$$- g(h + \Delta h + \eta)\frac{\partial \eta}{\partial x} + \frac{B(C_0)}{\rho_w}\frac{\partial p_a}{\partial x} + \frac{B(C_0)[F_S - \rho_w c_f u(u^2 + v^2)^{\frac{1}{2}}]}{\rho_w(h + \Delta h + \eta)} \tag{3.21}$$

$$\frac{\partial[(h + \Delta h + \eta)v]}{\partial t} + \frac{\partial[(h + \Delta h + \eta)uv]}{\partial x} + \frac{\partial[(h + \Delta h + \eta)vv]}{\partial y} + f u(h + \Delta h + \eta) =$$

$$- g(h + \Delta h + \eta)\frac{\partial \eta}{\partial y} + \frac{B(C_0)}{\rho_w}\frac{\partial p_a}{\partial y} + \frac{B(C_0)[G_S - \rho_w c_f v(u^2 + v^2)^{\frac{1}{2}}]}{\rho_w(h + \Delta h + \eta)} \tag{3.22}$$

Neglecting barometric forcing terms the governing Eqs. (3.20) to (3.22) reduce to

$$\frac{\partial \zeta}{\partial t} + \frac{\partial \tilde{u}}{\partial x} + \frac{\partial \tilde{v}}{\partial y} = 0 \tag{3.23}$$

$$\frac{\partial \tilde{u}}{\partial t} + \frac{\partial}{\partial x}(u\tilde{u}) + \frac{\partial}{\partial y}(v\tilde{u}) - f\tilde{v} = -g(h + \Delta h + \eta)\frac{\partial \eta}{\partial x} +$$

$$B(C_0)\{\frac{F_S}{(h + \Delta h + \eta)\rho_w} - \frac{c_f\tilde{u}(u^2 + v^2)^{\frac{1}{2}}}{(h + \Delta h + \eta)^2}\} \tag{3.24}$$

$$\frac{\partial \tilde{v}}{\partial t} + \frac{\partial}{\partial x}(u\tilde{v}) + \frac{\partial}{\partial y}(v\tilde{v}) + f\tilde{u} = -g(h + \Delta h + \eta)\frac{\partial \eta}{\partial y} +$$

$$B(C_0)\{\frac{G_S}{\rho_w(h + \Delta h + \eta)} - \frac{c_f\tilde{v}(u^2 + v^2)^{\frac{1}{2}}}{(h + \Delta h + \eta)^2}\} \tag{3.25}$$

where $\widetilde{u} = (h + \Delta h + \eta)u$ and $\widetilde{v} = (h + \Delta h + \eta)v$ are new prognostic variables and $(h + \Delta h + \eta)$ gives the total depth of the basin.
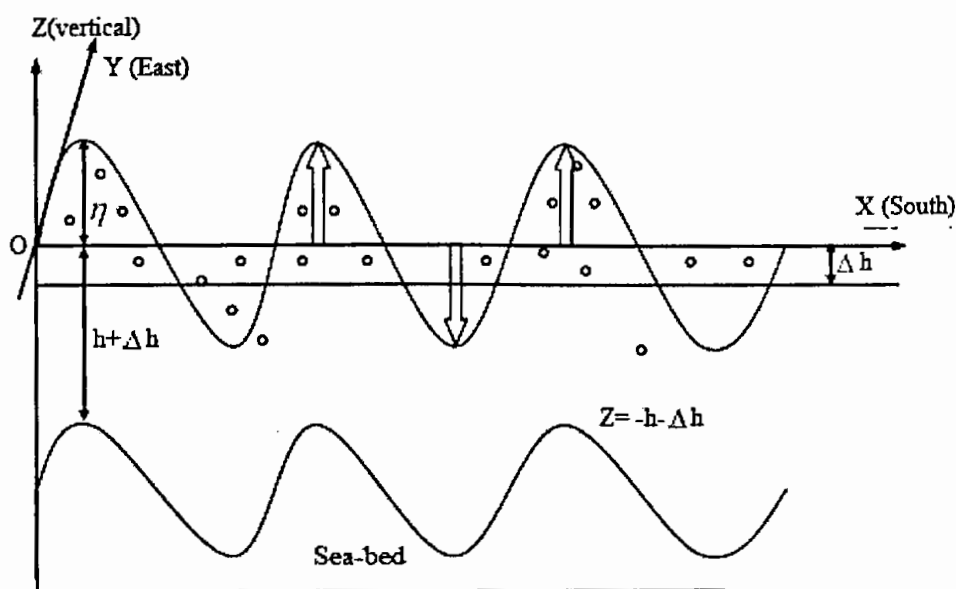
Figure 3.3: Storm surge coordinate representation

The head Bay of Bengal model is a coastal zone model, which covers an analysis area from 18° N to 23° N and 83.5° E to 94.5°E. The model has fixed the eastern boundary at about 250 km from the east coast of India at $x=b_2$ (y). The treatments of the coastal boundaries involve a procedure leading to a realistic curvilinear representation of both the western and the eastern sides of the Bay of Bengal. The analysis area of the head of the Bay of Bengal model is shown in the Fig. (3.4). The western coastal boundary (the east coast of India) is situated at $x = b_1(y)$ and the eastern coastal boundary is situated at $x = b_2(y)$. Southern open sea and northern coastal boundaries are at $y = 0$ and $y = L$ respectively (Fig. 3.5).
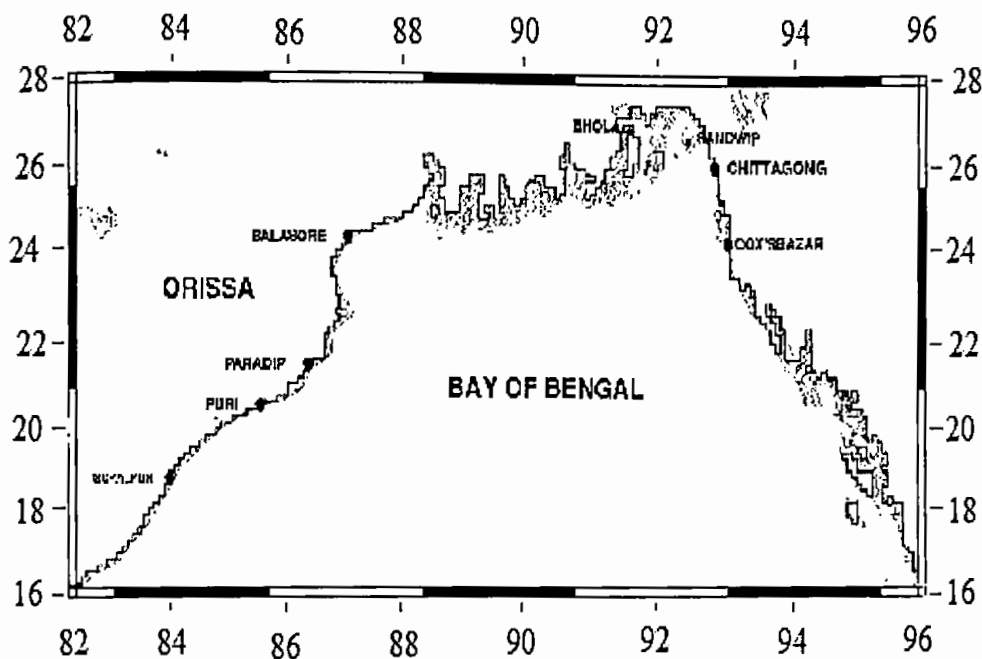
Figure 3.4: Analysis area of the head of the Bay of Bengal model (coast and islands are included in the stair step method).

3.3.1 Boundary conditions

The normal component of depth-averaged velocity is considered to be zero at the coast and is coastal sidewalls and so the condition of zero normal velocity at these may be given by

$$u - v \frac{\partial b_1}{\partial y} = 0 \quad \text{at} \quad x = b_1(y) \tag{3.26}$$

$$u - v \frac{\partial b_2}{\partial y} = 0 \quad \text{at} \quad x = b_2(y) \tag{3.27}$$

and $v = 0$ at $y = L$ \hfill (3.28)

where L is the distance between $y = 0$ and the coast.

Conceptually similar radiation conditions are applied at the open sea boundary the western ($84.5^0 E$), eastern ($94.5^0 E$) and southern ($18^0 N$) to yields

$$v + (\frac{g}{h + \Delta h})^{\frac{1}{2}} \eta = 0$$

$$v - (\frac{g}{h + \Delta h})^{\frac{1}{2}} \eta = 0 \qquad (3.29)$$

and $\qquad u - (\frac{g}{h + \Delta h})^{\frac{1}{2}} \eta = 0$
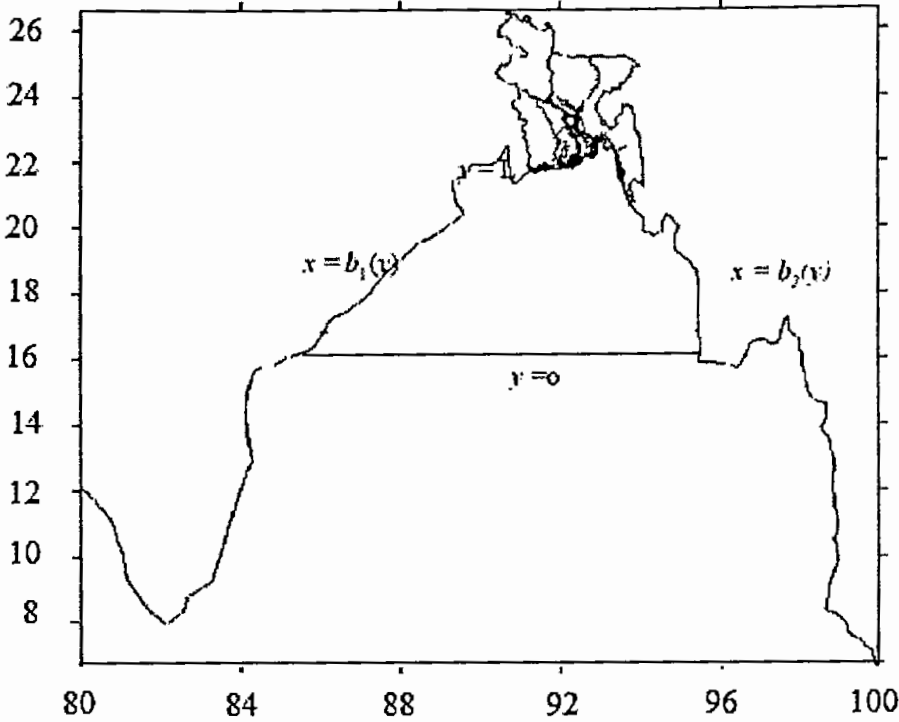
Figure 3.5: Map with boundary conditions.

3.3.2 Co-ordinate transformation

In storm surge work conformal mapping was considered by Reid et al. (1977) for curvilinear representation of coastal boundaries. But this treatment is of a different nature and is more similar to that reported by Jelesnianski (1976). This is achieved by applying a co-ordinate transformation in which

$$\xi = \frac{x - b_1(y)}{b(y)} \qquad (3.30)$$

where, $b(y) = b_2(y) - b_1(y)$.

Thus, the western and the eastern boundaries correspond to $\xi = 0$ and $\xi = 1$ respectively. Taking ξ, y, t as the new independent co-ordinates, the Eqs. (3.23 – 3.25) may be written as

$$\frac{\partial}{\partial t}(b\eta) + \frac{\partial}{\partial \xi}[bH\,U] + \frac{\partial}{\partial y}(bHv) = 0 \tag{3.31}$$

$$\frac{\partial \tilde{u}}{\partial t} + \frac{\partial}{\partial \xi}(U\tilde{u}) + \frac{\partial}{\partial y}(v\tilde{u}) - f\,\tilde{v} = -g\,H\frac{\partial \eta}{\partial \xi} + B(C_0)\{\frac{bF_S}{\rho_w H} - \frac{c_f \tilde{u}}{H^2}(u^2 + v^2)^{\frac{1}{2}}\} \tag{3.32}$$

$$\frac{\partial \tilde{v}}{\partial t} + \frac{\partial}{\partial \xi}(U\tilde{v})\frac{\partial}{\partial y}(v\tilde{v}) + f\,\tilde{u} = -gH\left[b\frac{\partial \eta}{\partial y} - \left(\frac{\partial b_1}{\partial y} + \xi\frac{\partial b}{\partial y}\right)\frac{\partial \eta}{\partial \xi}\right] +$$

$$+ B(C_0)\{\frac{bG_s}{\rho_w H} - \frac{c_f \tilde{v}}{H^2}(u^2 + v^2)^{\frac{1}{2}}\} \tag{3.33}$$

where, $\quad U = \frac{1}{b(y)}\left[u - \left(\frac{\partial b_1}{\partial y} + \xi\frac{\partial b}{\partial y}\right)v\right]$ \hfill (3.34)

$$\tilde{u} = Hbu, \quad \tilde{v} = Hbv, \quad H = h + \Delta h + \eta$$

From Eqs. (3.26) and (3.27) using Eq.(3.34) it can be seen that

$U = 0$, at $\xi = 0$ and $\xi = 1$. \hfill (3.35)

3.3.3 Numerical procedure

In order to estimate the surge height in the study area, a storm can move over the area at least for 3 days before crossing the coast. On the other hand, to include the major islands in the study area the mesh size (the distance between two consecutive grid points) should be smaller. To get the better performance a high-resolution numerical scheme (FMS) is nested into a coarse mesh scheme (CMS). Further, a very fine mesh scheme (VFMS) is nested in the FMS (Fig. 3.6). The CMS covers the area between 15^0 N to 23^0 N latitude and 85^0 E to 95^0 E longitudes. The mesh size along north-south direction (along x-axis) is $\Delta x = 15.08$ km and east-west direction (along y-axis) is $\Delta y = 17.52$ km. There are 60×61 grid points in the computational xy-plane.
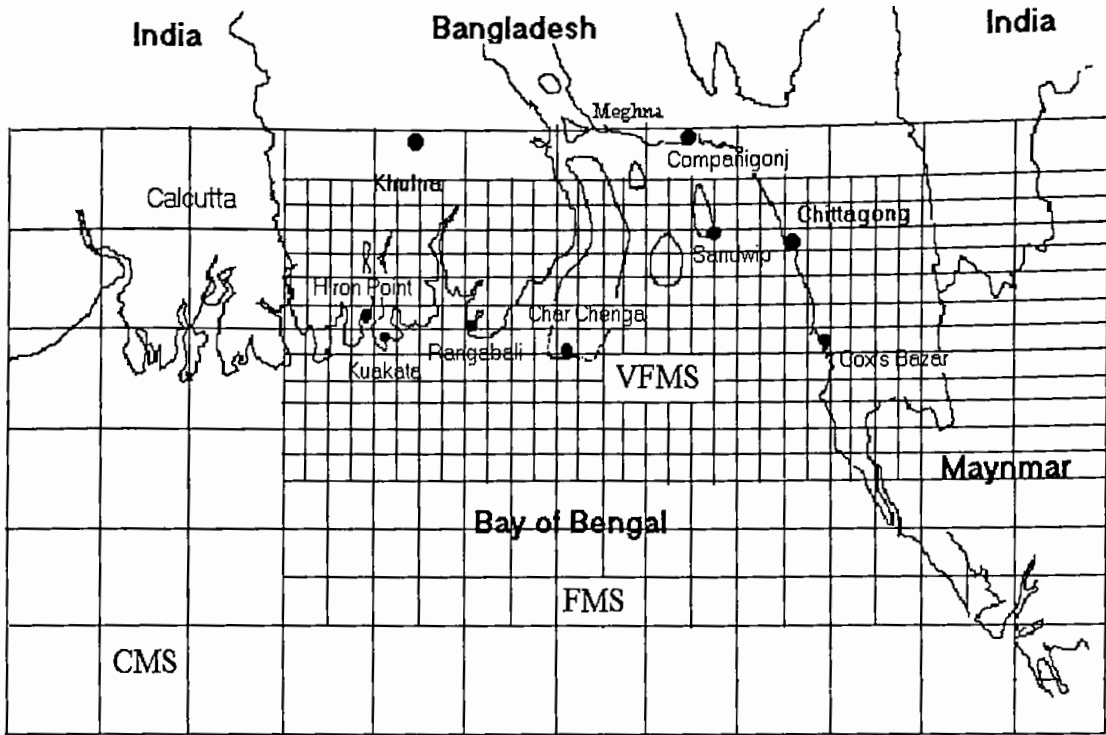
Figure 3.6: Physical domain of the analysis area

The FMS covers the area between 21^0-15′ N to 23^0 N latitude and 89^0 E to 92^0 E longitudes. This scheme area includes the study area and almost all the offshore islands. The mesh size along north-south direction (along x-axis) is Δx = 2.15 km and along east-west direction (along y-axis) is Δy = 3.29 km. There are 92×95 grid points in the computational xy-plane. The VFMS covers the area between 21.77^0 N to 23^0 N latitude and 90.40^0 E to 92^0 E longitudes. The mesh size along north-south direction (along x-axis) is Δx=720.73 m and along east-west direction (along y-axis) is Δy=1142.39 m. There are 190×145 grid points in the computational xy-plane.

Discrete co-ordinate points in the $\xi - y$ plane are given by

$$\xi = \xi_i = (i-1)\Delta \xi, \quad i = 1,2,....., m; \Delta \xi = 1/(m-1) \tag{3.36}$$

Along y direction

$$y = y_j = (j-1)\Delta y, \quad j = 1,2,3,........,n; \; \Delta y = L/(n-1) \tag{3.37}$$

48

and define a sequence of time instants by

$$t = t_p = p\Delta t, \quad p = 0,1,2,3\ldots\ldots\ldots \tag{3.38}$$

Since the model is non-linear, it requires the values of all the predictive variables at each and every grid point. Hence, the first and the simplest choice appear to be the unstaggered grid. But it is seen that (Ali, 1979) the unstaggered grid cannot handle properly the high frequency waves, particularly two grid waves. It is thought that the error developed at each grid point due to truncation or rounding off or due to some other reasons may give rise to two grid oscillations due to coupling of errors of adjacent points. Thus, the alternative is to apply some sort of filtering to remove the two grid computational waves, but it is found that (Ali, 1979) the application of filtering in a non-linear model produces unsatisfactory results. Calculations show that the use of staggered grid does not produce the two grid waves and hence staggered grids in which there are three distinct types of computational points are used. A suitable arrangement of grid points in (ξ, y) plane is shown in Fig. (3.7). The grid lines are all parallel to the co-ordinate axes and form a uniform network with a rectangular mesh having sides of length $\Delta\xi$ in the ξ- direction and Δy in the y direction. When i is even and j is odd, the point is a η point (marked by a black circle), at which η is computed. If i is odd and j is odd, the point is a u point (marked by a circle) at which both u and U are computed and finally if i is even and j is even, the point is a v point (marked by a square) at which v is computed.

The lateral boundaries of the finite difference grid are so chosen that the open sea boundary consist of η points and u-points. Any variable X, at a grid point (i, j) may be represented by

$$X(\xi_i, y_j, t_p) = X_{i,j}^p \tag{3.39}$$
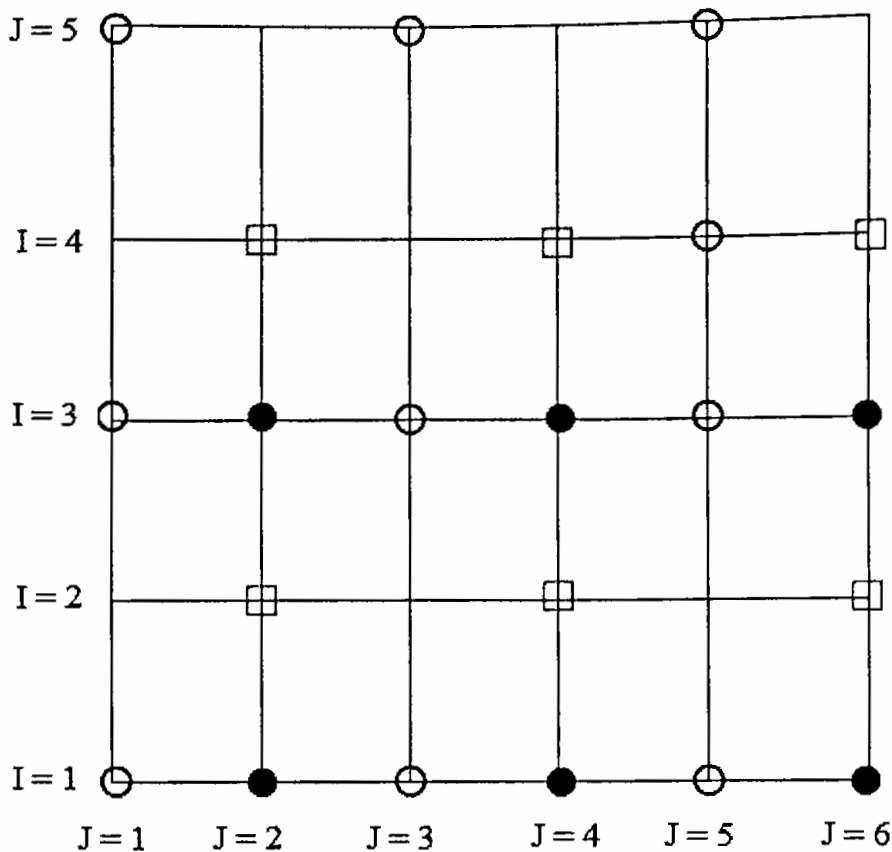
Figure 3.7: Staggered grid-points in ξ-y plane

Finite difference operators are defined as

$$\delta_t X = (X_{i,j}^{p+1} - X_{i,j}^{p})/\Delta t$$

$$\delta_\xi X = (X_{i+1,j}^{p} - X_{i-1,j}^{p})/(2\Delta\xi)$$

$$\delta_y X = (X_{i,j+1}^{p} - X_{i,j-1}^{p})/(2\Delta y)$$

(3.40)

Averaging operators are defined by

$$\left.\begin{aligned}
\overline{X}^\xi &= \frac{1}{2}(X_{i+1,j}^{p} + X_{i-1,j}^{p})\\
\overline{X}^y &= \frac{1}{2}(X_{i,j+1}^{p} + X_{i,j-1}^{p})\\
\overline{X}^{\xi y} &= \overline{X}^{\overline{\xi} y}
\end{aligned}\right\}$$

(3.41)

50

and a shift operator is defined by

$$E_t X = X_{i,j}^{p+1}$$ (3.42)

The discretization of the continuity equation may be written as

$$\delta_t(b\eta) + \delta_\xi(b(h + \Delta h + \overline{\eta}^\xi)U) + \delta_y(\widetilde{v}) = 0$$ (3.43)

The above equation (4.43) yields an updating procedure to compute the elevation at all the interior ξ-points consistent with the mass conservation in the system. The elevation at j = 1 and i = 2, 4, …., m −1 is determined by Eq. (4.33), in practice, this is applied at j = 2 and replaced by

$$\frac{1}{2}\left(\frac{g}{(h + \Delta h)_{i,2}}\right)^{\frac{1}{2}}\left[\eta_{i1}^{p+1} + \eta_{i3}^{p+1}\right] + v_{i2}^p = 0$$ (3.44)

Thus, leading to an updating procedure for the elevation on the southern open sea boundary in the form

$$\eta_{i,1}^{p+1} = -\eta_{i,3}^{p+1} - 2(\frac{(h + \Delta h)_{i2}}{g})^{\frac{1}{2}} v_{i,2}^p$$ (3.45)

The descretization of Eq. (3.32) is based on

$$\delta_t(\widetilde{u}) + \delta_\xi(U\,\overline{\widetilde{u}}^\xi) + \delta_y(\overline{v}^\xi\,\overline{\widetilde{u}}^y) - f\,\overline{\widetilde{v}}^{\xi y} = -g\,E_t\left((h + \Delta h + \overline{\eta}^\xi)\,\delta_\xi\eta)\right)$$

$$+ B(C_0)\{\frac{1}{\rho_w\,E_t(h + \Delta h + \overline{\eta}^\xi)}bF_s - \frac{c_f\left[u^2 + (\overline{v}^{\xi y})^2\right]^{\frac{1}{2}}E_t(\widetilde{u})}{E_t(h + \Delta h + \overline{\eta}^\xi)^2}\}$$ (3.46)

Equation (4.46) is used to update at $\widetilde{u}$ at the u points. Updated values of u may then be deduced from $\widetilde{u}$ and η by applying

$$u = \frac{\widetilde{u}}{b(h + \Delta h + \overline{\eta}^\xi)}$$ (3.47)

It may be seen that Eq. (3.46) is applied for i =3,5,…., m−2, and j =3, 5,… ,n −1. By virtue of Eq. (4.35), the boundary values of U at i =1 and i = m are identically zero. When j = n −1, the boundary value of v at j = n are identically zero by virtue of condition (3.28). When applied at j = 3, the averaging operator references the value of u at j = 1 and to overcome this difficulty, an appropriate one-sided definition of δ_y is then

used. With this procedure, values of $\tilde{u}$ (and hence u) may be updated at all the interior u-points. A similar discretization of Eq. (3.33) is based upon

$$\delta_t(\tilde{v}) + \frac{1}{F}\delta_\xi(\overline{U}^{\,y}\overline{\tilde{v}}^{\,\xi}) + \delta_y(\overline{v}^{\,y}\overline{\tilde{v}}^{\,y}) + E_t(f\,\overline{\tilde{u}}^{\,\xi y}) = -gE_t[b(h+\Delta h+\overline{\eta}^{\,y})\delta_y^\eta -$$

$$(\frac{\partial b_1}{\partial y}+\xi\frac{\partial b}{\partial y})(h+\Delta h+\overline{\eta}^{\,y})\delta_\eta\overline{\eta}^{\,\xi y}] + B(C_0)\{\frac{bG_S}{\rho_w(h+\Delta h+\overline{\eta}^{\,y})} - \frac{c_f[(\overline{u}^{\,\xi y})^2 + v^2]^{\frac{1}{2}}E_t(\tilde{v})}{E_t(h+\Delta h+\overline{\eta}^{\,y})^2}\}$$

$$(3.48)$$

Equation (3.48) is used for updating $\tilde{v}$ at the v-points. Updated values of v are then deduced from those of $\tilde{v}$ and η by using

$$v = \frac{\tilde{v}}{b(h+\Delta h+\overline{\eta}^{\,y})} \tag{3.49}$$

Equation (3.47) is applied for i = 2, 4, …, m −1 and j = 2, 4, …, n − 2. By virtue of (3.29), referenced values of U along i = 1 and i = m are identically zero. When applied at j = 2, averaging operator in eq. (3.48) references a value of v outside the analysis area. To overcome this difficulty, δ_y is replaced by an appropriate one-sided operator. After the updating of u and v, the updated value of U may be obtained by applying (3.33) in the descritized form

$$U = \frac{1}{b}\left[u - (\frac{\partial b_1}{\partial y} + \xi\frac{\partial b}{\partial y})\overline{v}^{\,\xi y}\right] \tag{3.50}$$

The ensuing values of U at the u points are then available for the next updating of the prognostic variables.

3.3.4   *Stability of the scheme*

The following general points are made about the descretizations. In Eqs. (3.46) and (3.48) the pressure gradient terms are evaluated at the advanced time level. This is possible explicitly using values of η previously updated by application of Eq. (3.43) and following Sieleki (1968), ensures computational stability subject only to the time step being limited by the space increment and gravity wave speed. This is governed by the CFL (Courant-Friedrich-Levy) criterion, i.e,

$$\sqrt{2g(h+\Delta h)_{max}}\,\frac{\Delta t}{\Delta x}\leq 1 \tag{3.51}$$

In Eq. (3.46), the Coriolis term is evaluated explicitly at the old time level where as in Eq. (3.48) it is evaluated at the advanced time level using the previously updated value of u. Finally in both Eqs. (3.46) and (3.48), the friction term is evaluated partly implicitly. The resulting difference equations being solved algebraically before their incorporation into the updating scheme. This ensures unconditional computational stability with reference to the treatment of the dissipative terms.

3.4 Conclusions

A nonlinear two-dimensional vertically integrated storm surge model considering air bubble effect has developed for prediction and evaluation of storm surges in the Bay of Bengal. The model founds to be capable of incorporating air bubble effects and bending of the coastline and island boundaries with a reasonably good accuracy. The model was included the analysis area of the full Bay of Bengal. This developed model is applied to simulate water levels in terms of air bubbles in the coastal region of Bangladesh due to cyclonic storm surges. Next chapter shows the computed results.

Chapter-4

Verification of the Storm Surge Model

Summary

In this chapter the storm surge model in terms of air bubble is used to simulate the surges of severe cyclonic storms with the 1991 cyclone and AILA, 2009. Initially six hourly and at the end part (towards landfall) three hourly data have been used for making gradual changes in the storm surge scenario. The model is found to higher water levels in presence of air bubbles. The results obtained from the model are in good agreement with the reported data. A comparison is made between the surges with and without air bubbles.

4.1 Introduction

The Bay of Bengal is the reason in the world over where about 5% of the global tropical cyclones form. About 80% global casualties occur in Bangladesh which lies at the northern tip of the Bay of Bengal (Debsarma, 2009). The prediction and analysis on storm surges and tide surge interaction in the Bay of Bengal have been investigated by many authors (e.g. Sinha et al, 1997; Henry et al., 1997; Roy et al, 2001; Roy, 1995; John and Ali, 1980; Ali et. al. 1997a, 1997b; Johns et. al. 1985). Sinha et. al. (1997) developed numerical model to simulate storm surges and sea level rise in the Indian coasts adjacent to the Bay of Bengal and the Arabian sea. Roy et. al. (2001) developed several models to simulate the surges associated with several severe cyclonic storms hitting the coast of Bangladesh. Ghosh *et. al.* (1983) made numerical simulation of storm surge envelopes associated with the recent severe cyclones impinging on the east and west coast of India. Johns and Ali (1980) incorporated the dynamic effect of the Ganges-Brahmaputra-Meghna river system

and off-shore islands in the nonlinear tide surge interaction model. Roy (1995) tested the sensitivity of wind velocity and surge route on water levels.

Though a number of studies are carried out on the analysis and prediction of tide, surge, their interaction and the effects of various factors on water levels, but studies incorporating air bubbles and their effect on water levels during storm surges are still limited. In this chapter we intend to simulate storm surges and sea level rise in the Bay of Bengal using storm surge model including air bubbles effect for the cyclone April, 1991 and AILA, 2009 and a comparison is made with and without air bubbles.

4.2 Cyclone of April, 1991

The Chittagong cyclone of 29 April 1991 was first detected as a depression on 23rd April 1991 from satellite imagery (NOAA-11) located at latitude 10.0^{o} N and longitude 89.0^{o}E at 0900 BST in the morning of 25 April (Fig. 4.1).
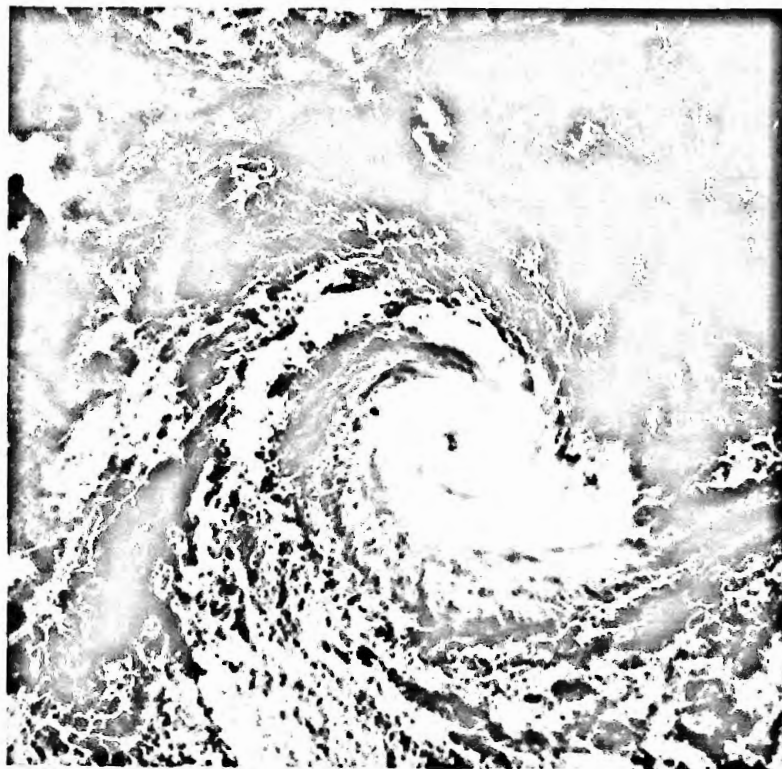

Figure 4.1: Satellite show of Bangladesh cyclone April, 1991(BMD).

The system again intensified into a deep depression in the evening and very quickly turned into a cyclonic storm at midnight on 25 April. The time series of the 1991 cyclone is shown in table 4.1. The maximum sustained wind speed was 65-87 km/h, having a central pressure of 996 Mb. It retained this intensity till 1500 BST of 27 April when it was found to have developed into a severe cyclonic storm. The maximum wind velocity was 90-115 km/h, having 990 Mb as the central pressure.
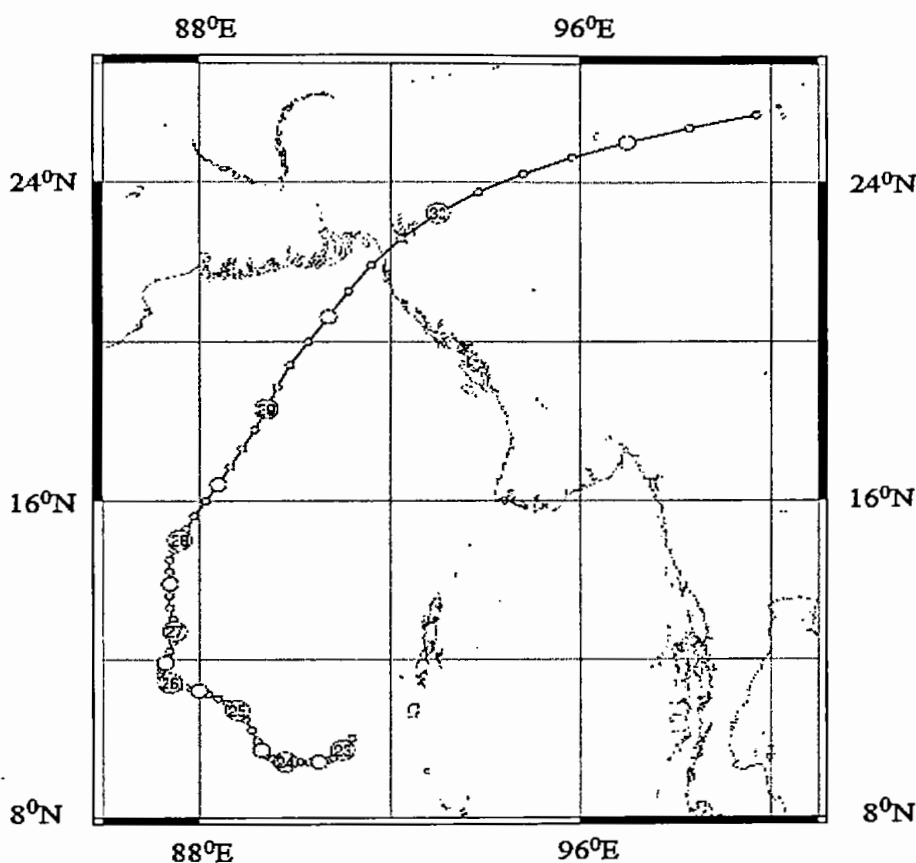
Figure 4.2: Observed track of cyclonic storm of April, 1991.

On the same day (27 April) at midnight, it turned into a storm with a core of hurricane wind that had wind speeds of more than 130 km/h. From 28 April, it started moving in a north-easterly direction and finally, crossed the coast north of Chittagong port in the early morning (0400 BST) of 30 April. The track of the April cyclone, 1991 is shown in figure 4.2. and the time series for the 1991 cyclone is given in table

4.2. The estimated maximum pressure drop was about 60 Mb (Talukdar et al., 1992).
The maximum wind speed observed at Sandwip was 235 km/h. The central pressure
of the 1991 cyclone was as low as 938 Mb, as measured by the Chittagong port
authority of Bangladesh. The storm surge was 4 to 8 meter high in different areas.
Vast areas in the districts of Cox's Bazar, Chittagong, Noakhali, and Bhola were
submerged. Fatality figures caused by the April cyclone varies between 130,000
(Bangladesh Bureau of Statistics, 1991) to 200,000 (Rashid,1991). The most
vulnerable points in the coastal area are indicated in figure 4.3.
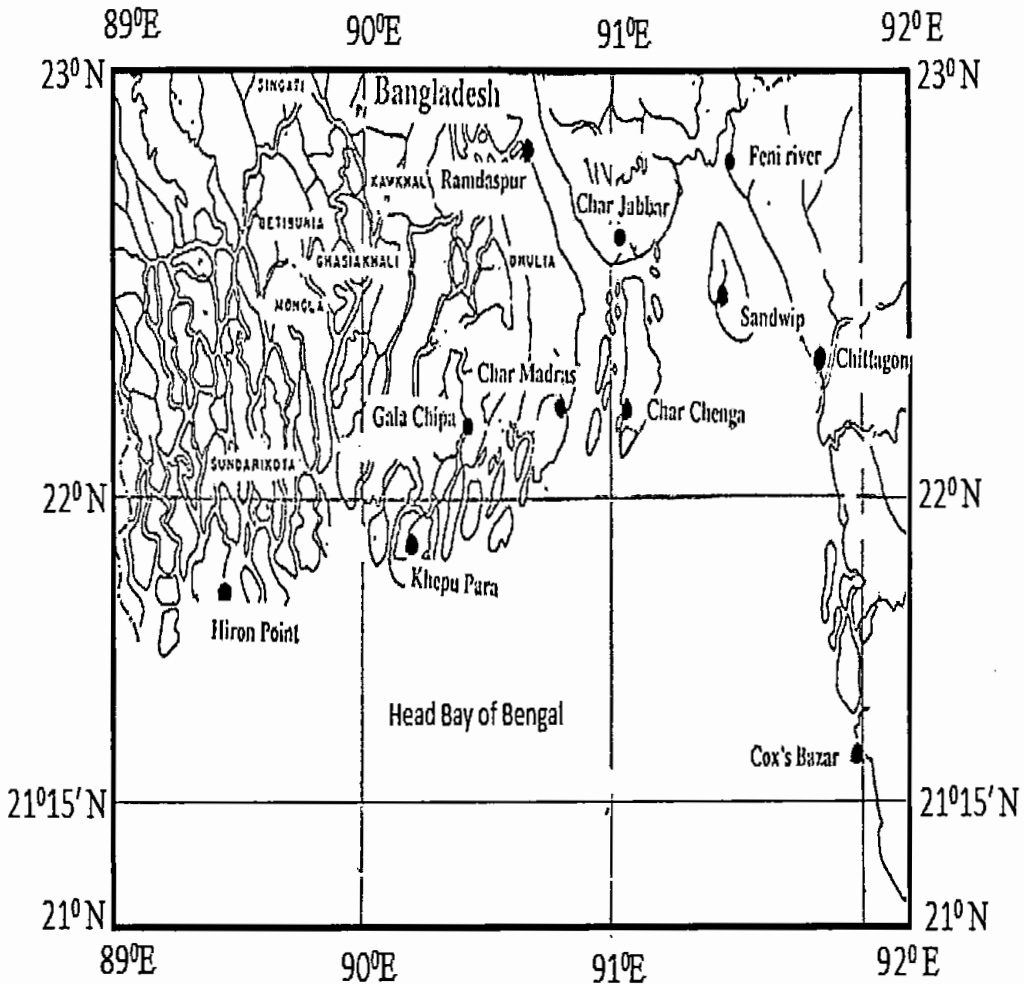

Figure 4.3: Positions of some coastal locations at which water levels are presented.

Casualties in the unprotected islands were on the average 40-50% of the total
population of the areas affected by the storm surge. Islands protected by

embankments, the figure may have been 30-40%; while on the mainland coast, which faced the fury of the surge, deaths were probably 20-30% of the population.

Table 4.1: Time series for the positions and the nature of the April 1991 cyclone (Source: BMD).

Date	Hour (UTC)	Latitude (^{0}E)	Longitude (^{0}N)	Nature of the storm
2604	1800	11.00	87.50	Cyclonic storm
2704	0000	11.80	87.50	Cyclonic storm
2704	0900	12.50	87.50	Cyclonic storm
2704	1200	13.00	87.50	Cyclonic storm
2704	1500	13.60	87.50	Severe cyclonic storm
2804	0000	14.50	87.50	Severe cyclonic storm with hurricane core
2804	1200	15.80	87.70	Severe cyclonic storm with hurricane core
2804	1400	16.50	88.00	Severe cyclonic storm with hurricane core
2904	0000	17.60	88.30	Severe cyclonic storm with hurricane core
2904	1200	19.80	88.40	Severe cyclonic storm with hurricane core
2904	1800	20.80	88.50	Severe cyclonic storm with hurricane core
3004	0000	22.00	91.00	Severe cyclonic storm with hurricane core
3004	0200	22.30	92.80	Severe cyclonic storm with hurricane core

4.3 Cyclone AILA, 2009

A low formed over South-West Bay and adjoining area at noon of 21 May 2009, moved northwards and intensified into a well marked low south-west Bay and adjoining west central Bay on 23 May (Fig. 4.4). Slightly moving north-westwards, the system again intensified into a depression near 16.0^0 N and 88.0^0 E at 0900 UTC on the same day.
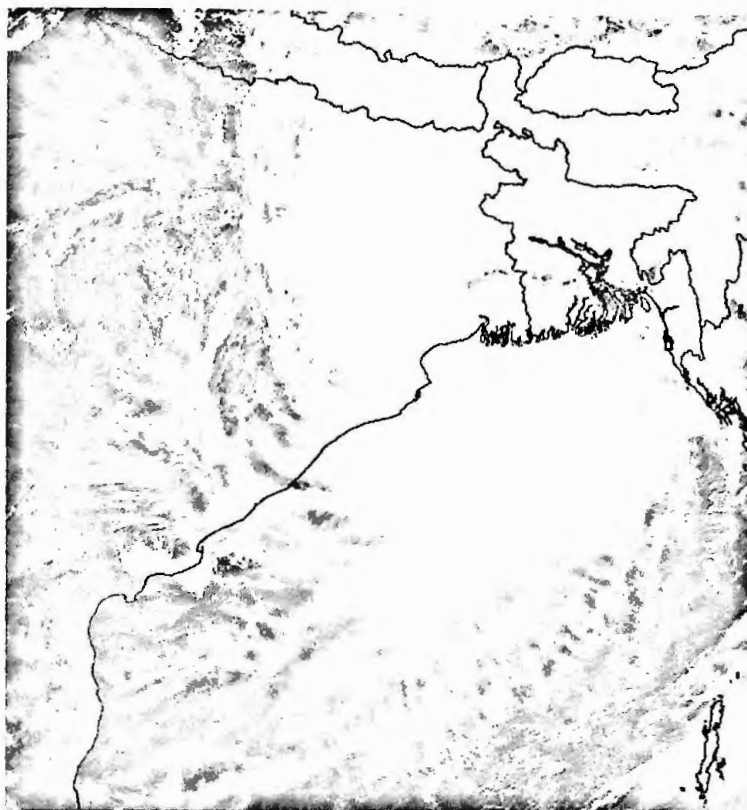
Figure 4.4: Satellite show of AILA, 2009 over India and Bangladesh (BMD).

Maximum sustained wind speed within 44 kms of the depression centre was about 40 kPh rising to 50 kPh. It became a deep depression near 17.8^0 N and 88.6^0 E at 0600 UTC on May 24 and intensified into a cyclonic storm "AILA"(EPC 994 hPa) at 1200 UTC near 18.3^0 N and 88.6^0 E on the same day. The cyclonic storm "AILA" moved slightly northwards over the same area centered at 0300 UTC near 18.6^0 N and 88.6^0 E on the same day. Finally, the cyclonic storm "AILA" started to cross West Bengal-Khulna (Bangladesh) coast near Sagar ilands of India and moving continuously northwards it completely crossed the west Bengal-Khulna (Bangladesh) coast on May 26. The track (path) of the cyclonic storm "AILA" associated rainfall wind distributions are given in figure 4.5. The time series of the cyclone AILA, 2009 is shown in table 4.2.

Table 4.2: Time series for the positions and the nature of the cyclone AILA, 2009 (Source: BMD).

| Date	Hour (UTC)	Latitude (^{0}E)	Longitude (^{0}N)	Nature of the storm
2305	0900	16.00	88.00	Depression
2305	1500	16.50	88.00	Depression
2405	0000	17.20	88.30	Depression
2405	0600	17.80	88.60	Deep depression
2405	0900	17.80	88.60	Deep depression
2405	1200	18.30	88.60	Cyclonic storm
2405	1800	18.80	88.60	Cyclonic storm
2405	2100	19.20	88.60	Cyclonic storm
2505	0000	19.40	88.60	Cyclonic storm
2505	0300	20.00	88.60	Cyclonic storm
2505	0600	21.60	88.30	Cyclonic storm
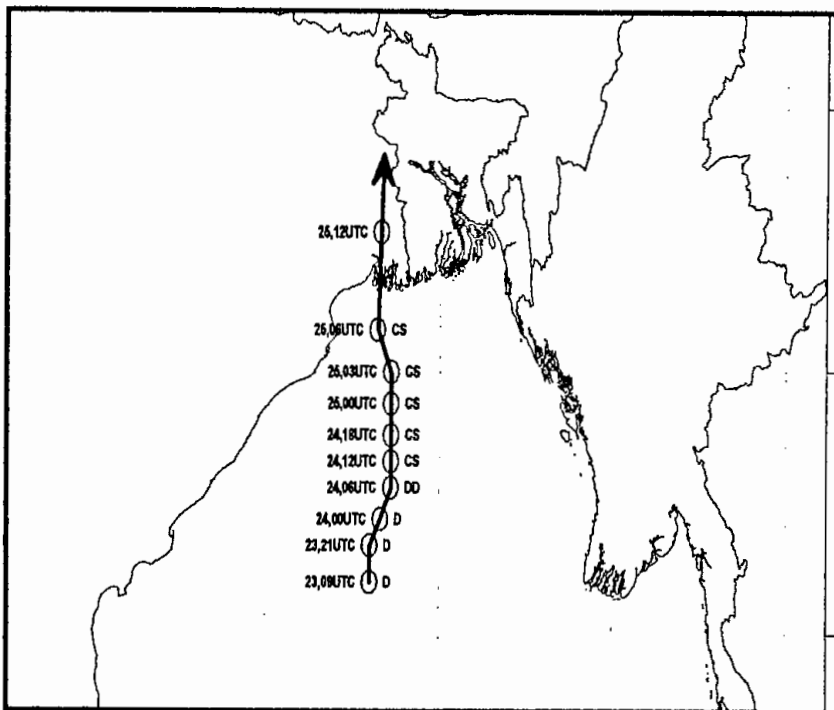
Figure 4.5: Observed track of cyclonic storm "AILA", May 2009 (BMD).

Maritime port of Mongla and the coastal districts of Bhola, Barisal, Patuakhali, Borguna, Pirozpur, Jhalokathi, Bagerhat, Khulna, Satkhira, Jessore and their offshore

islands and chars were under danger signal no. seven. On the other hand maritime ports of chittagong and cox's bazar and the coastal districts of cox's bazar, chittagong, noakhali, feni, laxmipur, comilla, chandpur and their offshore islands and chars were under danger signal number six. A maximum surge of about 06-08 ft was predicted to low lying areas of Bangladesh coast.

4.4 Results and Discussion

4.4.1 Cyclone of April, 1991

Due to the cyclone April, 1991 we have found the higher surge height in terms of air bubble at different locations in the coastal region of Bangladesh. At Hiron point the maximum surge height without air bubbles is 3.01m whereas the surge height is 3.05m when void fraction is 30% and with 70% void fraction the surge height is 3.10m (Fig. 4. 6). So, 1.33% sea level rise due to 30% void fraction and 2.99% sea level rise for 70% void fraction.
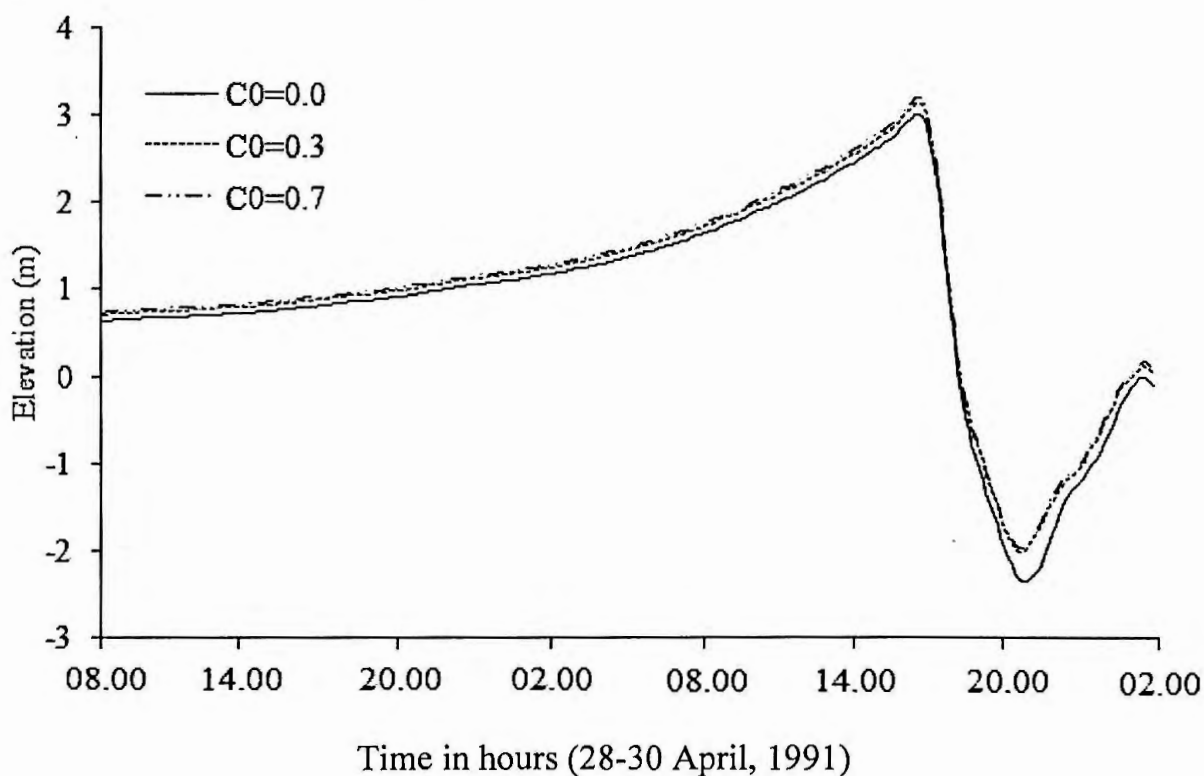

Time in hours (28-30 April, 1991)

Figure 4.6: Computed water levels with respect to the mean sea level at Hiron point of Bangladesh with $C_0 = 0.3$ and $C_0 = 0.7$ associated with the cyclone April, 1991.

At kuakata the maximum surge height without air bubbles is 3.52m whereas the surge height with 30% air bubbles is 3.57m and with 70% air bubbles the surge height is 3.63m (Fig. 4.7). So, 1.42% sea level rise due to 30% void fraction and 3.13% sea level rise for 70% void fraction.
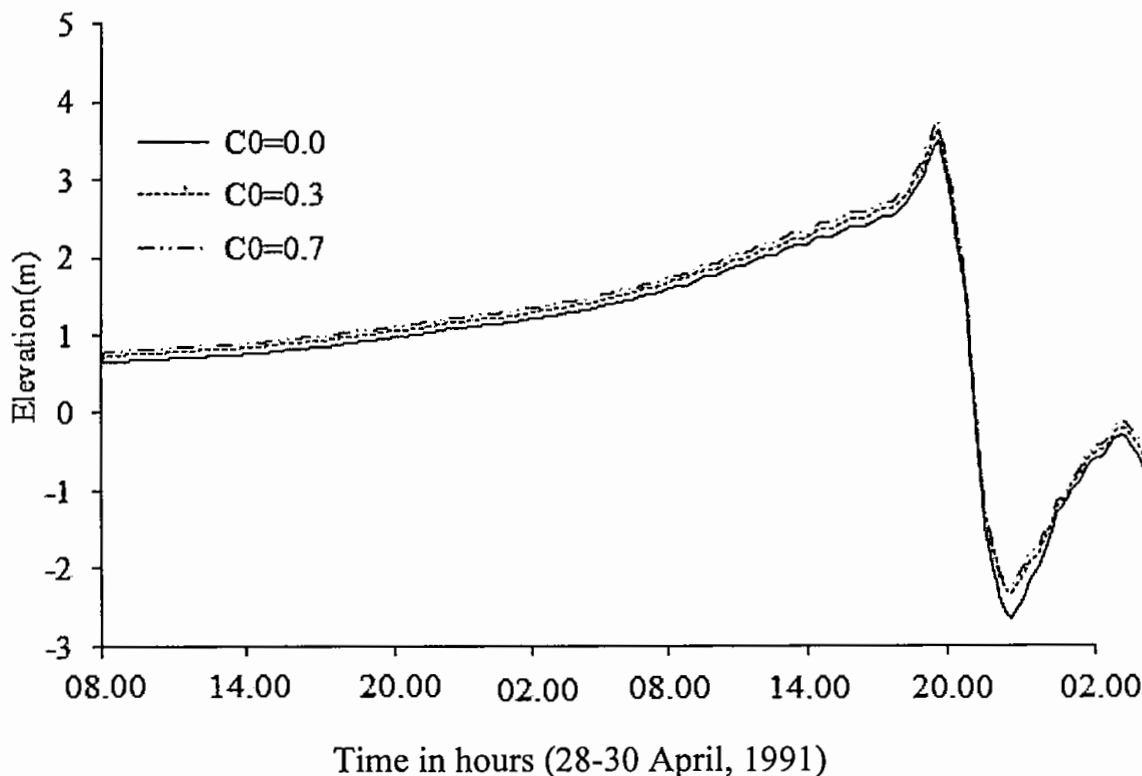

Figure 4.7: Computed water levels with respect to the mean sea level at Kuakata of Bangladesh with $C_0 = 0.3$ and $C_0 = 0.7$ associated with the cyclone April, 1991.

At Rangabali the maximum surge height without air bubbles is 4.18m whereas the surge height with 30% void fraction is 4.25m and with 70% void fraction the surge height is 4.35m (Fig. 4.8). So, 1.67% sea level rise due to 30% void fraction and 4.07% sea level rise for 70% void fraction.

At Char madras the maximum surge height without air bubbles is 5.18m whereas the surge height with 30% void fraction is 5.34m and with 70% void fraction the surge height is 5.54m (Fig. 4.9). So, 3.09% sea level rise due to 30% void fraction and 6.95% sea level rise for 70% void fraction.
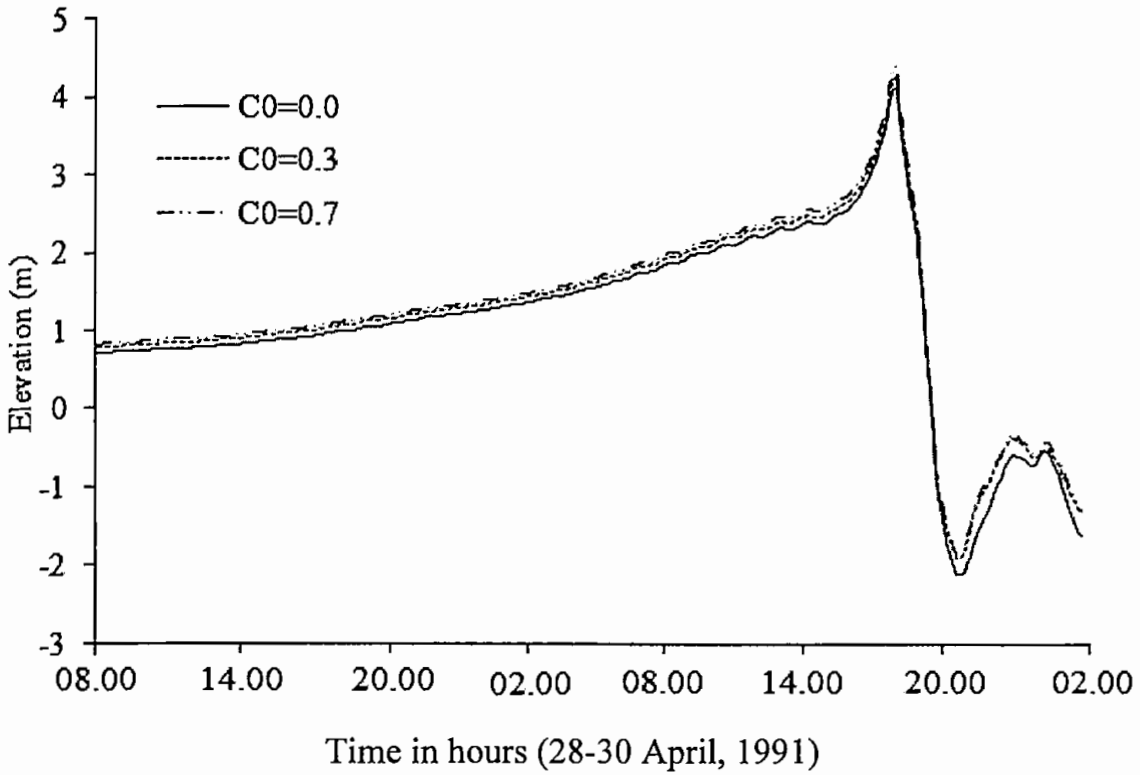
Figure 4.8: Computed water levels with respect to the mean sea level at Rangabali of Bangladesh with $C_0 = 0.3$ and $C_0 = 0.7$ associated with the cyclone April, 1991.
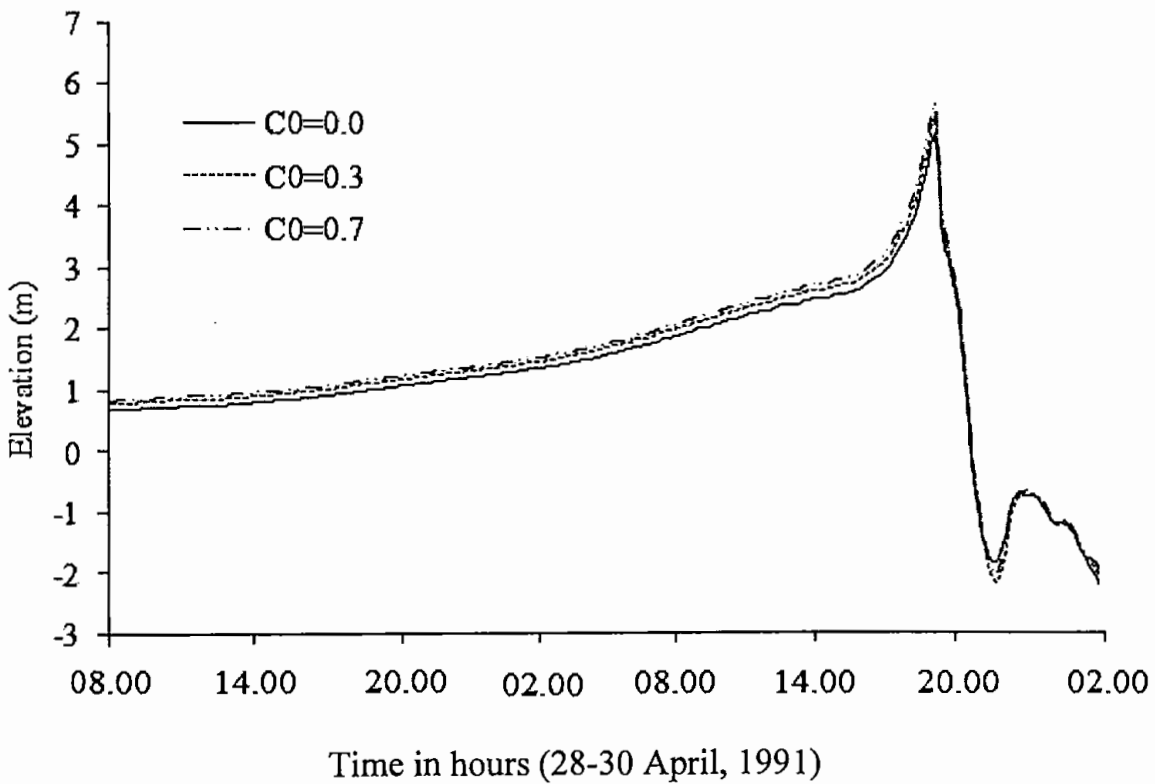

Figure 4.9: Computed water levels with respect to the mean sea level at Char madras of Bangladesh with $C_0 = 0.3$ and $C_0 = 0.7$ associated with the cyclone April, 1991.

At Char jabbar the maximum surge height without air bubbles is 5.88m whereas the surge height with 30% void fraction is 6.01m and with 70% void fraction the surge height is 6.18m (Fig. 4.10). So, 2.21% sea level rise due to 30% void fraction and 5.10% sea level rise for 70% void fraction.
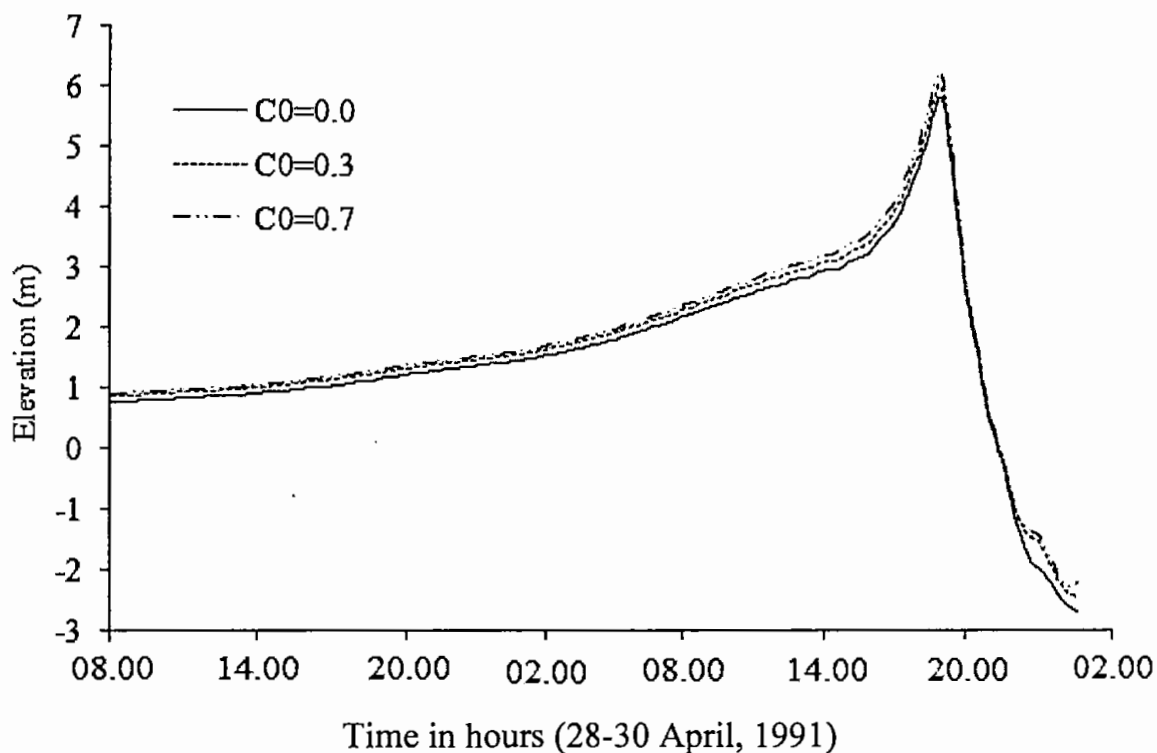

Figure 4.10: Computed water levels with respect to the mean sea level at Char jabbar of Bangladesh with $C_0 = 0.3$ and $C_0 = 0.7$ associated with the cyclone April, 1991.

At Char chenga the maximum surge height without air bubbles is 4.78m whereas the surge height with 30% void fraction is 4.94m and with 70% void fraction the surge height is 5.12m (Fig. 4.11). So, 3.35% sea level rise due to 30% void fraction and 7.11% sea level rise for 70% void fraction.

At Sandwip the maximum surge height without air bubbles is 5.08m whereas the surge height with 30% void fraction is 5.16m and with 70% void fraction the surge height is 5.26m (Fig. 4.12). So, 1.57% sea level rise due to 30% void fraction and 3.54% sea level rise for 70% void fraction.
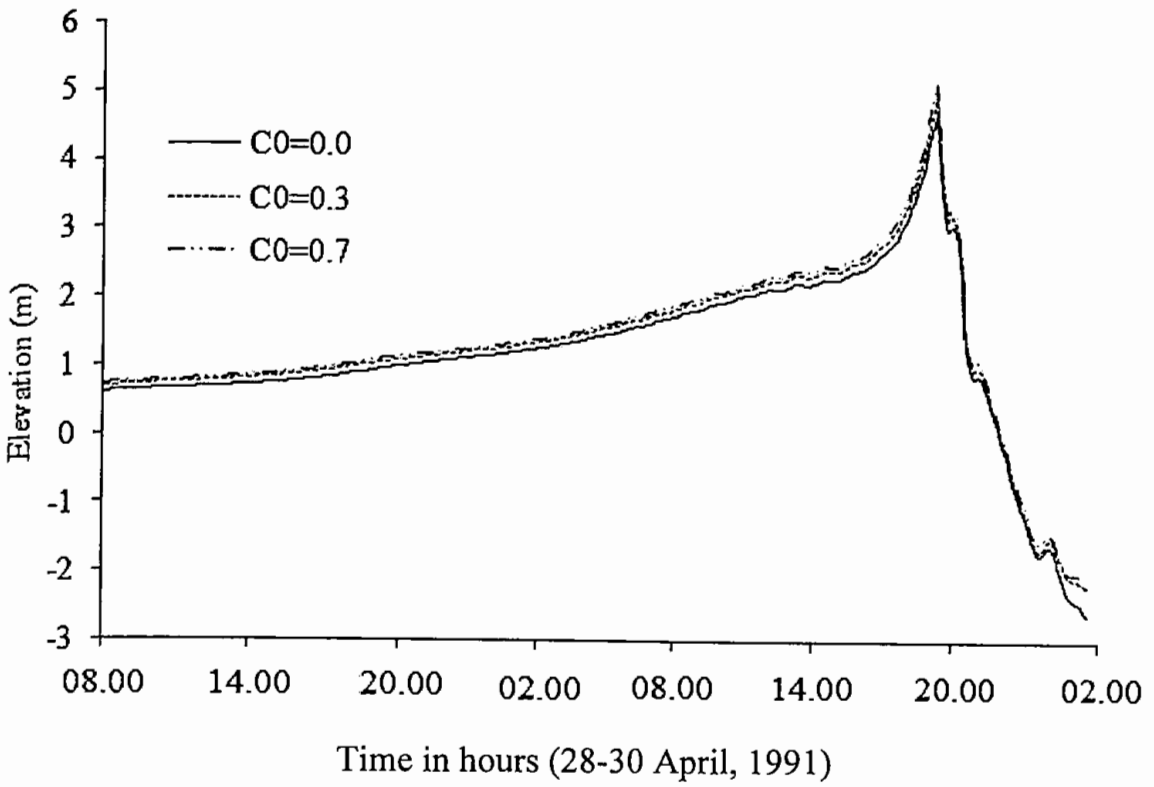
Figure 4.11: Computed water levels with respect to the mean sea level at Char chenga of Bangladesh with $C_0 = 0.3$ and $C_0 = 0.7$ associated with the cyclone April, 1991.
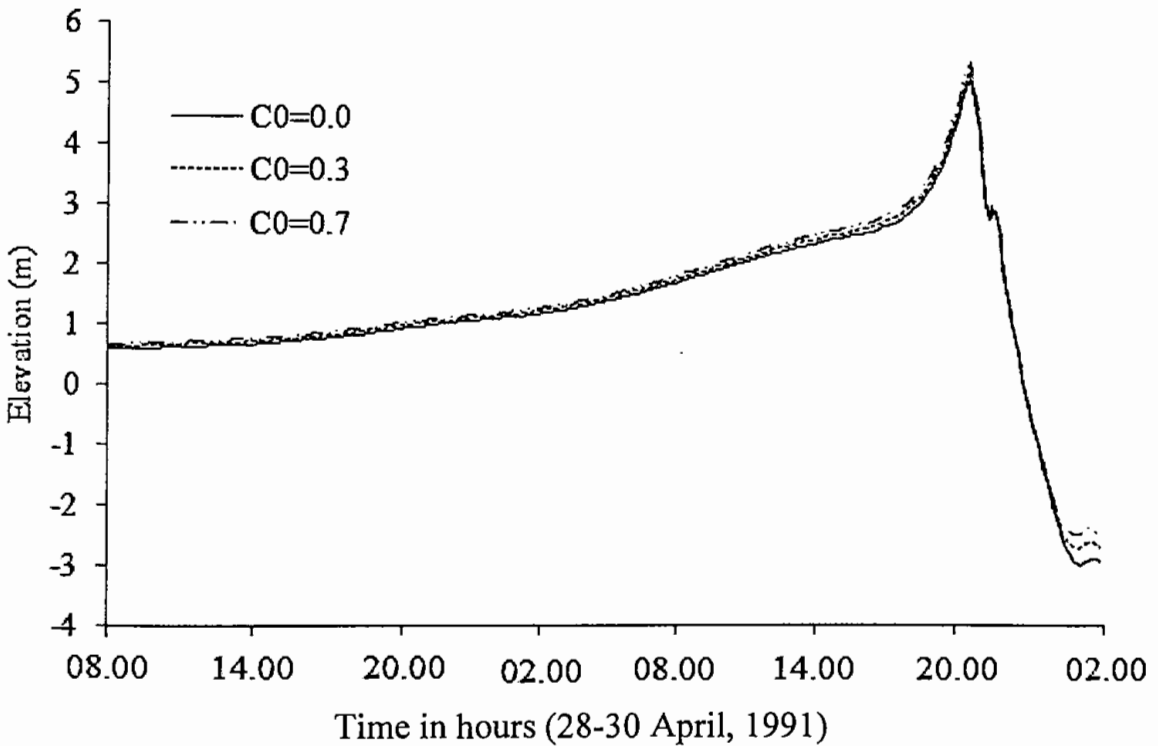

Figure 4.12: Computed water levels with respect to the mean sea level at Sandwip of Bangladesh with $C_0 = 0.3$ and $C_0 = 0.7$ associated with the cyclone April, 1991.

At Chittagang the maximum surge height without air bubbles is 5.15m whereas the surge height with 30% void fraction is 5.25m and with 70% void fraction the surge height is 5.37m (Fig. 4.13). So, 1.94% sea level rise due to 30% void fraction and 4.27% sea level rise for 70% void fraction.
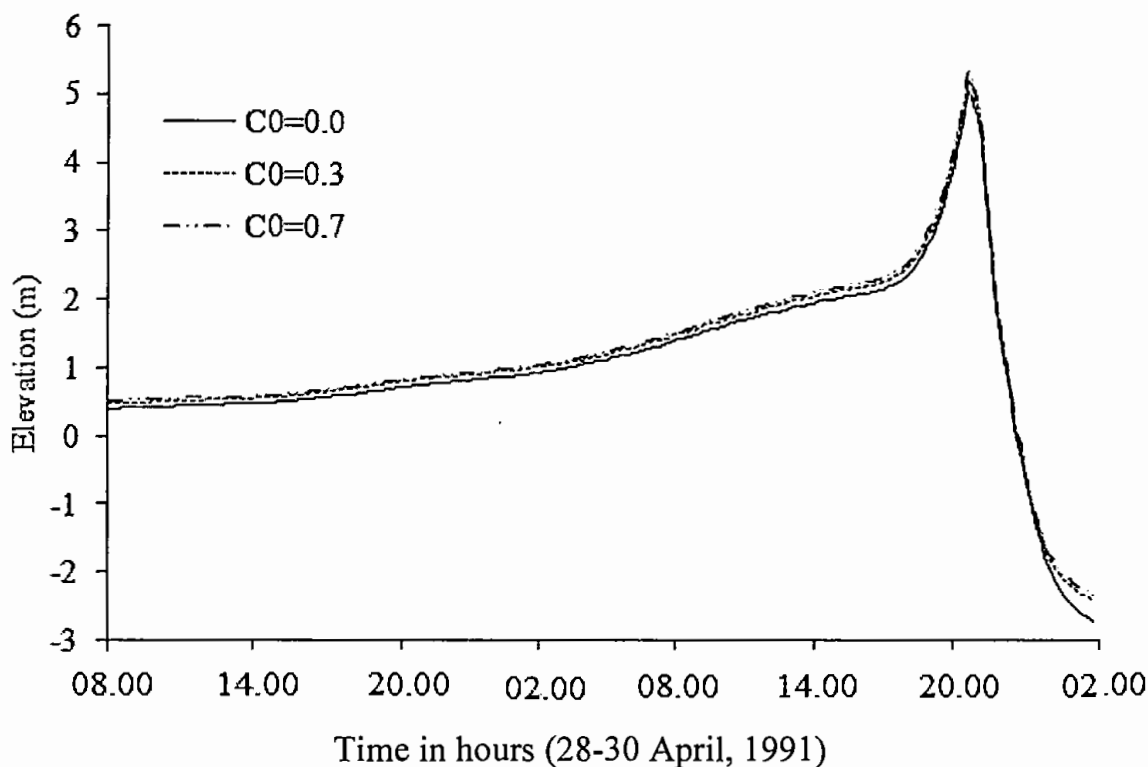

Figure 4.13: Computed water levels with respect to the mean sea level at Chittagang of Bangladesh with $C_0 = 0.3$ and $C_0 = 0.7$ associated with the cyclone April, 1991.

At Cox's bazar the maximum surge height without air bubbles is 2.17m whereas the surge height with 30% void fraction is 2.19m and with 70% void fraction the surge height is 2.22m (Fig. 4.14). So, 0.92% sea level rise due to 30% void fraction and 2.30% sea level rise for 70% void fraction.

At Companiganj the maximum surge height without air bubbles is 5.89m whereas the surge height with 30% void fraction is 5.99m and with 70% void fraction the surge height is 6.17m (Fig. 4.15). So, 1.70% sea level rise due to 30% void fraction and 4.75% sea level rise for 70% void fraction.
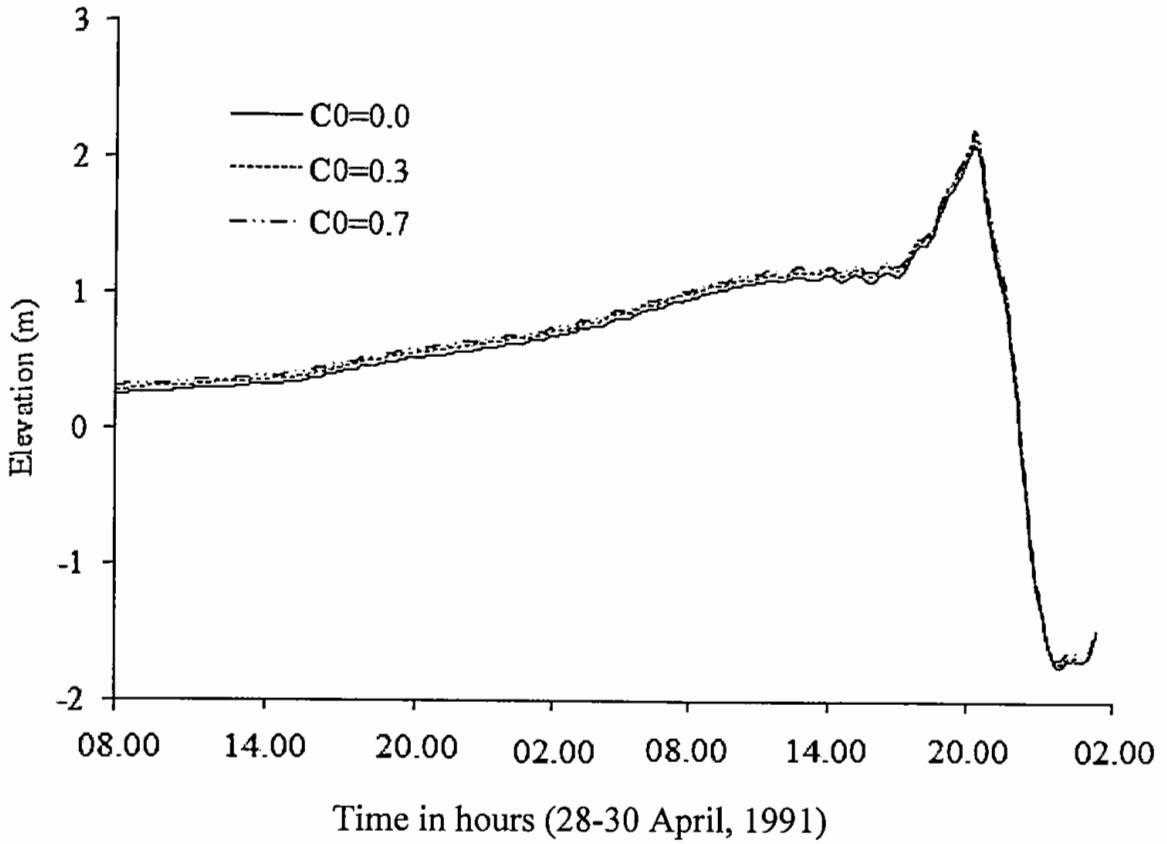
Figure 4.14: Computed water levels with respect to the mean sea level at Cox's bazar of Bangladesh with $C_0 = 0.3$ and $C_0 = 0.7$ associated with the cyclone April, 1991.
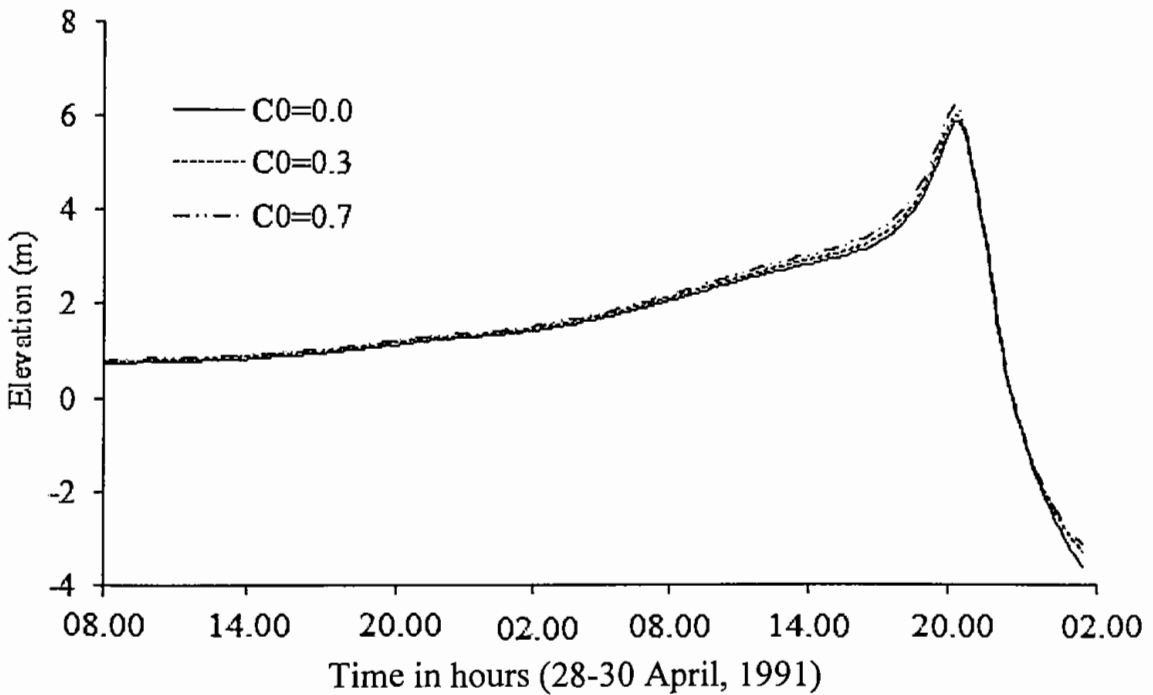

Figure 4.15: Computed water levels with respect to the mean sea level at Compani- ganj of Bangladesh with $C_0 = 0.3$ and $C_0 = 0.7$ associated with the cyclone April, 1991

.

At Tiger point the maximum surge height without air bubbles is 4.03m whereas the surge height with 30% void fraction is 4.09m and with 70% void fraction the surge height is 4.18m (Fig. 4.16). So, 1.49% sea level rise due to 30% void fraction and 3.72% sea level rise for 70% void fraction.

Figure 4.16: Computed water levels with respect to the mean sea level at Tiger point of Bangladesh with $C_0 = 0.3$ and $C_0 = 0.7$ associated with the cyclone April, 1991.

At Kotoali the maximum surge height without air bubbles is 5.49m whereas the surge height with 30% void fraction is 5.57m and with 70% void fraction the surge height is 5.67m (Fig. 4.17). So, 1.46% sea level rise due to 30% void fraction and 3.28% sea level rise for 70% void fraction.
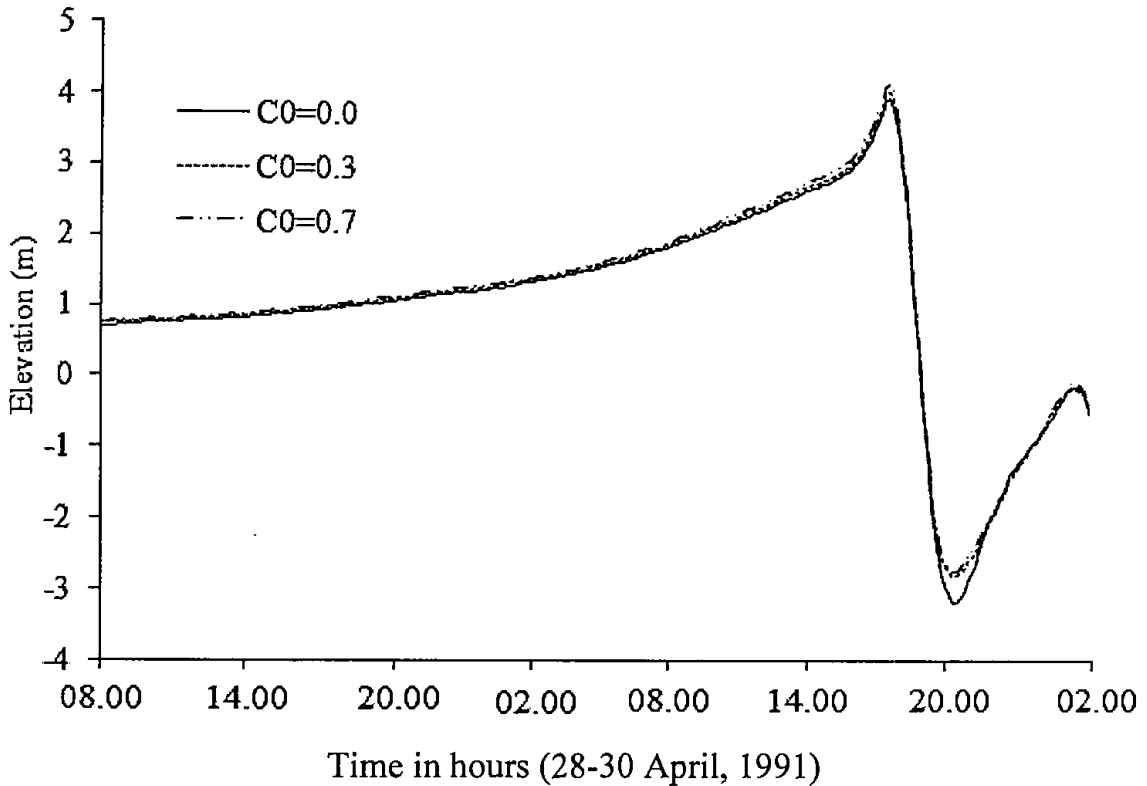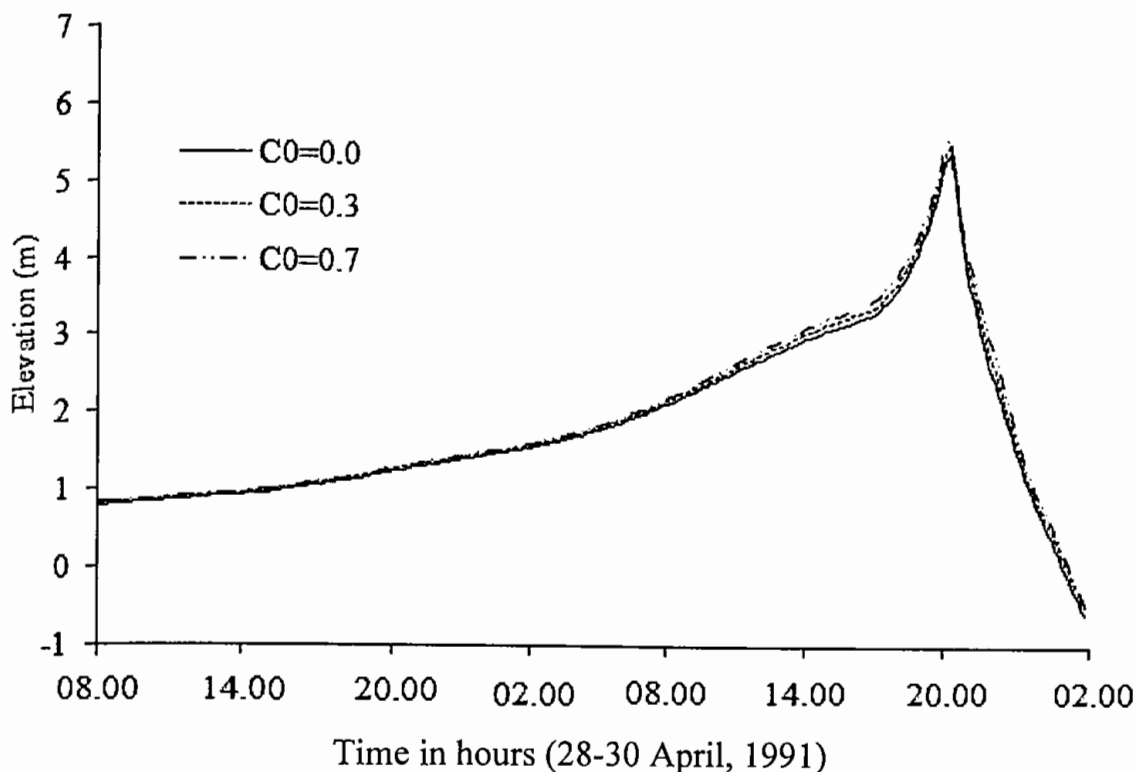
Figure 4.17: Computed water levels with respect to the mean sea level at Kotoali of Bangladesh with $C_0 = 0.3$ and $C_0 = 0.7$ associated with the cyclone April, 1991.

The time series of the over-all surge levels with 30% void fraction associated with the storm April, 1991 at 9 coastal and island locations from Hiron point to Cox's bazaar is depicted (Figs. 4.18 and 4.19). It has been seen that the maximum surge level is increasing with time due to air bubbles when approaches towards coast and the air bubbles affects the wave height more for larger wave height. At every location, the peak surge is attained before the time of land fall of the storm. This is also our expectation, as the circulatory wind intensity is highest along the coast when the storm reaches near the coast. Due to unavailablity of data we could not compare comprehensively and thoroughly our computed time series elevation data to the observed one. Maximum surge level calculated by the model at the Companiganj coast associated with the storm April, 1991 was found to be nearly 5.99 m and minimum surge level at Cox's bazar with 30% void fraction also the maximum surge height is calculated at Companiganj nearly 6.17m and minimum at Cox's bazaar with 70% void fraction as shown in Fig. (4.20).

Figure4.18: Computed water levels with respect to the mean sea level due to surge at some coastal and island locations of Bangladesh with $C_0 = 0.3$ associated with the cyclone April, 1991.
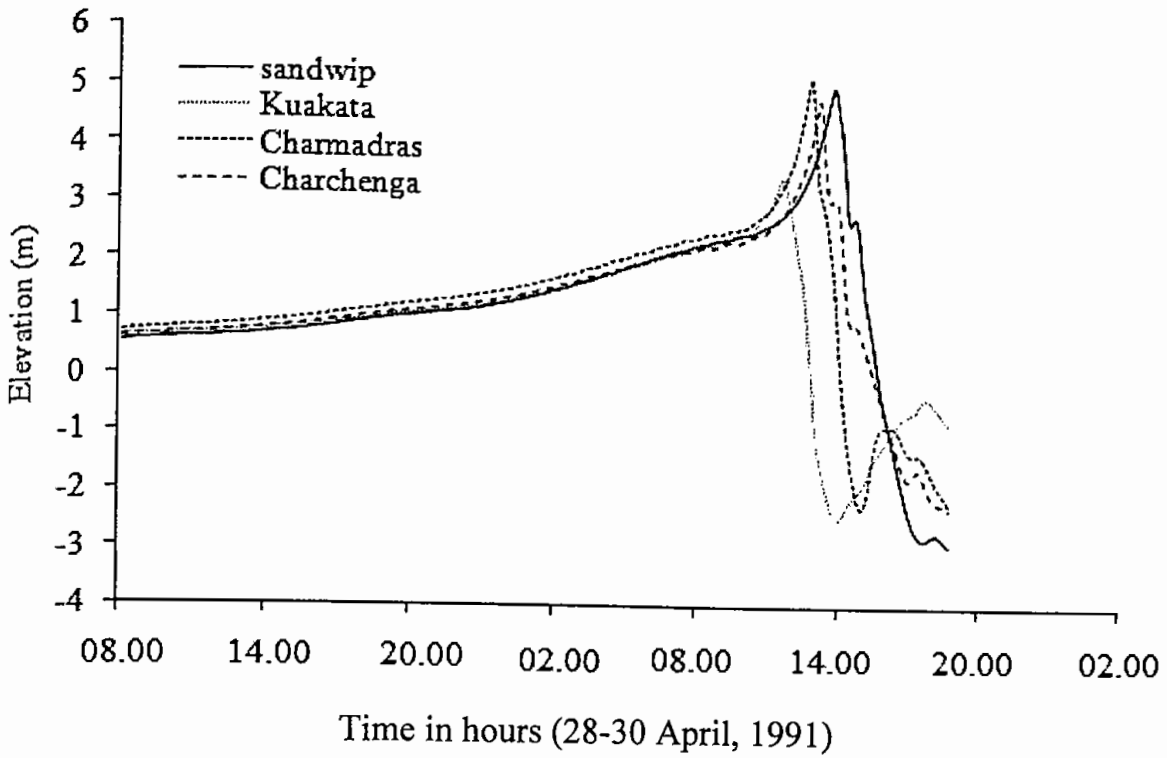

Figure 4.19: Computed water levels with respect to the mean sea level due to surge at some coastal and island locations of Bangladesh with $C_0 = 0.3$ associated with the cyclone April, 1991.
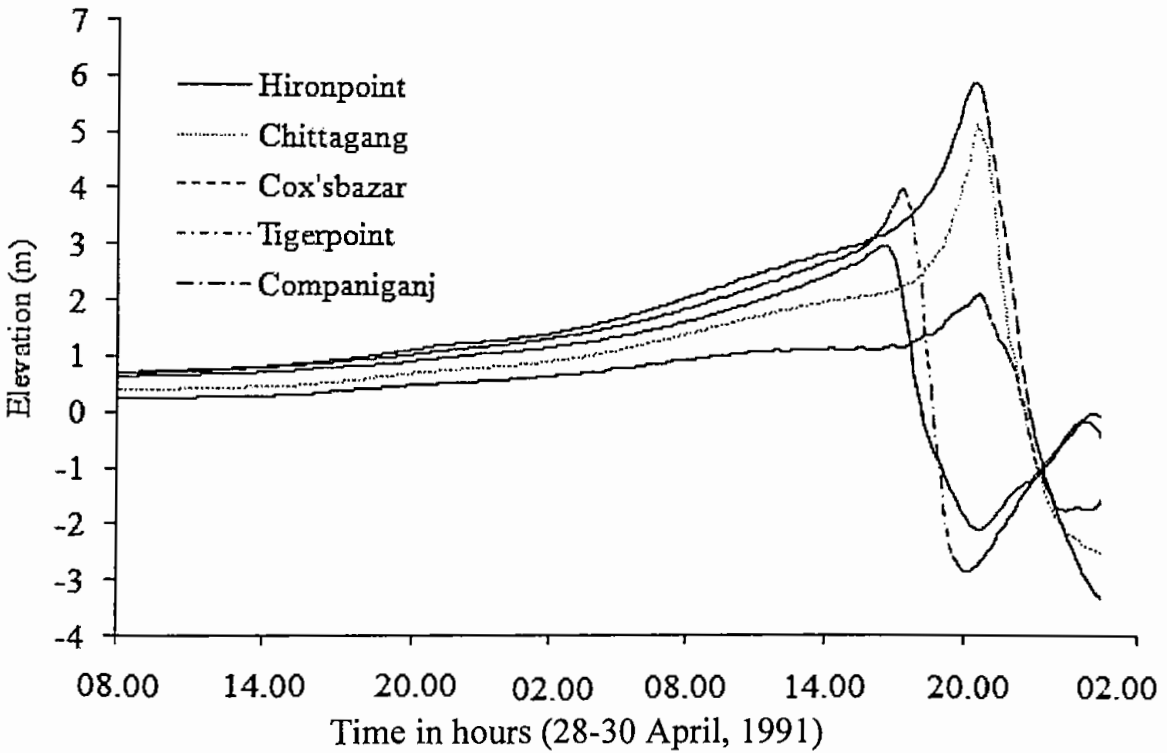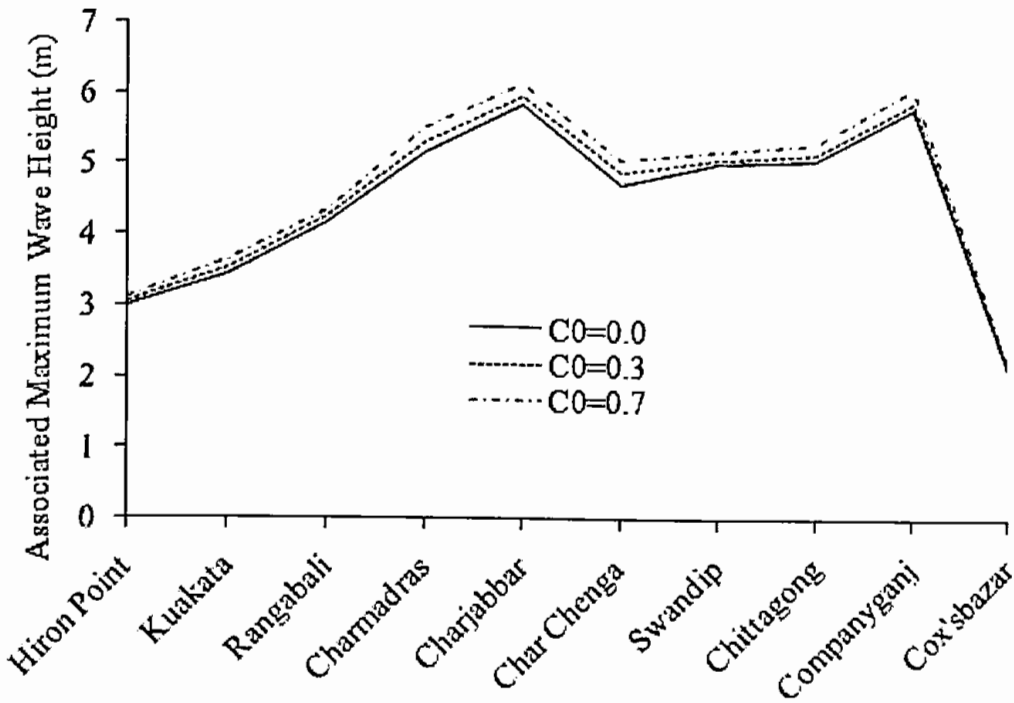
70

Figure 4.20: Peak water levels (overall) at some coastal and island locations of Bangladesh due to the cyclone April, 1991.

4.4.2 Cyclone AILA, 2009

We have found the higher surge height in terms of air bubble at different locations in the coastal region of Bangladesh due to cyclone AILA, 2009. At the Hiron point the maximum surge height without air bubbles is 2.87m whereas the surge height with 30% void fraction is 2.90m and with 70% void fraction the surge height is 2.94m (Fig. 4.21). So, 1.05% sea level rise due to 30% void fraction and 2.44% sea level rise for 70% void fraction.

At Kuakata the maximum surge height without air bubbles is 2.53m whereas the surge height with 30% void fraction is 2.55m and with 70% void fraction the surge height is 2.58m (Fig. 4.22). So, 0.8% sea level rise due to 30% void fraction and 1.98% sea level rise for 70% void fraction.

At Rangabali the maximum surge height without air bubbles is 2.26m whereas the surge height with 30% void fraction is 2.28m and with 70% void fraction the surge height is 2.31m (Fig. 4.23). So, 0.9% sea level rise due to 30% void fraction and 2.21% sea level rise for 70% void fraction.
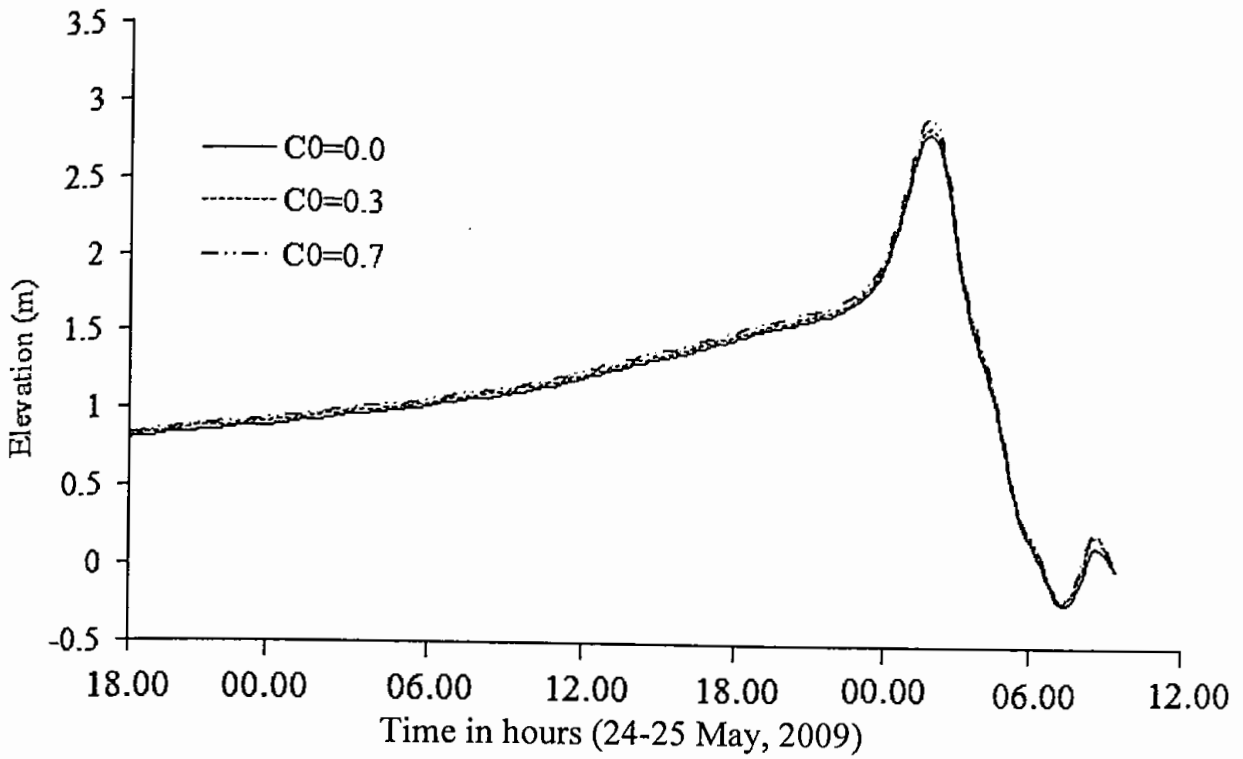
71

Figure 4.21: Computed water levels with respect to the mean sea level at Hiron point of Bangladesh with $C_0 = 0.3$ and $C_0 = 0.7$ associated with the storm AILA, 2009.
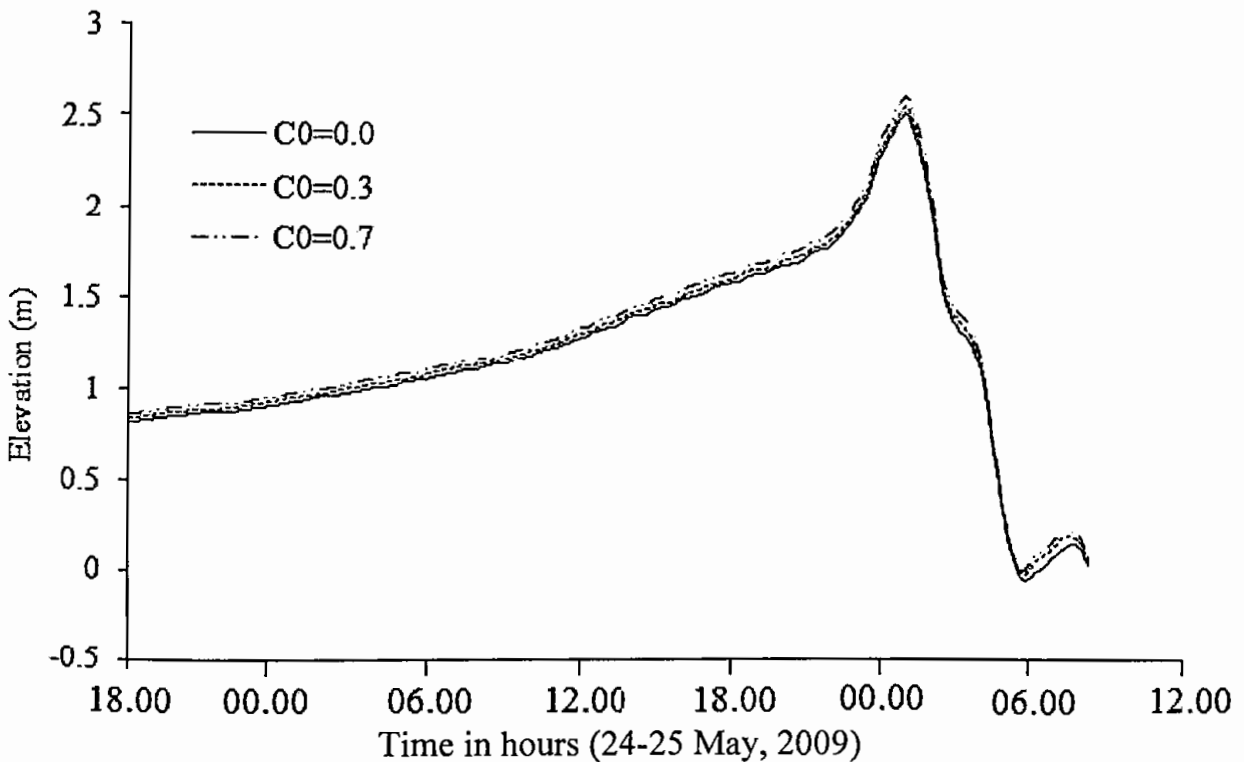

Figure 4.22: Computed water levels with respect to the mean sea level at Kuakata point of Bangladesh with $C_0 = 0.3$ and $C_0 = 0.7$ associated with the storm AILA, 2009.

Figure 4.23: Computed water levels with respect to the mean sea level at Rangabali of Bangladesh with $C_0 = 0.3$ and $C_0 = 0.7$ associated with the storm AILA, 2009.

At Char madras the maximum surge height without air bubbles is 2.35m whereas the surge height with 30% void fraction is 2.38m and with 70% void fraction the surge height is 2.42m (Fig. 4.24). So, 1.3% sea level rise due to 30% void fraction and 2.98% sea level rise for 70% void fraction. At char jabbar the maximum surge height without air bubbles is 3.12m whereas the surge height with 30% void fraction is 3.19m and with 70% void fraction the surge height is 3.27m (Fig. 4.25). So, 2.24% sea level rise due to 30% void fraction and 4.81% sea level rise for 70% void fraction. At char chenga the maximum surge height without air bubbles is 2.28m whereas the surge height with 30% void fraction is 2.31m and with 70% void fraction the surge height is 2.35m (Fig. 4.26). So, 1.32% sea level rise due to 30% void fraction and 3.07% sea level rise for 70% void fraction.

Figure 4.24: Computed water levels with respect to the mean sea level at Char madras of Bangladesh with $C_0 = 0.3$ and $C_0 = 0.7$ associated with the storm AILA, 2009.

Figure 4.25: Computed water levels with respect to the mean sea level at Char jabbar of Bangladesh with $C_0 = 0.3$ and $C_0 = 0.7$ associated with the storm AILA, 2009.
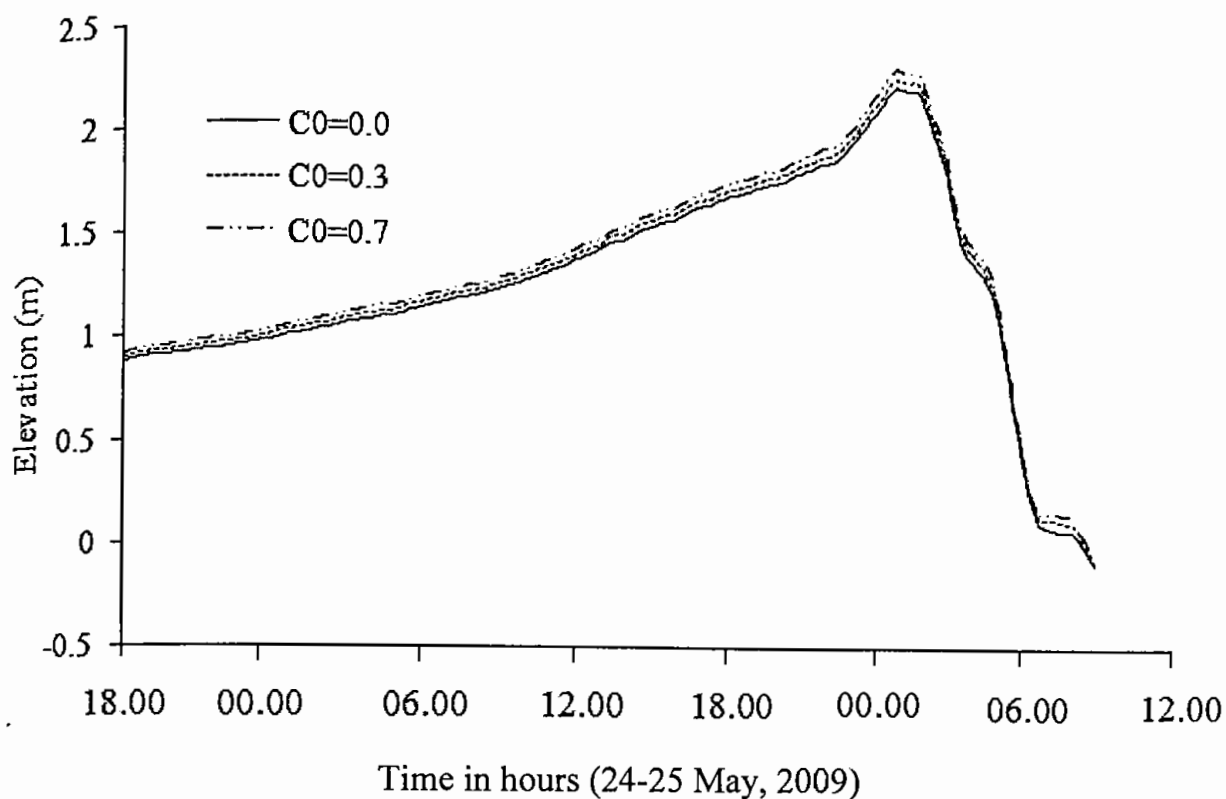
Figure 4.26: Computed water levels with respect to the mean sea level at Char chenga of Bangladesh with $C_0 = 0.3$ and $C_0 = 0.7$ associated with the storm AILA, 2009.

At Sandwip the maximum surge height without air bubbles is 2.82m whereas the surge height with 30% void fraction is 2.87m and with 70% void fraction the surge height is 2.93m (Fig. 4.27). So, 1.77% sea level rise due to 30% void fraction and 3.90% sea level rise for 70% void fraction.

At Chittagang the maximum surge height without air bubbles is 2.55m whereas the surge height with 30% void fraction is 2.58m and with 70% void fraction the surge height is 2.63m (Fig. 4.28). So, 1.18% sea level rise due to 30% void fraction and 3.14% sea level rise for 70% void fraction.
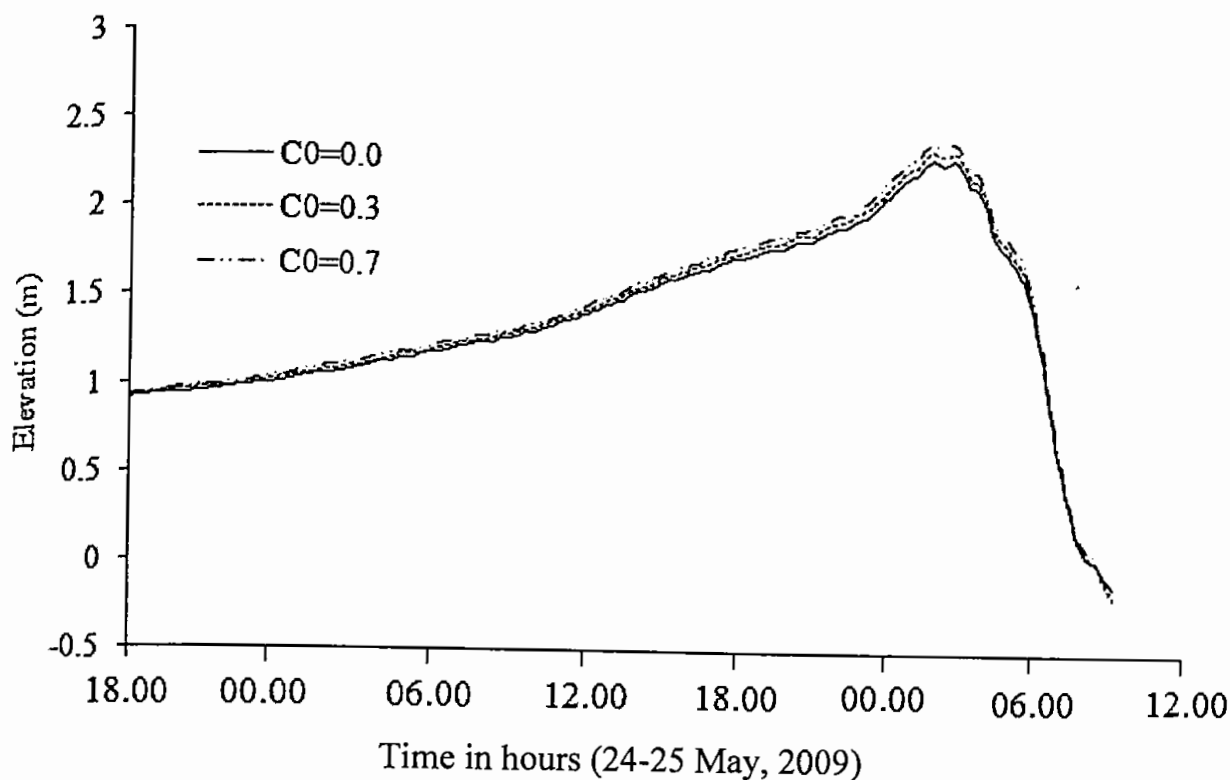
Figure 4.27: Computed water levels with respect to the mean sea level at Sandwip of Bangladesh with $C_0 = 0.3$ and $C_0 = 0.7$ associated with the storm AILA, 2009.

Figure 4.28: Computed water levels with respect to the mean sea level at Chittagang of Bangladesh with $C_0 = 0.3$ and $C_0 = 0.7$ associated with the storm AILA, 2009.
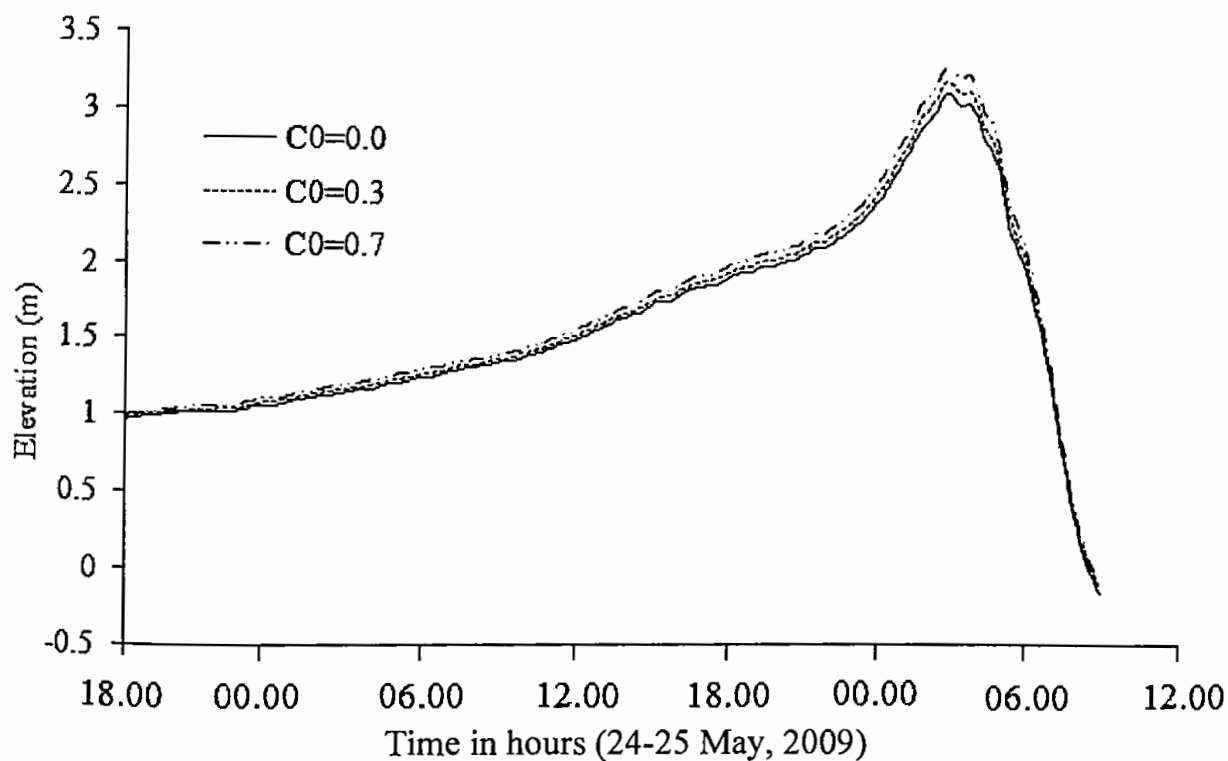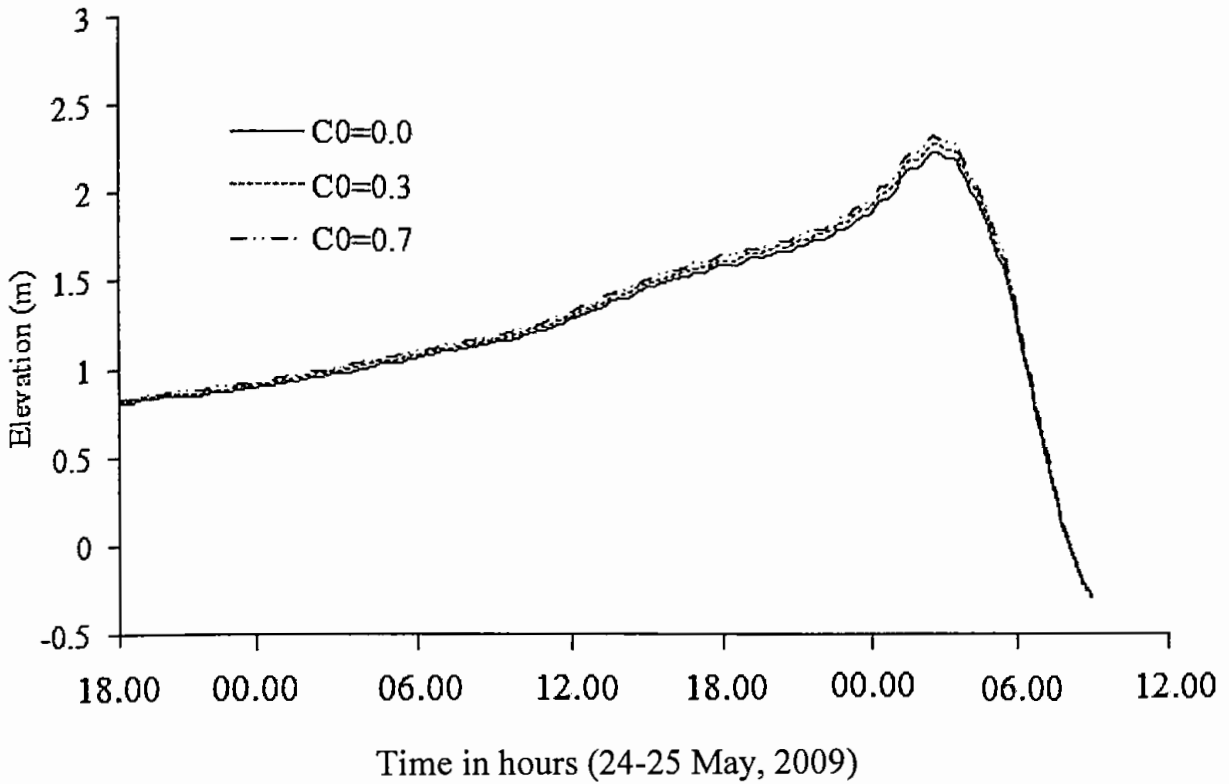
At Companiganj the maximum surge height without air bubbles is 3.46m whereas the surge height with 30% void fraction is 3.54m and with 70% void fraction the surge height is 3.64m (Fig. 4.29). So, 2.31% sea level rise due to 30% void fraction and 5.20% sea level rise for 70% void fraction.

Figure 4.29: Computed water levels with respect to the mean sea level at Companiganj of with $C_0 = 0.3$ and $C_0 = 0.7$ associated with the storm AILA, 2009.

At Tiger point the maximum surge height without air bubbles is 3.01m whereas the surge height with 30% void fraction is 3.05m and with 70% void fraction the surge height is 3.09m (Fig. 4.30). So, 1.33% sea level rise due to 30% void fraction and 2.66% sea level rise for 70% void fraction.

At Kotoali the maximum surge height without air bubbles is 3.36m whereas the surge height with 30% void fraction is 3.43m and with 70% void fraction the surge height is 3.53m (Fig. 4.31). So, 2.08% sea level rise due to 30% void fraction and 5.06% sea level rise for 70% void fraction
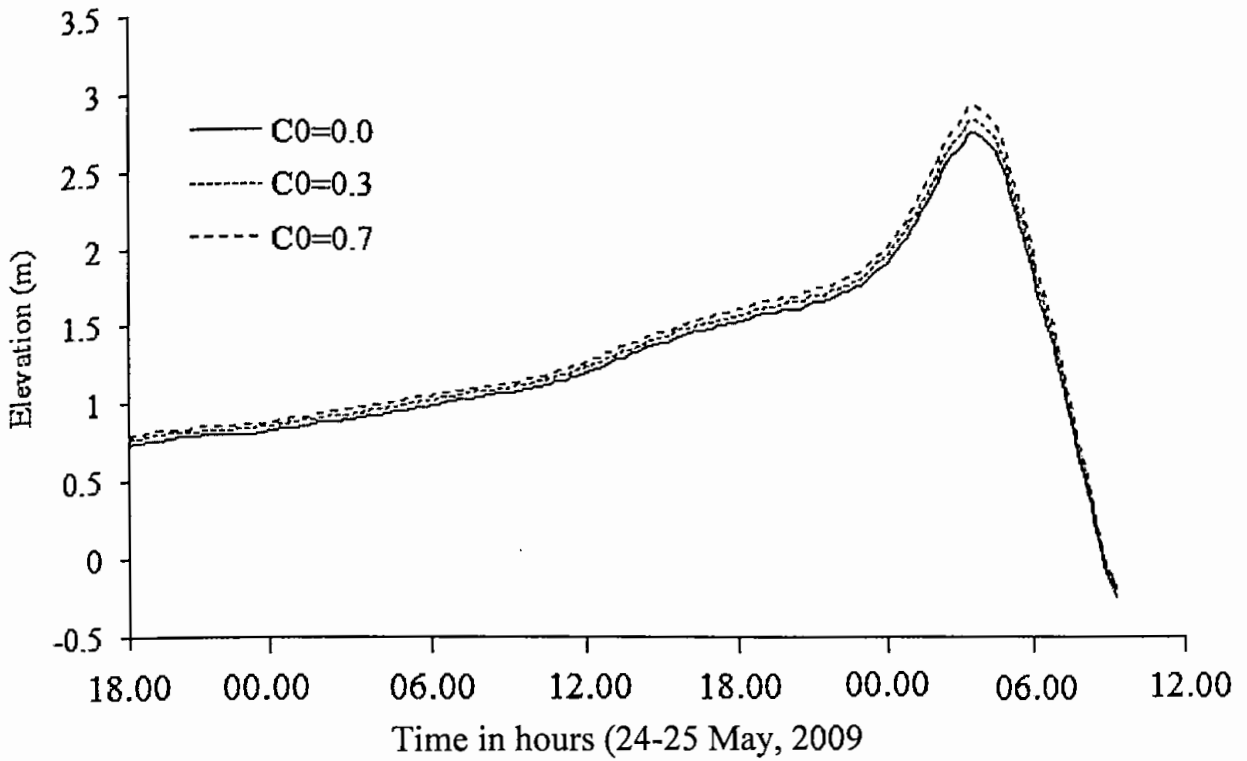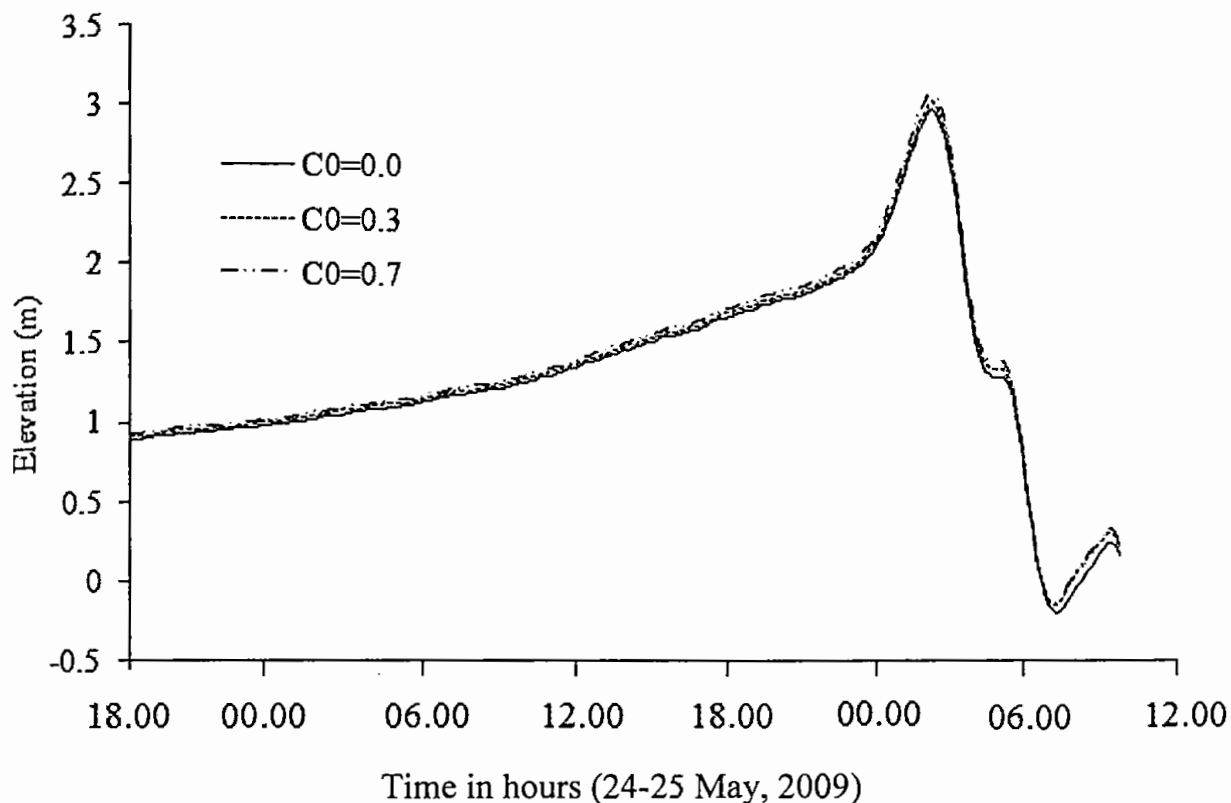
Figure 4.30: Computed water levels with respect to the mean sea level at Tiger point of with $C_0 = 0.3$ and $C_0 = 0.7$ associated with the storm AILA, 2009.
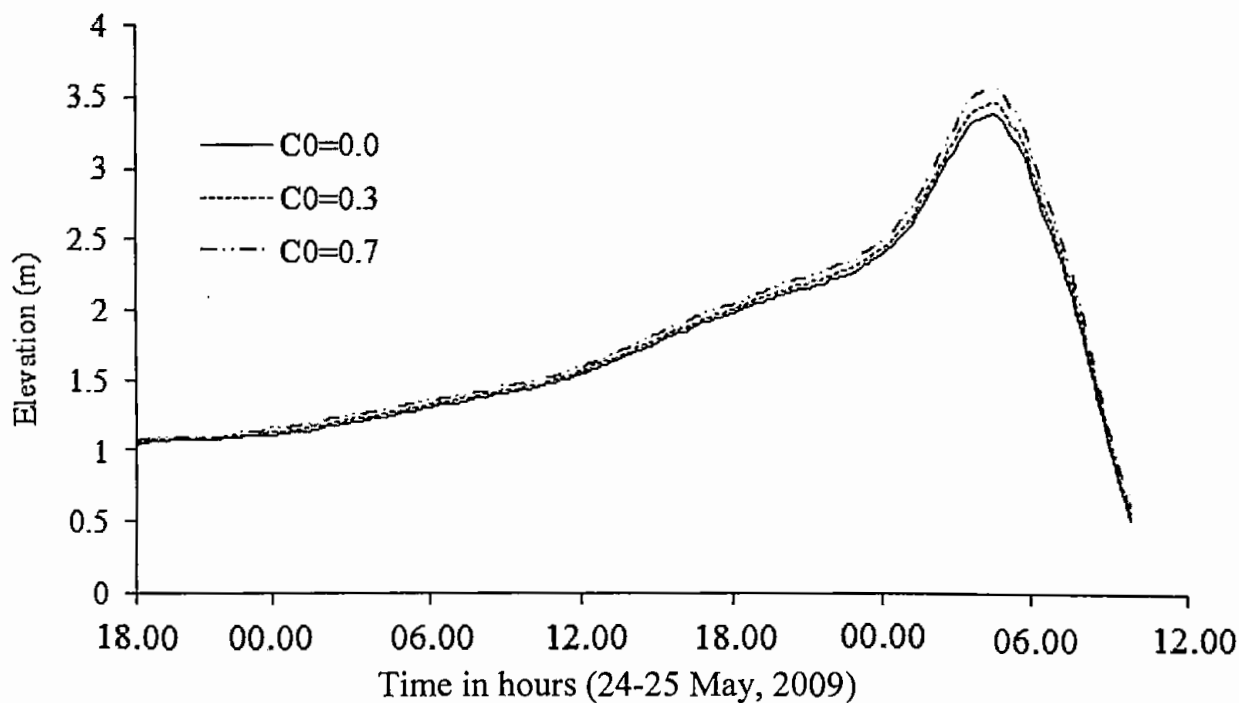
Figure 4.31: Computed water levels with respect to the mean sea level at Kotoali of with $C_0 = 0.3$ and $C_0 = 0.7$ associated with the storm AILA, 2009.

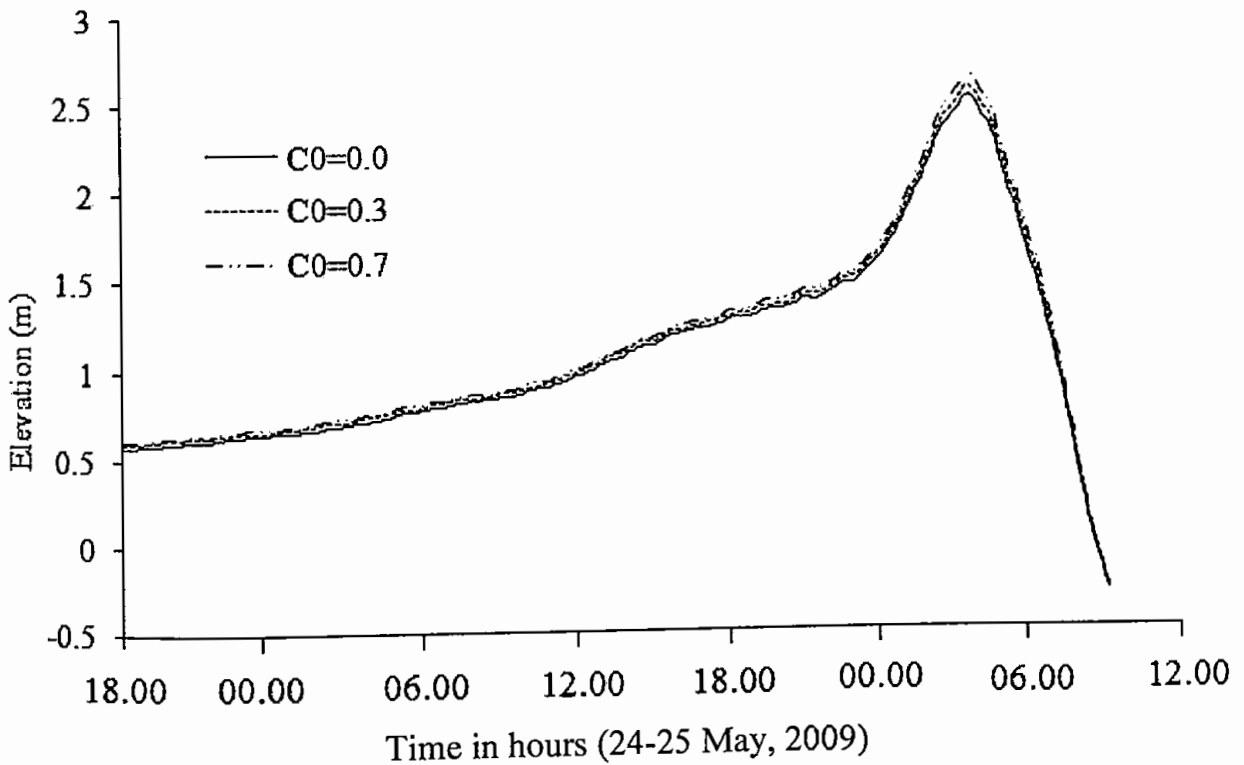At Cox's bazar the maximum surge height without air bubbles is 1.28m whereas the surge height with 30% void fraction is 1.29m and with 70% void fraction the surge height is 1.30m (Fig. 4.32). So, 0.78% sea level rise due to 30% void fraction and 1.56% sea level rise for 70% void fraction.
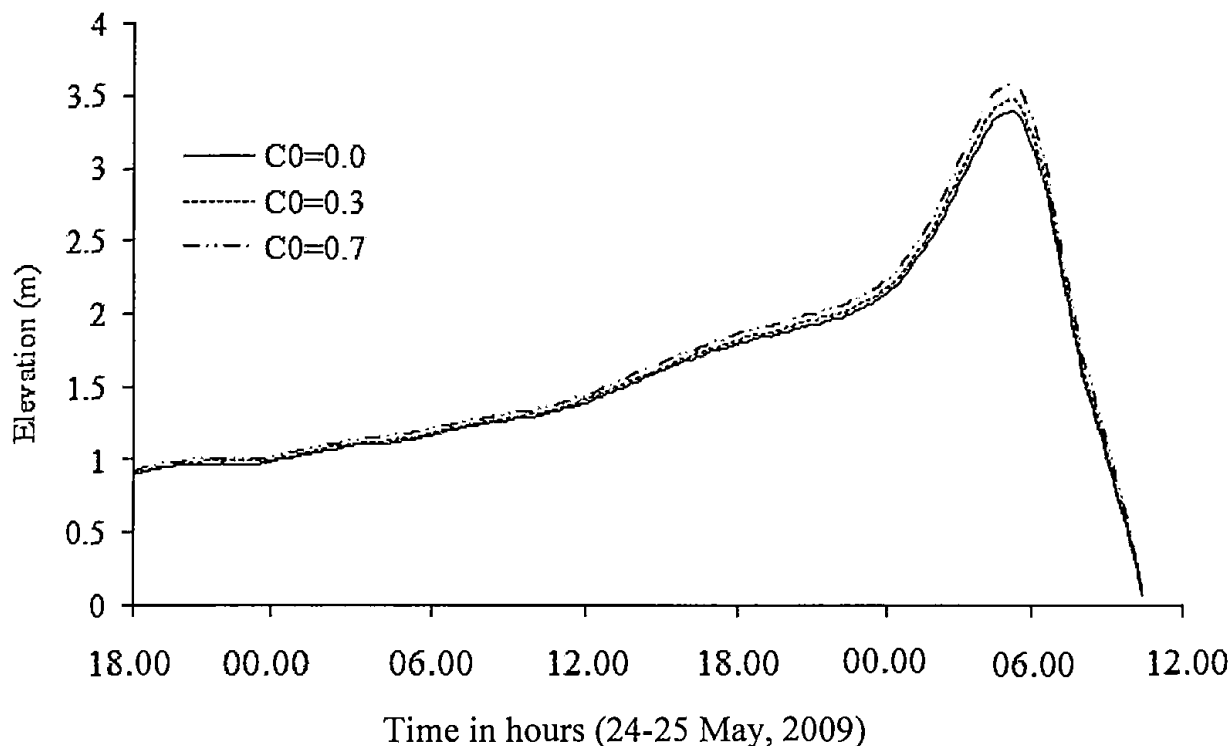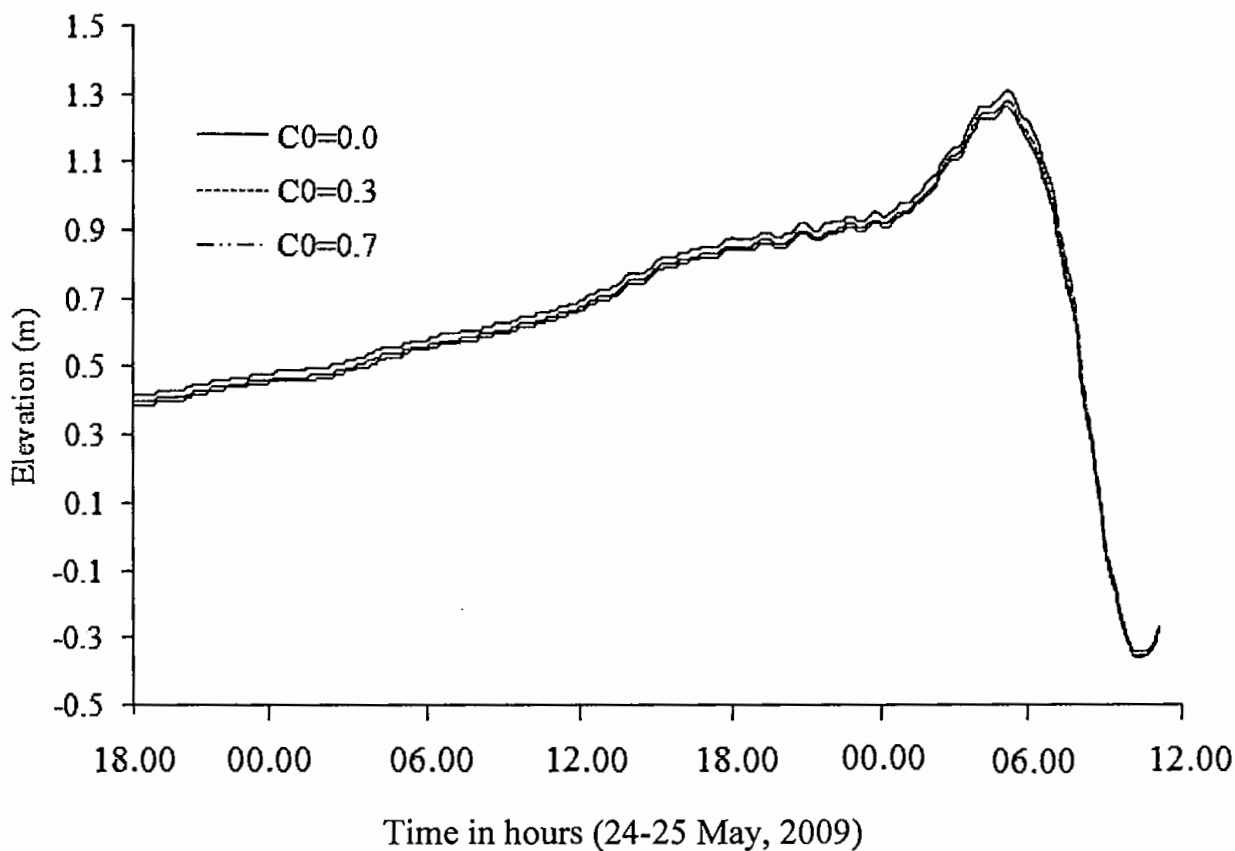

Figure 4.32: Computed water levels with respect to the mean sea level at Cox's bazar of with $C_0 = 0.3$ and $C_0 = 0.7$ associated with the storm AILA, 2009.

The time series of the over-all surge levels with 30% void fraction associated with the storm AILA, 2009 at 9 coastal and island locations from Rangabali to Cox's bazaar is depicted (Figs. 4.33 and 4.34). It has been seen that the maximum surge level is increasing with time due to air bubbles when approaches towards coast and the air bubbles affects the wave height more for larger wave height. At every location, the peak surge is attained before the time of land fall of the storm. This is also our expectation, as the circulatory wind intensity is highest along the coast when the

storm reaches near the coast. Due to unavailablity of data we could not compare comprehensively and thoroughly our computed time series elevation data to the observed one.
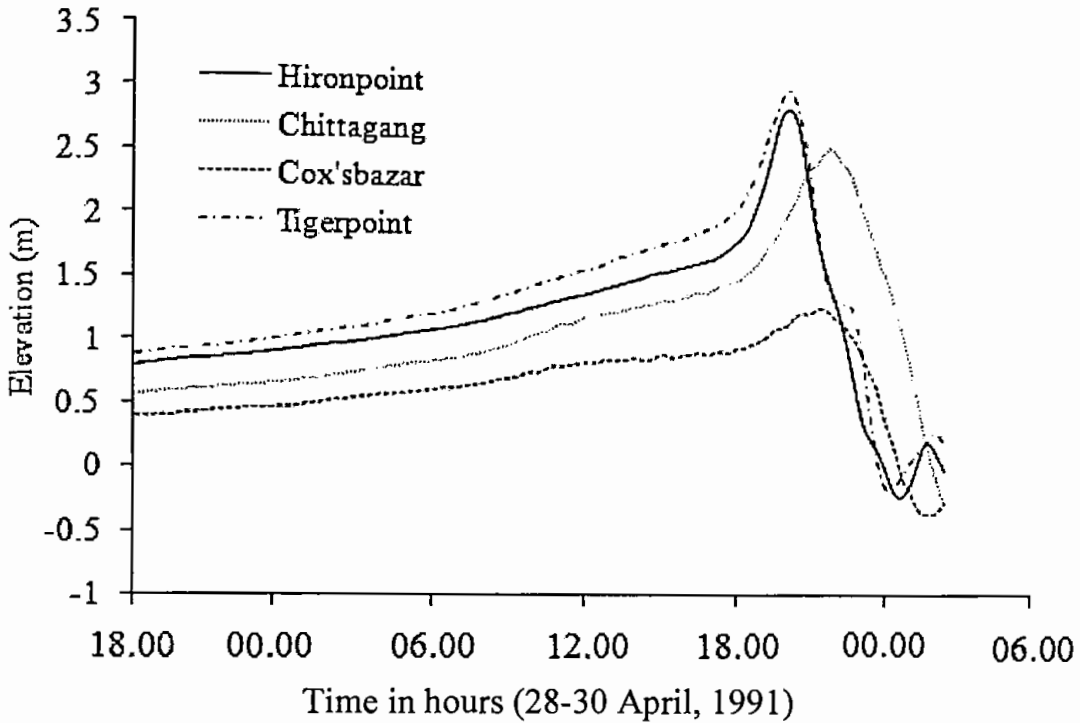
Figure4.33: Computed water levels with respect to the mean sea level due to surge at some coastal and island locations of Bangladesh with $C_0 = 0.3$ associated with the cyclone AILA, 2009.

Maximum surge level calculated by the model at the Companiganj coast associated with the storm AILA, 2009 is found to be nearly 3.54m and minimum surge level at Cox's bazar is nearly 1.29 with 30% void fraction. Furthermore, the maximum surge height is calculated at Companiganj nearly 3.64m and minimum at cox's bazaar nearly 1.3m with 70% void fraction as shown in Fig. (4.35).
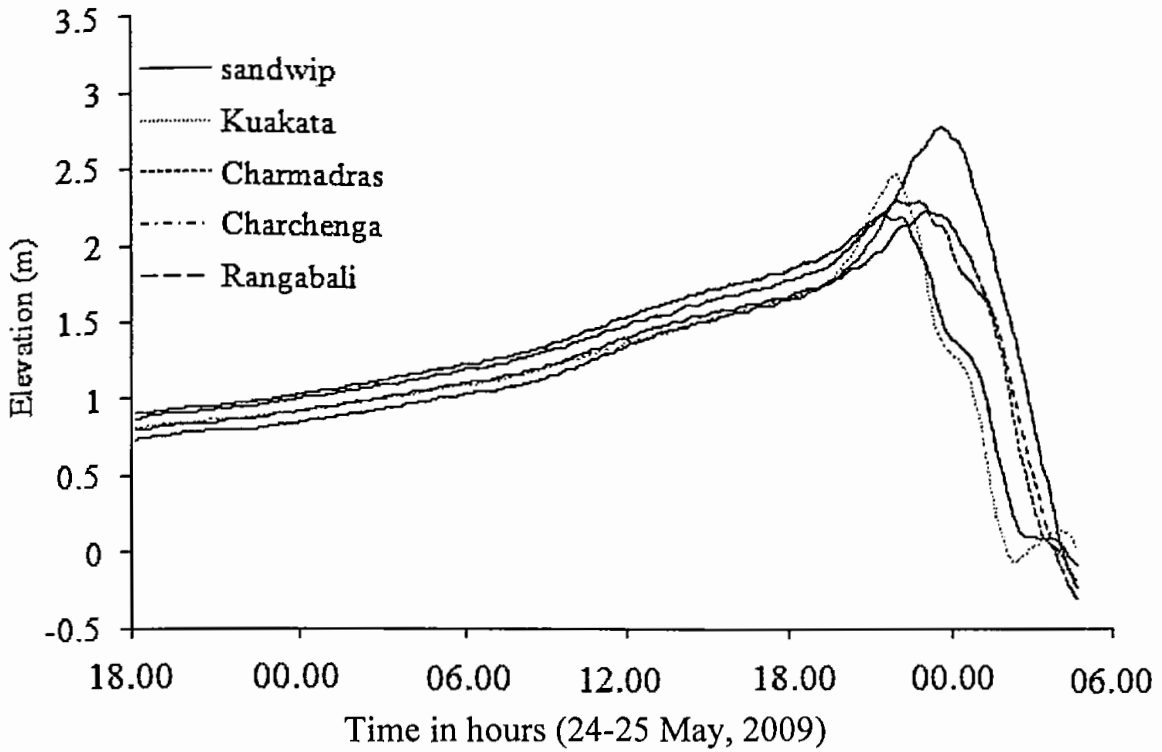
Figure4.34: Computed water levels with respect to the mean sea level due to surge at some coastal and island locations of Bangladesh with $C_0 = 0.3$ associated with the cyclone AILA, 2009.
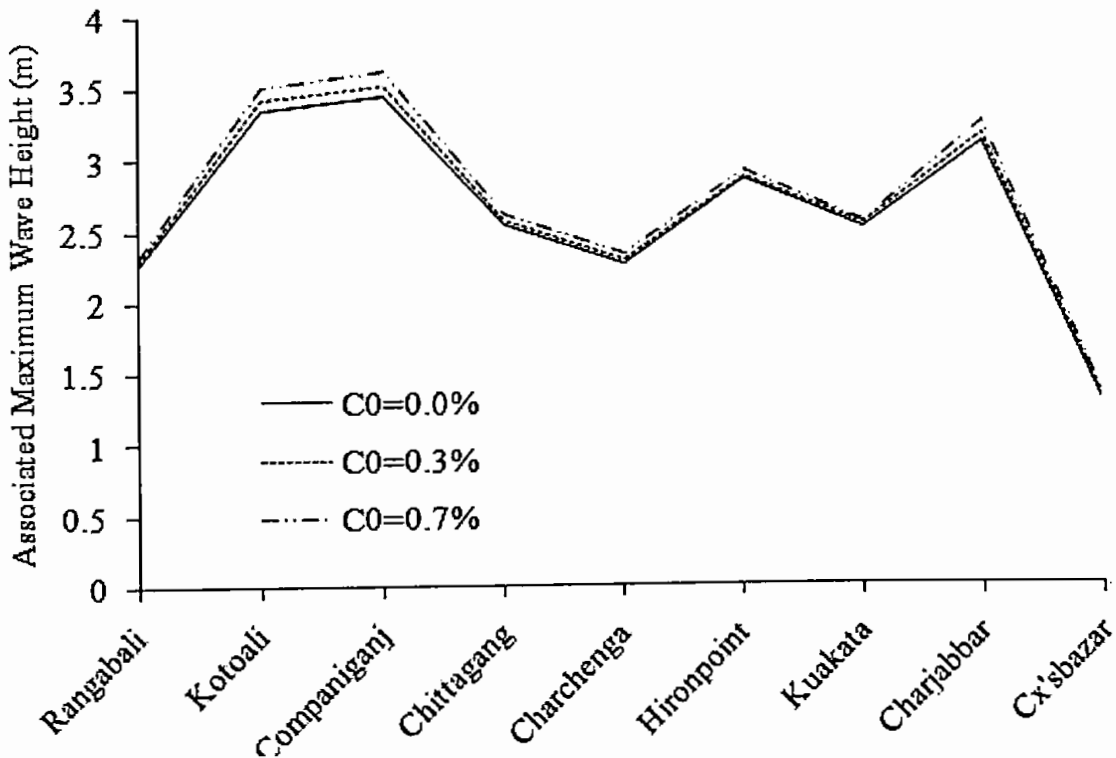
Figure 4.35: Peak water levels (overall) at some coastal and island locations of Bangladesh due to cyclone AILA, 2009.

4.5 Conclusions

In this chapter we have simulated the storm surges due to cyclones AILA, 2009 and the Bangladesh cyclone of April, 1991 considering air bubbles effects during wave breaking in the surf zone. The simulation is made at some coastal and island location of Bangladesh. The model simulation result is found to be reasonable. The model can be found to simulate higher water levels in the presence of air bubbles. That is, it was observed that approximately 1.5%-3.5% water level increases with the increasing of void fraction from 10%-70% associated with AILA, 2009 and approximately 2%-4.5% water level increases with the increasing of void fraction from 10%-70% associated with the cyclone April, 1991. The results are in good agreement with the reported post storm survey information.

Chapter 5

General Conclusions

Summary

This chapter concerns with the brief discussion about the results obtained throughout the thesis. The model is found to higher water levels in presence of air bubbles. The results obtained from the model are in good agreement with the reported data.

5.1 Conclusions

In this study we have developed two dimensional vertically integrated hydrodynamic storm surge model including air bubble effects in Cartesian co-ordinates for the forecasting and evaluation of surge levels in the Bay of Bengal along Bangladesh coast. The model uses finite difference method to solve the wave equations where the coasts and islands are included in the stair step method. The model included the analysis area of the head Bay of Bengal. The developed model is applied to simulate water levels in terms of air bubbles in the coastal region of Bangladesh due to cyclonic storms in April, 1991 and AILA, 2009. The computed results are at nine locations along Bangladesh coast as shown in Fig. (4.3). History about positions and nature of the above-mentioned storms is shown in Tables 4.1 and 4.2, where the data were received from the Bangladesh Meteorological Department. Figures 4.18, 4.19, 4.33 and 4.34 depict the time series of the over-all surge levels with 30% void fraction associated with the storms April 1991 and AILA, 2009 at 9 locations of the coastal region of Bangladesh from Hiron Point to Cox's bazar. For prediction of storm surge each storm should allow to move for at least 72 hours over the analysis area (Roy, 1999b). The model is found to higher water levels in presence of air bubbles. The results obtained from the model are in good agreement with the reported data. A comparison is made between the surges with and without air bubbles. The model can

be found to simulate higher water levels in the presence of air bubbles. That is, it was observed that approximately 1.5%-3.5% water level increases with the increasing of void fraction from 10%-70% associated with AILA, 2009 and approximately 2%-4.5% water level increases with the increasing of void fraction from 10%-70% associated with the cyclone in April, 1991. Ali (1999), in his study, found the maximum surge height along the coastal region of Bangladesh as 7.69 m associated with the cyclone April 1991. Debsharma (2009) observed the maximum surge height at Chittagong as 5m associated with the cyclone April, 1991 and according to the report of Bangladesh Meteorological Department, the water level for the storm at Chittagong was 5.5 m. while our model calculated the surge height with 30% void fraction as 5.25m with maximum level 5.99m at Companiganj. According to the disaster Management Bureau (DMB) the low-lying areas of the coastal districts of Satkhira, Khulna, Bagerhat, Borguna, Bhola, Patuakhali, Barisal, Pirozpur, Jhalokathi, Laxmipur, Noakhali, Feni, Chandpur, Chittagong, Cox's Bazar and their offshore islands and chars are likely to be inundated by wind driven surge of height 05-07 feet above normal astronomical tide. Surge level calculated by our model associated with the storm AILA was found to be 1.15 m to 3.54 m with 30% void fraction along the coast of Bangladesh with maximum level 3.54 m at Companiganj.

Thus, in both storms, the computed surge heights are in reasonably good agreement with those observed.

5.2 Recommendation

The coastal geometry of Bangladesh is complex (Fig. 3.2) and there are many islands in the Bay of Bengal. So, the model in curvilinear coordinate system with finite element method may give the better result for storm surge level in the Bay of Bengal.

References

[1]   Aimin Shi. (2005): Propagation of Long water waves thorugh   Branching channels. J. Engineering Mechanics. Vol. 131, No. 8, August, 859-871.

[2]   Ali, A. (1979): Storm surges in the Bay of Bengal and some related problems. Ph.D, Thesis, University of Reading, England, 227 pp.

[3]   Ali, A. (1996): Vulnerability of Bangladesh to Climate Change and Sea Level Rise through tropical cyclones and storm surges. Water, Air and Soil Pollution, 92, 171-179.

[4]   Ali, A. (1980a): The dynamic effects of barometric forcing on storm surges in the Bay of Bengal, Mausam (formerly Indian J. Met.   Hydrol and Geophys.), vol. 31, No. 4, 517 – 522.

[5]   Ali, A.; Rahman, H.; Sazzard S. and Choudhary H. (1997a): River discharge, storm surges and tidal interaction in the Meghna river mouth in Bangladesh. Mausam. 48, 531-540.

[6]   Ali, A.; Rahman, H.; Choudhary, S.S.H. And Begum, Q.N. (1997b): Back water effect of tides and storm surges on fresh water discharge through the Meghna estuary. J. Remote Sensing & Environment, 1, 85-95.

[7]   Chanson, H. and Toombes, L. (2002): Energy dissipation and air entrainment in a stepped storm waterway: An experimental study, J. Irrig. Drain. Eng., ASCE 128(5), 305-315.

[8]   Cheng, T.T. (1967): Storm Surges in Hong Kong, Royal Observatory, Hong Kong, Tech. Note No. 26.

[9]   Chittibabu, P. (1999): Developement of storm surge prediction models for the Bay of Bengal and the Arabian sea. Ph. D. Thesis , IIT Delhi, India, 200 pp.

[10]   Choudhury, A.M. and Ali, M.A. (1974): Prediction of maximum wind speed in cyclones in the Bay of Bengal-A preliminary investigation, Nucl. Sci. Appl. 7 (B), 109–113.

[11] Conner, W.C.; Kraft, R.H. and Harris, D.L. (1957): Empirical methods for forecasting the maximum storm tide due to hurricanes and other tropical storms. Mon. Wea. Rev., 85, 113-116.

[12] Das P.K. (1972): A prediction model for storm surges in the Bay of Bengal. Nature, vol. 239, 211-213.

[13] Das P.K. (1994a): Prediction of storm surges in the Bay of Bengal. Proc.Inidan natn. Sci. Acad.,60, 513-533.

[14] Das P.K. (1994b): On the Prediction of storm surges. Sadhana, 19,583-595.

[15] Das, P.K.; Sinha, M.C. and Balasubramanyam, V. (1974): Storm Surges in the Bay of Bengal, Quart. J. Roy. Met. Soc., 100, 437-449.

[16] Das P.K.; Dube, S.K.; Mohanty, U.C.; Sinha, P.C. and Rao, A.D. (1983): Numerical simulation of the surge generated by the June 1982 Orissa cyclone. Mausam, 34, 359-366.

[17] Dean, R.G. and Dalrymple, R.A. (1984): Water wave mechanics for Engineers and Scientists, prentice-Hall, Englewood Cliffs, NJ.

[18] Debsarma, S.K. (1997): Visualization of May 1997 storm surge by using IIT model, Proc. Of SAARC seminar on tropical cyclone and storm surges in the south Asian region, 20-22, Dec. 2003 (held in Dhaka, Bangladesh), 23-48.

[19] Debsarma, S.K. (2009): Simulations of storm surges in the Bay of Bengal, Mar. Geod. 32, 178-198.

[20] Devendra, R.A. (1982): Storm Surge modeling in the Bay of Bengal, Ph. D thesis, IIT, Delhi, India, 1-38.

[21] Dube S.K.; Sinha, P.C. and Rao, A.D. (1982): The effect of coastal geometry on the location of peak surge. Mausam 33, 445-450.

[22] Dube S.K.; Sinha, P.C.; Rao, A.D. and Rao, G.S. (1985): Numerical modelling of storm surges in the Arabian Sea. Applied Math , Modelling, 9 , 289-294

[23] Dube, S.K.; Singh, P.C. and Roy, G.D. (1986): Numerical simulation of storm surges in Bangladesh using multi-level model; Int. J. for Num. Methods in fluids 6, 305-311.

[24] Dube, S.K. and Rao, A.D. (1989): Coastal flooding due to storm surges in the Bay of Bengal. In: Coastal Zone Management in India (Editors: S. N. Dwiwedi, V. S. Bhatt and Pradeep Chaturvedi), Indian Association for the Advancement of Science, 136-144.

[25] Dube, S.K. and Rao, A.D. (1991): Sea level rise and coastal flooding by storm surges in the Bay of Bengal. Proc. Indian National Sci. Acad., 57A, 565-572.

[26] Dube S.K.; Rao, A.D.; Sinha, P.C.; Murty, T.S. and Bahulayan, N. (1997): Storm Surges in the Bay of Bengal and Arabian Sea: The problem and its prediction, Mausam, Vol. 48, No. 2, 283-304.

[27] Flather, R.A. (1976): Results from a storm surge prediction of the northern Bay of Bengal with application to the cyclone disaster in April 1991. Jr. Phys. Oceanogr. Vol. 24. 172-190.

[28] Frank, N.L. and Hussain, S.A. (1971): The deadliest tropical cyclone in history. Bulletin of the American Meteorological Society, Vol. 57, 438-444.

[29] Fuhrboter, A. (1970): Air entrainment and energy dissipation in breakers. Proc. ICCE, 391-398.

[30] Ghosh, S. K. (1981): Objective prediction of storm surges on Indian coasts, Proc. Symp. on Meteorological and Oceanic Fluid dynamics, 7-8 February, 1981, Jadavpur University, Calcutta , India.

[31] Ghosh, S.K.; B.N. Dewan and Singh, V.B. (1983): Numerical simulation of storm surge envelopes associated with the recent severe cyclones impinging on the east and west coast of India, Mausam, Vol. 34, 399-404.

[32] Heaps, N.S. (1967): Storm surges, Oceanogr. Mar. Biol. Ann. Rev., vol. 5, 11-47.

[33] Heaps, N.S. (1973): Three dimensional numerical model of the Irish sea, Gyophys. J. astron. Soc. Vol. 35, 99-120.

[34] Henry, R.F.; Duncalf, D.S.; Walters, R.A.; Osborne, M.J. and Murty, T.S. (1997): A study of tides and storm surges in offshore waters of the Meghna estuary using a finite element method, Mausam, 48(4), 519-530.

[35] Hicks, S.D. (2006): Understanding of tides, National oceanic and admini station, US department of commerce.

[36] Hoque, A. (2002): Air bubble entrainment by breaking waves and associated energy dissipation. Ph.D. thesis. Toyohashi Univ. of Technology, p151.

[37] Hoque, A. (2008): Studies of water level rise by entrained air in the surf zone, Exp. Therm. Fluid Sci. 32, 973–979.

[38] Hoque, A. and Aoki, S. (2008): Air Entrainment and Associated Energy Dissipation in Steady and Unsteady Plunging Jets at Free Surface, Applied Ocean Research, 30/1, 37-45.

[39] Hoque, A. and Rahman, A. (2006): A study of Coriolis Effects on Long Waves Propagating in an Unbounded Ocean, Channel and Basin, Journal of Ocean Engineering, Elsevier, Vol. 34, 1701-1705.

[40] Horikawa, K. and Kuo, C. T. (1966): A study on wave transformation inside surf zone. Proc. 10th Coastal Engng. Conf., 217-233.

[41] Huq, S.; Ali, S.I. and Rahman, A.A. (1995): "Sea-level rise and Bangladesh: A preliminary analysis." Journal of Coastal Research Special Issue 14:44-53.

[42] IPCC (2007): Fourth Assessment Report of the Intergovernmental Panel on Climate Change, paris, February.

[43] Isojaki, I. (1970): An investigation on the variations of sea level due to meteorological disturbances in the coast of Japanese Islands (VI), Paper on Meteorological Geophysics, Tokyo, XXI, 3, 291-321.

[44] Jelesnianski, C.P. (1965): A numerical calculation of storm tides induced by a tropical storm impinging on a continental shelf. Mon. Wea. Rev. 93, 343-358.

[45] Jelesnianski, C.P. (1972): SPLASH (Special Program to List Amplitudes of Surges from Hurricanes) I. Landfall Storms. NOAA Tech. Man. NWS TDI/-46, 52pp.

[46] Jelesnianski, C.P. (1976): A sheared coordinate system for storm surge equations of motion with a mildly curved coast. NOAA Tech. Memo., NWS/TOL-61, 55 pp.

[47] Johns, B. (1981): Numerical simulation of storm surges in the Bay of Bengal, Proc. Of Conf. On Monsoon Dynamics, New Delhi, Dec., 5-9, 1997, Cambridge University press.

[48] Johns, B. and Ali, A., (1980): The numerical modeling of storm surges in the Bay of Bengal. Quart. J.R. Met. Soc., 106, 1-18.

[49] Johns, B.; Rao, A.D.; Dube, S.K. and Sinha, P.C. (1985): Numerical modelling of Tide-surges interaction in the Bay of Bengal, Philos. T. Roy. Soc. A 313, 507-535.

[50] Karim, N. (2006): Options for cyclone protection: Bangladesh context. Climate Institute. 6 July 2006.

[51] Kraus, E.B. and Businger, J.A. (1994): Atmosphere–Ocean Interaction, second ed. Oxford University Press, pp. 362.

[52] Lagrange, J.L. (1781): Mémoire sur la théorie du mouvement des fluides. Nouv. Mém. Acad. Berlin, p. 196. Also in 1867–1892. Oeuvres de Lagrange 4:695–748. Paris: Gauthier-Villars.

[53] Miyazaki, M. (1957): On storm surges which recently struck the Japanese coast. Oceanogr. Mag., vol. 9, 209-225.

[54] Murty, T.S. (1984): Storm surges - meteorological ocean tides. Can. Bull. Fish. & Aquat. Sci., 212, 897 pp.

[55] Murty, T.S.; Flather, R.A. and Henry, R.F. (1986): The storm surge problem in the Bay of Bengal. Prog. Oceanog.16, 195-233.

[56] Nihoul, J.C.J. (1975): Modeling of marine systems. Elsevier Scientific Pub. Co. 272pp.

[57] Paul Glaister (1988): Approximate Riemann solutions of the shallow water equations, Journal of Hydraulic Research Vol. 26, Issue 3, 293 –306.

[58]   Prandle, D. (1975): Storm surges in the southern north sea and river thames, Proc. R. Soc. Lond., A, vol. 344, 509-539.

[59]   Proudman, J. (1955): The propagation of tide and surge in an estuary, Proc. R. Soc. Lond., A, vol. 231, 8-24.

[60]   Rao, N.S. and Mazumdar, B.S. (1966): A technique for forecasting storm waves. Indian Journal of Meteorology and Geophysics. 17, 333-346.

[61]   Rashid, H.E. (1991): Geography of Bangladesh, 2nd edition, University Press, Dhaka, 87-88.

[62]   Reid, R.O.; Vastano, A.C.; Whitaker, R.E. and Wanstrath, J.J. (1977): Experiments on storm surge simulation, Wiley interscience publication, New York, London, Sydney, Toronto, vol. 6, 145-168.

[63]   Rao, A.D. (1982): Numerical storm surge prediction in India. Ph.D. Thesis. Centre for Amos. & Fluid Sc., IIT, New Delhi.

[64]   Roy, G.D. (1995): Estimation of expected maximum possible water level along the Meghna estuary using a tide surge interaction model; Environment International 25(1), 671-677.

[65]   Roy, G.D. (1999a): Sensitivity of water level associated with tropical storms along the Meghna estuary in Bangladesh. Environ. Int. 25, 109-116.

[66]   Roy, G.D. (1999b): Inclusion of off-shore islands in a transformed coordinate shallow water model along the coast of Bangladesh. Environ. int. 25, 67-74.

[67]   Roy, G.D. and Hussain, F. (2001): A nearly orthogonal 2D grid system in solving the shallow water equations in the head Bay of Bengal, Preprint Abdus Salam (ICTP).

[68]   Sielecki, A. (1968): An energy conserving difference scheme for the storm surge equations. Mon. Wea. Rev., 96, 150-156.

[69]   Sinha, P.C.; Dube, S.K.; Rao, A.D. and Rao, G.S. (1984): Numerical simulation of the surge generated by the November 1982 Gujarat cyclone, Vayu Mandal, 14, 31-33.

[70]   Sinha, P.C.; Rao, Y. R.; Dube, S. K. and Murty, T. S. (1997): Effect of sea level rise on tidal circulation in Hoogly Estuary, Bay of Bengal. Marine Geodesy. 20, 341-366.

[71] Soloviev, A. and Lukas, R. (2010): Effects of bubbles and sea spray on air-sea exchange in hurricane conditions, Bound.-lay. meteorol. 136, 365–376.

[72] Talukdar, J.; Roy, G.D. and Ahmed, M. (1992): Living with cyclone, *Community Development library*, Dhaka, 86-102.

[73] Terray, E.A.; Donelan, M.A.; Agrawal, Y.C.; Drennan, W.M., Hwang, P.A. and Williams, A.J. (1996): Estimates of kinetic energy dissipation under breaking waves, Journal of physical Oceanography, vol. 26 (5).

[74] World Bank (2002): World Development Indicators. On CD Rom. The World Bank, Washington, DC. WRI. 2001. World Resources: 2000-2001. World Resources Institute, Washington, DC.

[75] Welendar, P. (1961): Numerical prediction of storm surges. Advances in Geography., B., 316-379.

[76] Wu, J. (1981a): Bubble populations and spectra in near- surface ocean: Summary and review of field measurements. J. Geophys. Res. 86, 457-463.